MARINE PHYSICAL LABORATORY

SCRIPPS INSTITUTION OF OCEANOGRAPHY

San Diego, California 92152

200 Hz Matched Field Processing on the September 1987 VLA Data Set

Jean-Marie Q.D. Tran and William S. Hodgkiss

MPL TECHNICAL MEMORANDUM 417

MPL-U-6/90
September 1990

UNCLASSIFIED

SECURITY CLASSIFICATION OF THIS PAGE

REPORT DOCUMENTATION PAGE

Form Approved
OMB No. 0704-0188

1a. REPORT SECURITY CLASSIFICATION UNCLASSIFIED	1b. RESTRICTIVE MARKINGS
2a. SECURITY CLASSIFICATION AUTHORITY	3. DISTRIBUTION / AVAILABILITY OF REPORT Approved for public release; distribution unlimited.
2b. DECLASSIFICATION / DOWNGRADING SCHEDULE	
4. PERFORMING ORGANIZATION REPORT NUMBER(S) MPL Technical Memorandum 417 [MPL-U-6/90]	5. MONITORING ORGANIZATION REPORT NUMBER(S)
6a. NAME OF PERFORMING ORGANIZATION University of California, San Diego 6b. OFFICE SYMBOL (*If applicable*) MPL	7a. NAME OF MONITORING ORGANIZATION Office of Naval Research Department of the Navy
6c. ADDRESS (*City, State, and ZIP Code*) Marine Physical Laboratory Scripps Institution of Oceanography San Diego, California 92152	7b. ADDRESS (*City, State, and ZIP Code*) 800 North Quincy Street Arlington, VA 22217-5000
8a. NAME OF FUNDING / SPONSORING ORGANIZATION Office of Naval Research 8b. OFFICE SYMBOL (*If applicable*) ONR	9. PROCUREMENT INSTRUMENT IDENTIFICATION NUMBER N00014-89-K-0038
8c. ADDRESS (*City, State, and ZIP Code*) 800 North Quincy Street Arlington, VA 22217-5000	10. SOURCE OF FUNDING NUMBERS PROGRAM ELEMENT NO. / PROJECT NO. / TASK NO / WORK UNIT ACCESSION NO.

11. TITLE (*Include Security Classification*)
200 Hz Matched Field Processing on the September 1987 VLA Data Set

12. PERSONAL AUTHOR(S)
Jean-Marie Q.D. Tran and William S. Hodgkiss

13a. TYPE OF REPORT	13b. TIME COVERED	14. DATE OF REPORT (*Year, Month, Day*)	15. PAGE COUNT
technical memorandum	FROM _____ TO _____	September 1990	79

16. SUPPLEMENTARY NOTATION

17. COSATI CODES			18. SUBJECT TERMS (*Continue on reverse if necessary and identify by block number*)
FIELD	GROUP	SUB-GROUP	vertical line array, matched field processing, towed source transmission

19. ABSTRACT (*Continue on reverse if necessary and identify by block number*)

This technical report demonstrates, based on data collected at sea during the September 1987 Vertical Line Array (VLA) Experiment in the North East Pacific, that matched field processing is a viable processing technique at 200 Hz and on a 900 m long vertical line array. The sound speed information derived from the CTD and XBT data collected during the experiment allows a good acoustic modeling by the ATLAS normal mode model of the CW transmissions. Although mismatch still exists, matched field processing produces good estimates of the source ranges for both fixed station transmissions and towed source transmissions. Source depth estimation appears, in this data set, a more difficult problem. The VLA system has acoustic navigation capabilities which show that the array, generally, has a tilt on the order of 1°. This tilt corresponds to a 15 m horizontal displacement from the top to the bottom of the array or two wavelengths at 200 Hz. Simulations indicate that array tilt can result in large losses and significant pattern changes in the range-depth ambiguity surfaces and is the main source of mismatch.

20. DISTRIBUTION / AVAILABILITY OF ABSTRACT	21. ABSTRACT SECURITY CLASSIFICATION
☐ UNCLASSIFIED/UNLIMITED ■ SAME AS RPT. ☐ DTIC USERS	UNCLASSIFIED
22a. NAME OF RESPONSIBLE INDIVIDUAL W. S. Hodgkiss	22b. TELEPHONE (*Include Area Code*) (619) 534-1798 22c. OFFICE SYMBOL MPL

DD Form 1473, JUN 86 *Previous editions are obsolete*

SECURITY CLASSIFICATION OF THIS PAGE

UNCLASSIFIED

200 Hz Matched Field Processing On The September 1987 VLA Data Set

Jean-Marie Q.D. Tran
William S. Hodgkiss

Marine Physical Laboratory
Scripps Institution of Oceanography
San Diego, CA 92152

ABSTRACT

This technical report demonstrates, based on data collected at sea during the September 1987 Vertical Line Array (VLA) Experiment in the North-East Pacific, that matched field processing is a viable processing technique at 200 Hz and on a 900 m long vertical line array. The sound speed information derived from the CTD and XBT data collected during the experiment allows a good acoustic modeling by the ATLAS normal mode model of the CW transmissions. Although mismatch still exists, matched field processing produces good estimates of the source ranges for both fixed station transmissions and towed source transmissions. Source depth estimation appears, in this data set, a more difficult problem. The VLA system has acoustic navigation capabilities which show that the array, generally, has a tilt on the order of 1°. This tilt corresponds to a 15 m horizontal displacement from the top to the bottom of the array or two wavelengths at 200 Hz. Simulations indicate that array tilt can result in large losses and significant pattern changes in the range-depth ambiguity surfaces and is the main source of mismatch.

Table of Contents

1. Introduction

This technical memorandum contains the results of matched field processing on 200 Hz CW tone propagation data collected during the September 1987 Vertical Line Array (VLA) experiment in the North-East Pacific. The Marine Physical Laboratory (MPL) digital array, long of 900 m and filled with 120 hydrophones with 7.5 m interelement spacing, was deployed for several weeks from the R/P FLIP, approximately 400 km southwest of Monterey, California. The R/P FLIP was in a three-point moor at 34°58.69′ N 125°58.43′ W. Previous work [Tran1989] dealt with the conventional processing of the 200 Hz CW tone propagation data recorded by the VLA, first, when the source ship kept a fixed stations 89 nm from the R/P FLIP on Julian 271 and, second, when the ship towed the source away from the R/P FLIP for ten hours on Julian 272. In both cases, the top of the VLA was at a nominal depth of 400 m. The acoustic source was an HX90 deployed from the USNS NARRAGANSETT. It projected the 200 Hz CW tone with a nominal source level of 184 dB ref 1 μPa at 1 m.

The results of the conventional processing and of the acoustic modeling of the propagation presented in [Tran1989] demonstrate the good quality of the data and the ability to model the propagation with the available environmental information. Based on these results, it is natural to attempt matched field processing on the data set. Since the source level is high in this propagation experiment, detectability is not an issue here. The signal is easily detected on individual phones using conventional techniques. Therefore the focus is on the range and depth localization capability of matched field processing.

2. Outline of the Matched Field Processing

Conventional beamforming can be interpreted as a spatial matched filtering operation. The Bartlett processor, for a particular frequency f is given by

$$P_B = \frac{1}{M} \mathbf{E}^H \mathbf{R} \mathbf{E} \tag{2.1}$$

where $\mathbf{R}$ is the array covariance matrix at the frequency f based on the data given by

$$\mathbf{R} = \frac{1}{K} \sum_{i=1}^{K-1} \mathbf{X}_i \mathbf{X}_i^H \tag{2.2}$$

where $\mathbf{X}_i$ is the vector of Fourier coefficients across the array at the selected frequency f corresponding to the time snapshot i. In Equation 2.1, $\mathbf{E}(\theta)$ is a normalized replica vector containing the phase variations across the array, assuming a given arrival angle and a wavefront shape. The replica vector $\mathbf{E}$ is such that $\mathbf{E}^H \mathbf{E} = 1$. The beamformer searches peaks in angle to find arrivals. Such processor can be generalized to search spaces other than angle. The matched field processing techniques search in the range-depth space, that is the replica vector $\mathbf{E}$ is now $\mathbf{E}(r, z)$ [Baggeroer1988]. Matched field processing consists in measuring the match or the mismatch of a field probed by a vertical array with a predicted field for a particular source range and depth. Matched field processing provides detection as well as localization. The main difficulty is to compute a realistic prediction of the pressure field for a source and receiver geometry. The replica vectors are computed by propagation models such as normal mode models where environmental information is critical. The literature provides multiple examples of the great sensitivity of matched field processing to an imperfect knowledge of the environment parameters such as sound speed profile, geoacoustic parameters of the bottom, water depth [Porter1987, Del.Bazo1988, Feuillade1989, Tolstoy1989, Baxley1989]. The acoustic modeling performed in [Tran1989] is used with the ATLAS normal mode model [Gordon1984] to create the replica vectors using a sound speed profile based on the CTD and the XBT data collected at the R/P FLIP during the experiment. The range-depth search space is sampled every 250 m in range and every 5 m in depth up to a maximum depth of 600 m.

Several processors can be used in matched field processing [Fizell1987]. In addition to the conventional Bartlett processor given in Equation 2.1, with $\mathbf{E}(r,z)$, the Minimum Variance (MV) processor [Capon1969], which yield more resolution but is less robust, is used in the following. The MV processor is given by

$$P_{MV} = \frac{1}{M} \frac{1}{\mathbf{E}^H \mathbf{R}^{-1} \mathbf{E}} \tag{2.3}$$

where $\mathbf{R}$ is defined like in Equation 2.1, and $\mathbf{E}$ is the replica vector corresponding to a particular source range and depth. $\mathbf{E}(r,z)$ is normalized to unit norm. In order to be inverted, the array covariance matrix $\mathbf{R}$ must be stabilized, that is, its main diagonal loaded by a small amount of spatially white noise [Capon1969]. The matrix $\mathbf{R}$ is augmented by $\gamma \frac{tr(\mathbf{R})}{M} \mathbf{I}$, where $\mathbf{I}$ is the identity matrix, tr the trace operation, M the number of sensors and γ the fraction of white noise, also called stabilization factor with values between 10^{-3} and 10^{-1}. The selected values for the stabilization in this study are 10^{-3}, 10^{-2} and 10^{-1}.

A preliminary step is to estimate the array covariance matrix at the transmission frequency, 200 Hz. The covariance matrix is computed by averaging 126 dyad products $\mathbf{X}_i \mathbf{X}_i^H$ in Equation 2.2. The array Fourier vectors $\mathbf{X}_i$ are derived from two blocks of 64 K data points (1 K = 1024 point) using 50 % overlapped 2048-point FFTs (244 mHz binwidth), and a Kaiser-Bessel window with α parameter of 2.5 (first side-lobe level at -57 dB). Each covariance matrix corresponds to 4 minutes and 22 seconds worth of data. The 2048-point FFT corresponds to 4 seconds worth of data and yields a positive signal-to-noise ratio on an individual hydrophone.

3. Fixed Station Matched Field Processing

3.1. Description of the Experiment

On Julian Day 270, the 200 Hz CW tone was projected for various time lengths and various source depths, 89 nm (or 165.5 km) from the R/P FLIP. The first transmission with the source at a nominal depth of 300 m began at 20:50 GMT and lasted for 15 minutes. The corresponding data were recorded on Tape 915 (which starts at 20:48:04 GMT). The source was raised to a depth of 150 m and the transmission resumed at 21:30 GMT for 10 minutes. The data were recorded on Tape 917 (which starts at 21:34:59 GMT). The source finally was raised to a depth of 20 m and projected for 18 minutes from 21:57 GMT. The data were recorded on Tape 918 (which starts at 21:58:27 GMT).

Environmental data were collected on the R/P FLIP. Swell heights on Julian Day 270 were visually measured between 5 and 10 feet. A northern wind was blowing with speeds between 20 and 25 kts. XBT casts were collected at the R/P FLIP before and after the transmissions

3.2. Fixed Station Modeling

The modeling of the propagation data was described in [Tran1989] for the three different depths at which transmissions were performed using both the Generic Sonar Model (GSM) [Weinberg1985] and the ATLAS normal mode model [Gordon1984]. Information relevant to the calculation of the replica vectors with the ATLAS model is presented here, more detailed information can be found in [Tran1989].

3.2.1. Sound Speed Profiles

As mentioned earlier, a CTD was collected in the vicinity of the R/P FLIP on Julian Day 267, up to a depth of 3885 m. Another CTD, collected at 37°04.19′ N 134°46.75′ W on Julian Day 264, was used to extend the FLIP CTD down to the nominal bottom depth at the R/P FLIP, 4667 m. The sound speed profile, based on the CTD, was

derived using the UNESCO equations relating conductivity to practical salinity and sound speed to temperature, salinity and pressure [Fofonoff1983].

XBT casts were collected at the R/P FLIP before and after the fixed station transmissions on Julian Day 270 at 13:00 GMT (a 400 m XBT) and on Julian Day 272 at 03:00 GMT (a 750 m XBT). These XBT data were used in the state equation of [Mackenzie1981] to produce sound speed profiles.

This information allows the synthesis of the sound speed profile used with the ATLAS model to produce the replica vectors. The model sound speed profile is plotted in Figure 1 for the whole water column and for the top 750 m. The two XBT sound speed profiles are also plotted in dashed lines. A 30 m deep mixed layer was observed at the R/P FLIP, followed by a shallow duct above 100 m, which evolves with time, as shown by the two XBT sound speed profiles taken only 14 hours apart. The deep sound axis as at a depth of about 550 m.

3.2.2. Modeling with ATLAS

The replica vectors produced by the ATLAS normal mode model are based on the sound speed profile in Figure 1 and a bottom loss table which corresponds to a GSM Bottom Province Type 3, given in Table 1. A range independent medium with a water depth of 4667 m is considered here.

The source is at a nominal range of 165.5 km and modeling indicates that the VLA is in the trailing edge of the third convergence zone, which becomes sharper as the source is raised in the water column [Tran1989]. The angular spectrum of the pressure field produced by the ATLAS model was found in good agreement with the beamformed experimental data. The replica vectors are calculated for ranges going from 152.5 km to 177.5 km, every 250 m, for sources every 5 m from 5 to 600 m.

Angle (deg)	Loss (dB)
0°	0.0
10°	0.4
20°	3.2
30°	5.2
40°	6.8
50°	7.6
60°	8.2
70°	8.2
80°	8.2
90°	8.4

Table 1: Bottom Loss Table in dB (GSM Province Type 3)

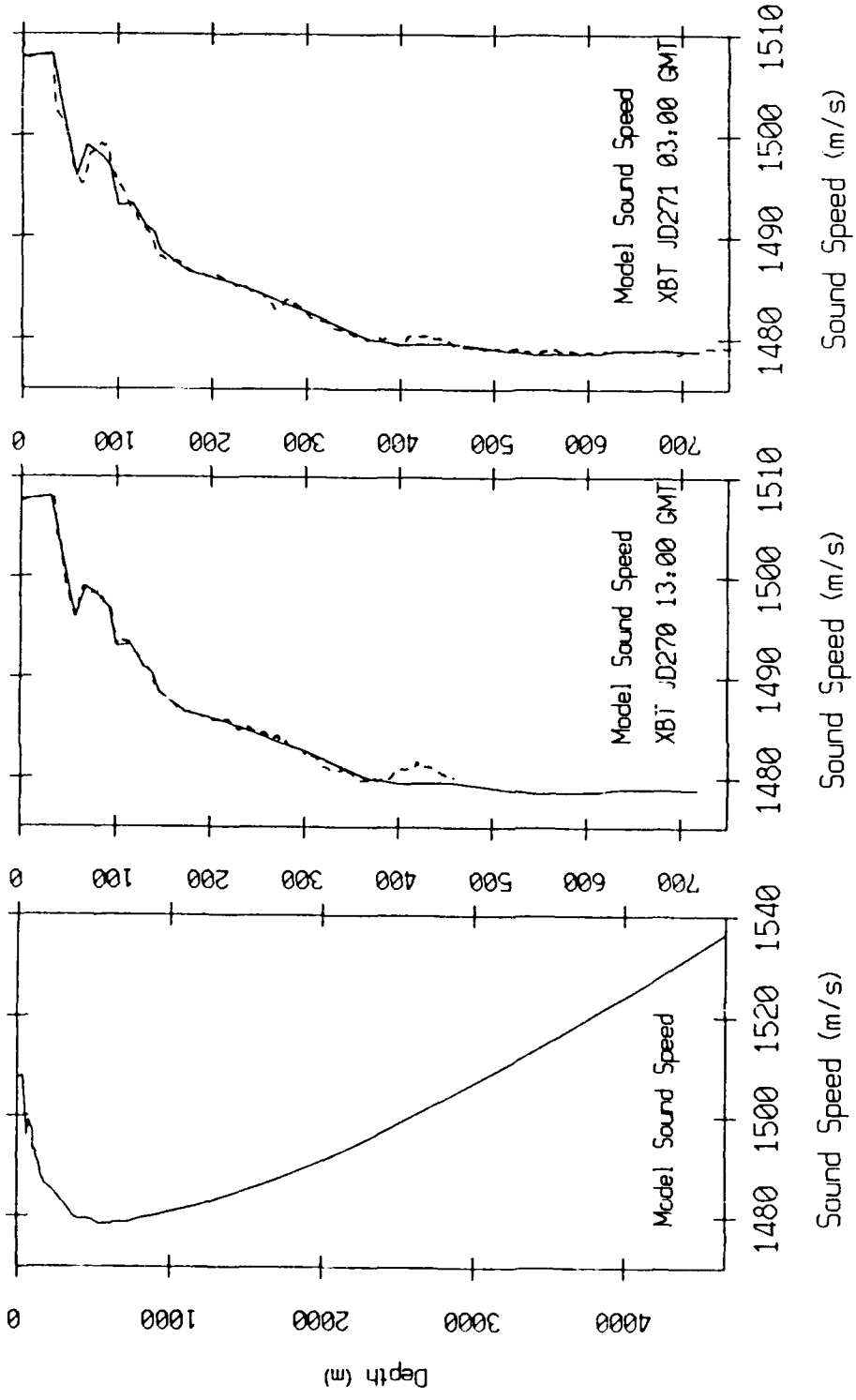

Figure 1: Fixed station sound speed profile.

3.3. Matched Field Processing Results

Matched field processing is performed with the Bartlett processor and the MV processor with stabilization factors equal to 10^{-3}, 10^{-2} and 10^{-1}. Table 2 references the 4 minute and 22 second long data segments used to estimate the covariance matrix for each station. The sequence of three source depths (300, 150 and 20 m) provides an opportunity to test on real data the capabilities of matched field processing to localize in depth.

For the three source depths, the covariance matrix is computed by keeping the frequency bin # 1844 in the 2048-point FFT (200.195 Hz) where the signal is the strongest across the array.

Tape number	GMT data segment start time	Source depth (m)
915	20:54:37	300
917	21:34:59	150
918	22:02:49	20

Table 2: GMT time reference for the covariance matrix estimate

The results are gray-level displayed in Figure 2 to 7. In each case, the gray levels span the full dynamic range of the ambiguity surface and correspond to a scale of dB re μpa. Each ambiguity surface is normalized by the level of its maximum peak which is characterized by its calibrated power level in dB re μPa, its range and depth. This highest peak can be used to localize the source. Table 3 summarizes the results of matched field processing on the experimental data. First, one observes that the ambiguity surfaces exhibit their maximum peaks near the nominal source range, 165.5 km. One notes the great granularity of the range-depth ambiguity surfaces and the large number of sidelobes. The Bartlett processor has the most sidelobes but has also the largest dynamic range. The MV processor suffers large loss due to mismatch, the replica are imperfect. An increase in the fraction of noise γ for the MV processor results in more robustness [Cox1988], but reduces the relative signal level in the ambiguity surfaces. A stabilization factor of 10^{-2} is

best based on a subjective inspection of the range-depth ambiguity surfaces.

Wnile localization in range is successful, localization in depth produces mixed results. When the source is at 300 m depth, the Bartlett processor produces a highest level peak at a depth of 195 m, while the MV processors find shallower source depths. When the source is at a depth of 100 m, the Bartlett processor and the MV processor with a stabilization factor γ of 10^{-3} indicate a very shallow source. On the other hand, the stabilized MV processor with γ equal to 10^{-2} and 10^{-1} find the correct source depth at 110 m. Finally when the source is at 20 m, all the processors correctly estimate the source depth.

Tape		Processor			
		Bartlett	MV $\gamma = 10^{-3}$	MV $\gamma = 10^{-2}$	MV $\gamma = 10^{-1}$
915 (Source at 300 m)	Depth of Max.	195 m	15 m	15 m	15 m
	Range of Max.	163.25 km	163 km	163 km	167 km
	Surface Max.	72.2 dB	44.8 dB	49.1 dB	54.9 dB
	Dynamic Range	25 dB	7.5 dB	5.5 dB	4 dB
	Figure	2	2	3	3
917 (Source at 100 m)	Depth of Max.	15 m	20 m	110 m	110 m
	Range of Max.	163 km	166.25 km	165.75 km	165.75
	Surface Max.	72.7 dB	43.7 dB	48.2 dB	53.8 dB
	Dynamic Range	25 dB	8 dB	6 dB	4.5 dB
	Figure	4	4	5	5
918 (Source at 20 m)	Depth of Max.	25 m	20 m	20 m	20 m
	Range of Max.	163.5 km	164.25 km	164.25 km	164.25 km
	Surface Max.	79.0 dB	49.6 dB	54.4 dB	60.0 dB
	Dynamic Range	30 dB	10 dB	8 dB	5.5 dB
	Figure	6	6	7	7

Table 3: Summary of matched field processing (fixed station data)

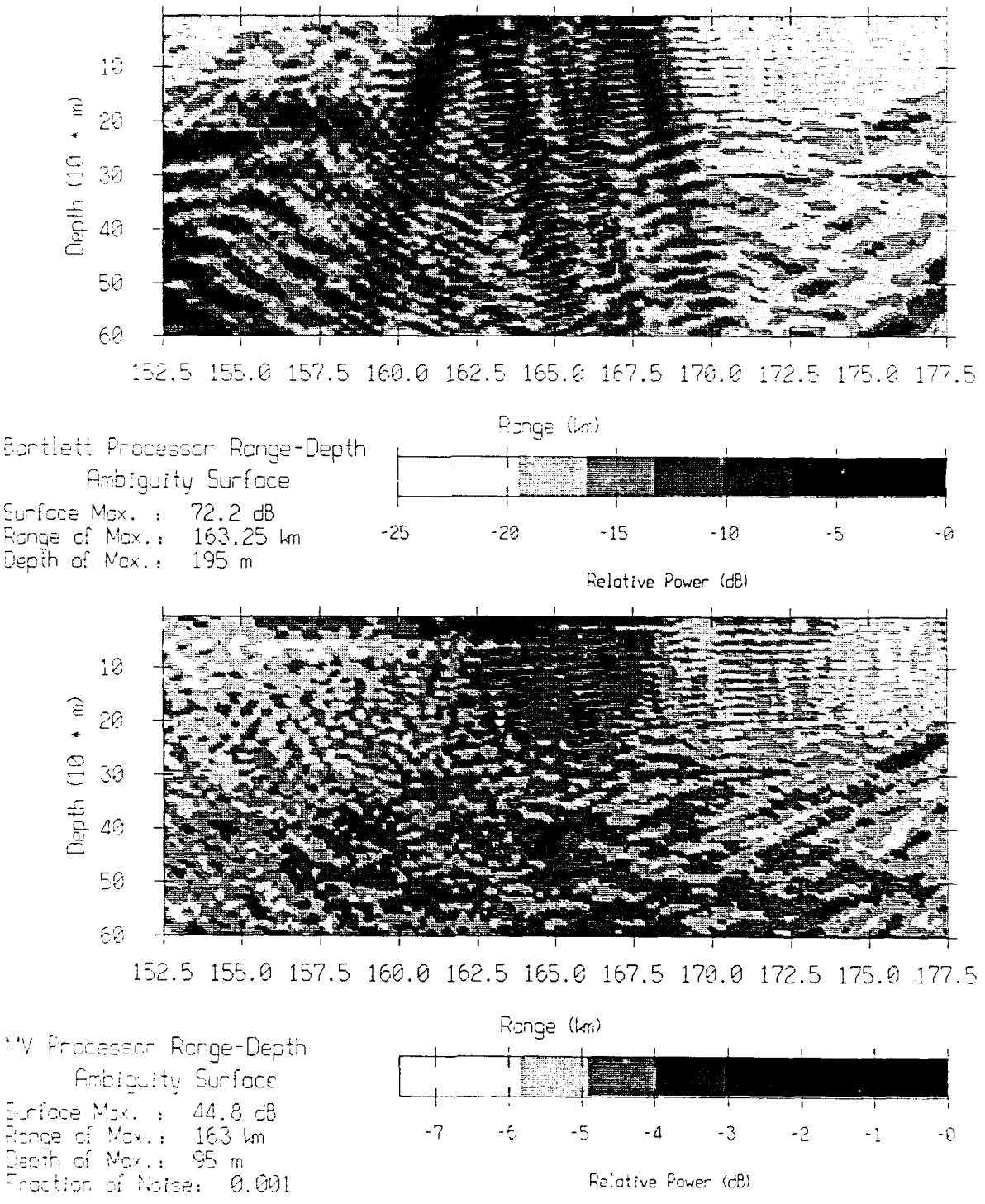

Figure 2: Matched field processing on the data of Tape 915, part 1.

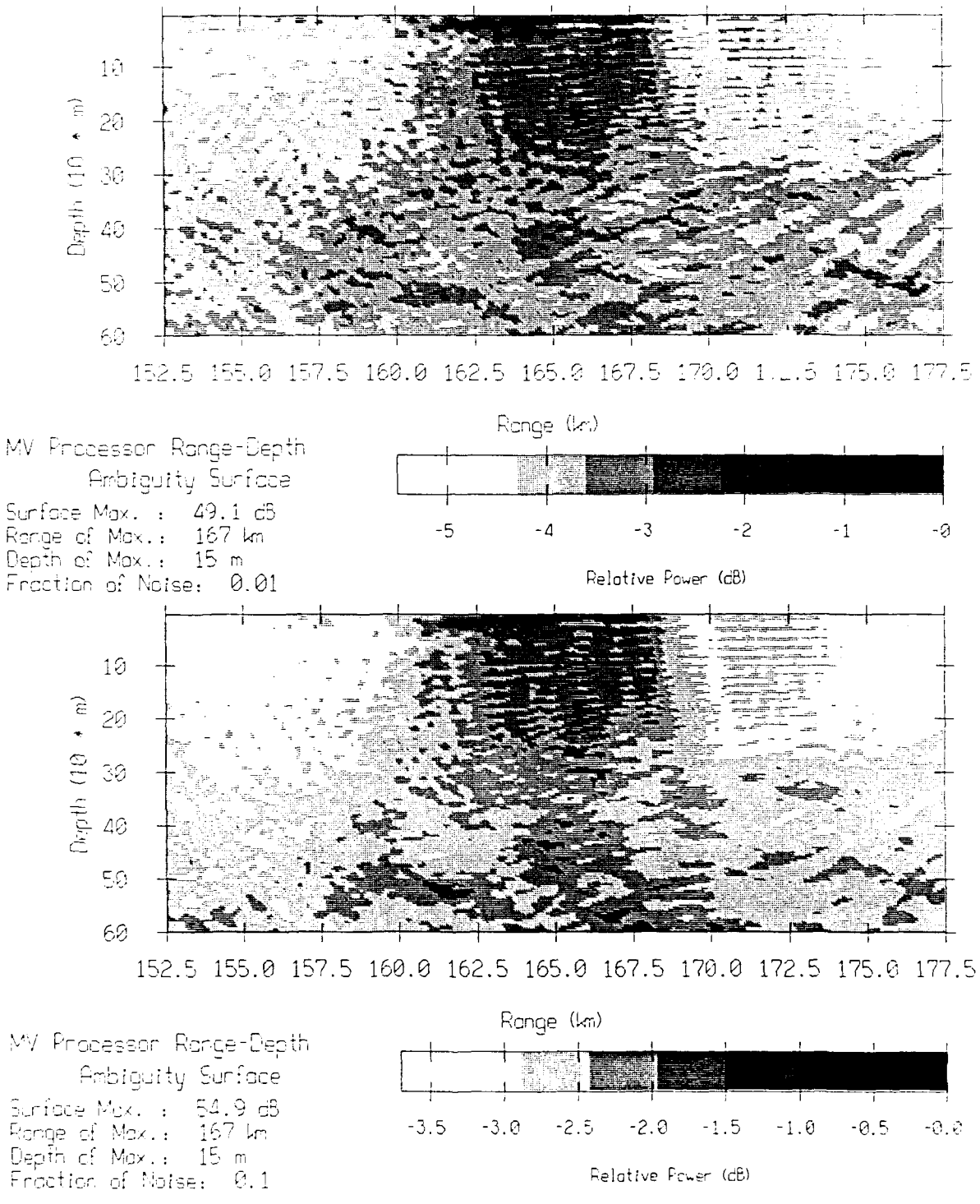

Figure 3: Matched field processing on the data of Tape 915, part 2.

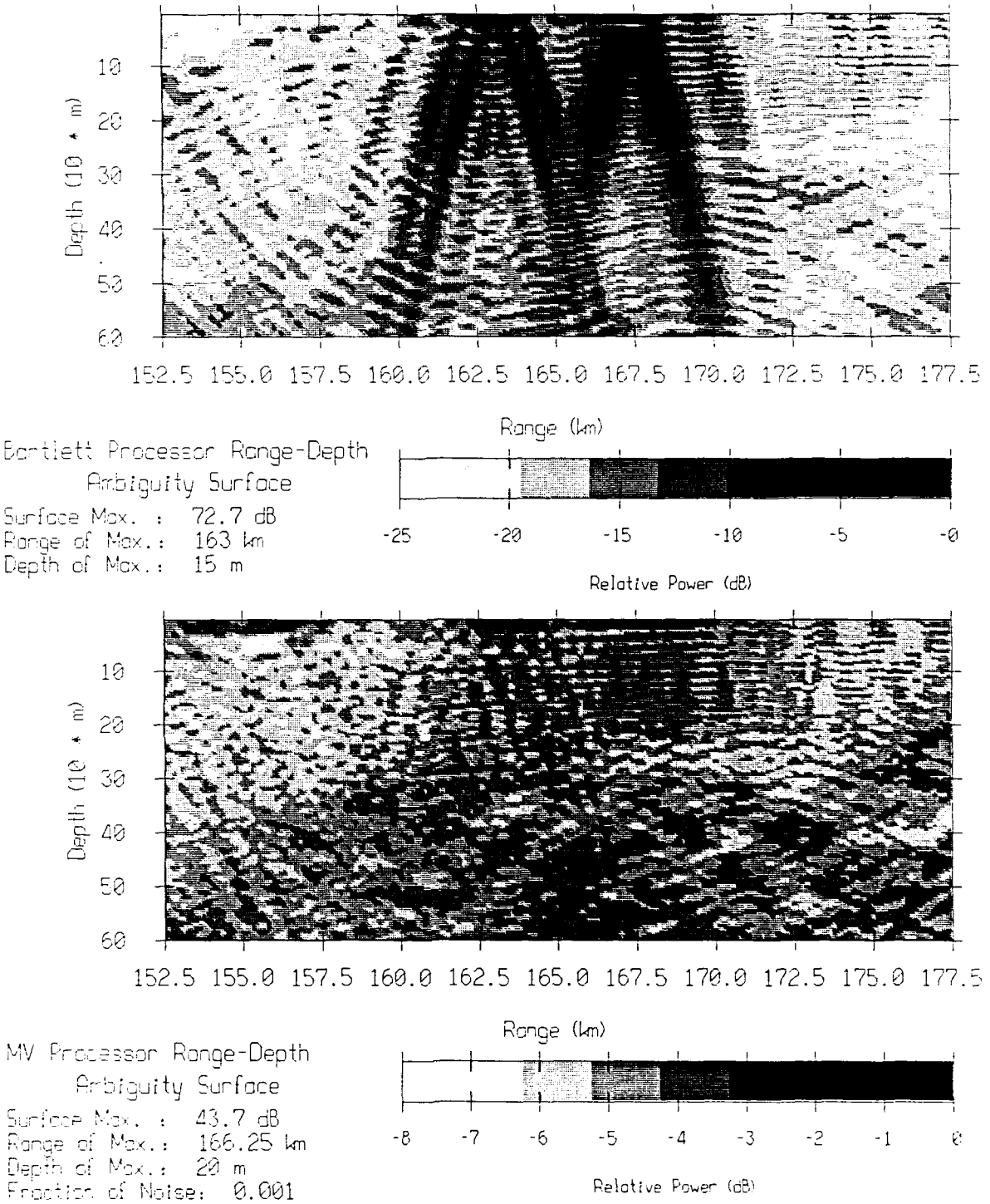

Figure 4: Matched field processing on the data of Tape 917, part 1.

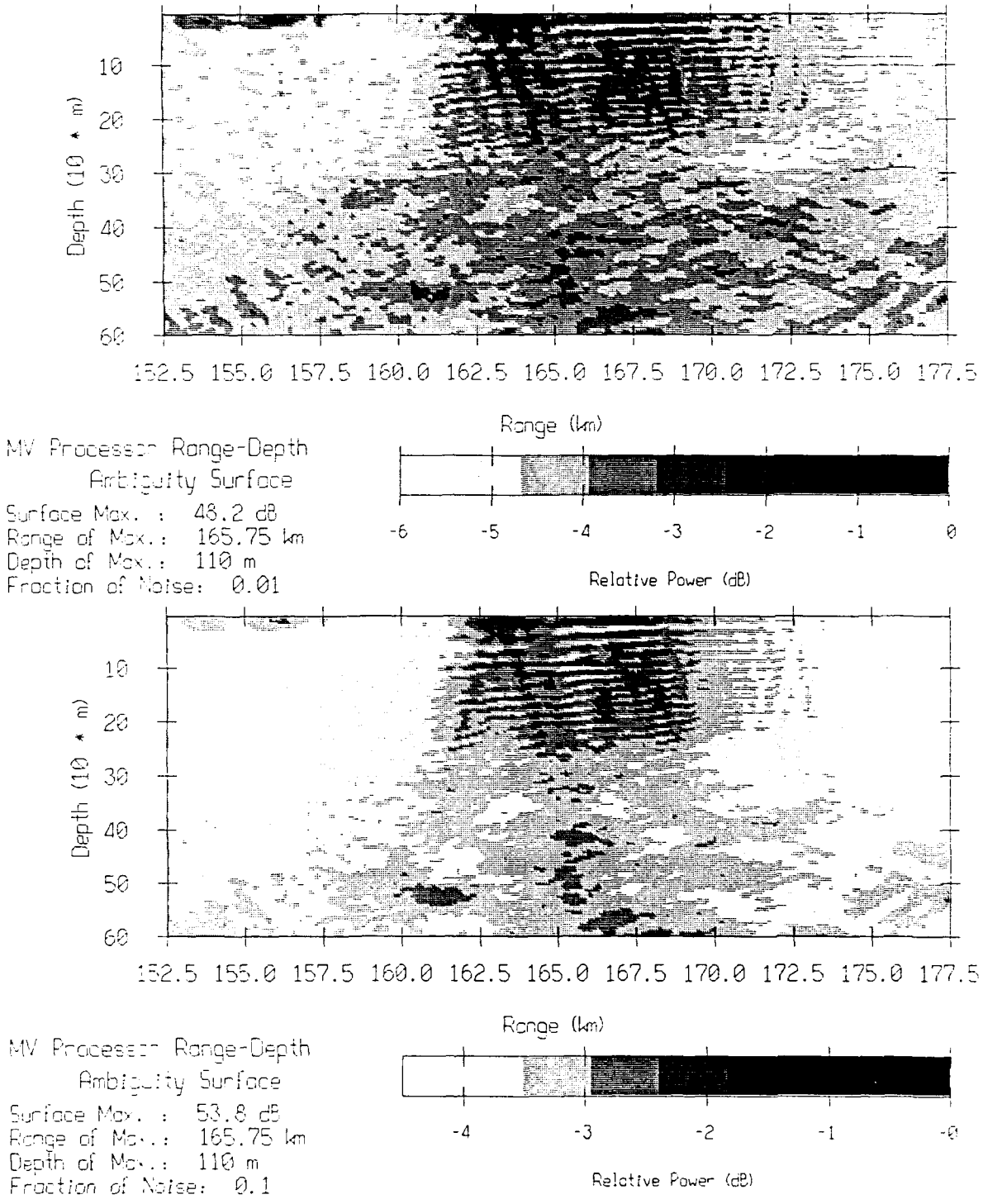

Figure 5: Matched field processing on the data of Tape 917, part 2.

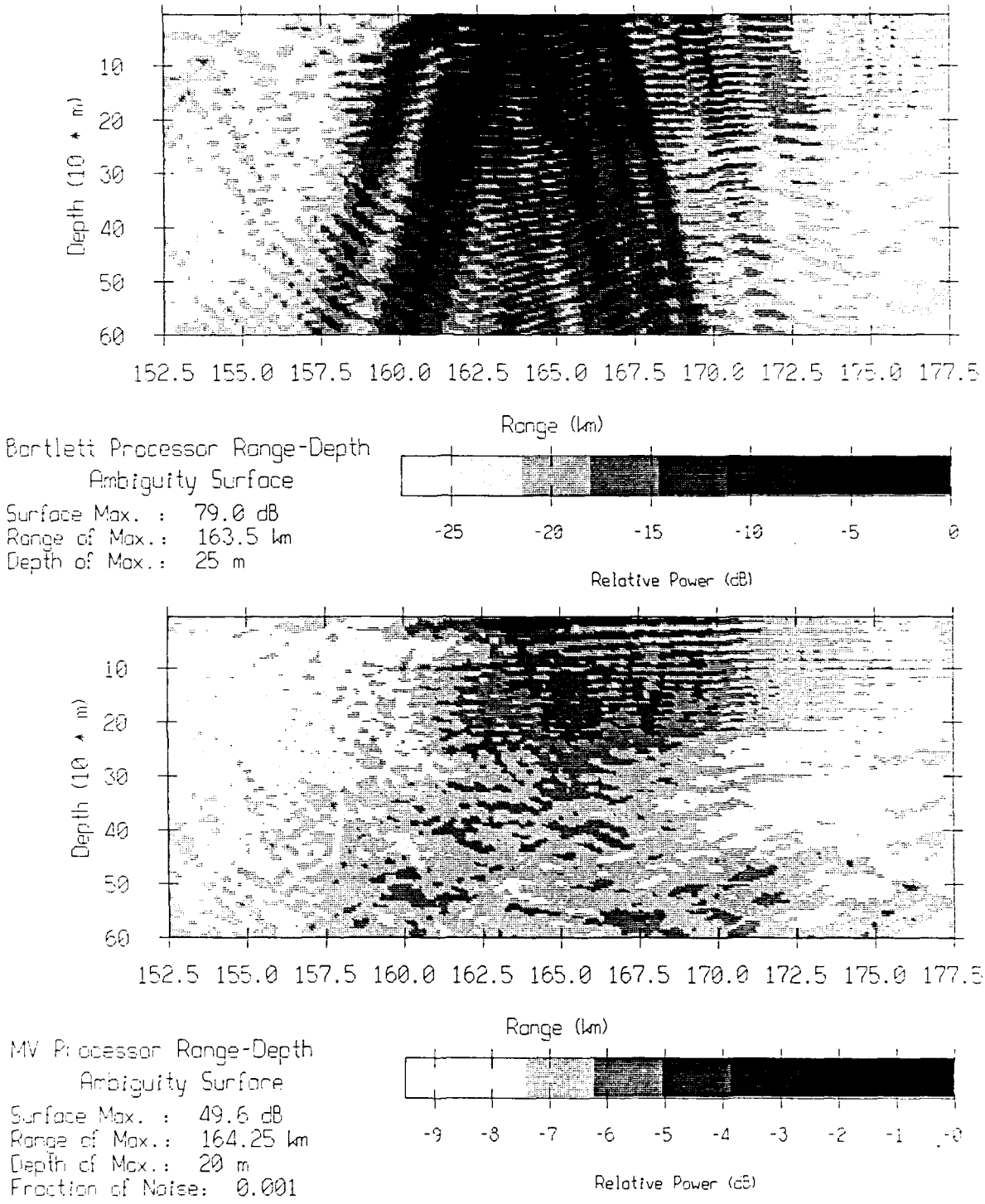

Figure 6: Matched field processing on the data of Tape 918, part 1.

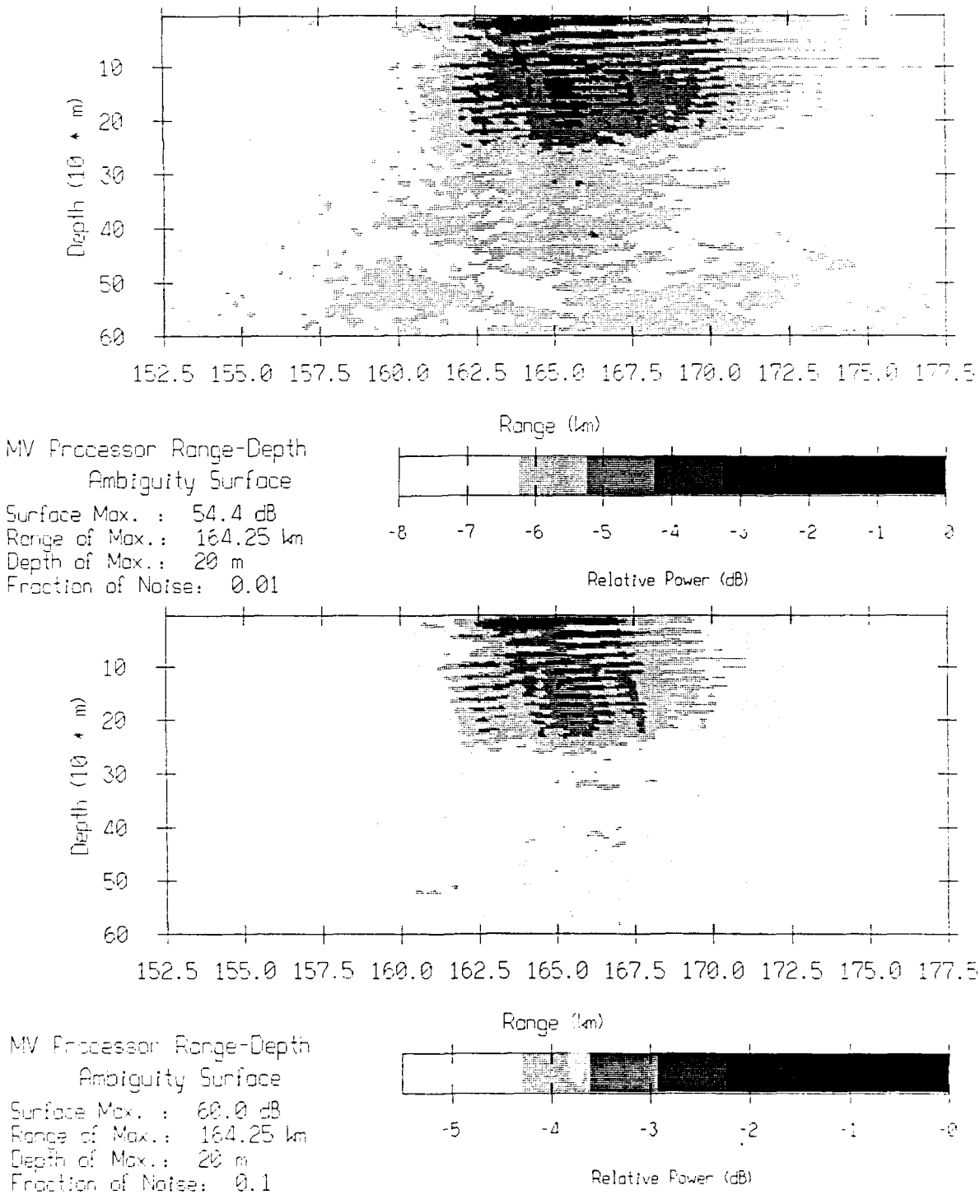

Figure 7: Matched field processing on the data of Tape 918, part 2.

3.4. Matched Field Processing Simulations

In an effort to understand the results of the matched field processing on the real data, simulation results are now presented in the case where there is no mismatch. Then, causes for mismatch are analyzed and simulations involving array tilt are performed.

3.4.1. No Mismatch Simulations

A perfect situation is now assumed where there is no noise and no mismatch (that is the replica vectors computed by the ATLAS model constitute the "truth"). A 200 Hz source is simulated at a range of 165 km and a depth of 300, 100 and 20 m. The ambiguity surfaces for the Bartlett processor and the three different implementations of the MV processor are computed and plotted in Figures 8 to 13.

Since there is no mismatch and no noise, the source is correctly localized in all cases and the dynamic range of the ambiguity surfaces is much larger than for the real data. It is on the order of 50 dB for the Bartlett processor and the MV processor with a stabilization factor γ of 10^{-3}, and on the order of 40 and 30 dB for the MV processor with stabilization factors equal to 10^{-2} and 10^{-1}. In the case of the real data, there is loss due to mismatch or an incorrect modeling of the wavefield. The Bartlett processor produces, in all these simulation cases, a large number of sidelobes. It exhibits the usual hat shape also observed in the real data ambiguity surfaces. The MV processor is a high resolution processor and produces a single peak in the range-depth cell of the simulated source. These simulation results for the MV processor are far apart from what is observed in the real data case. It is well known that the MV processor is very sensitive to mismatch and lacks robustness. These simulations indicates that the errors in the replica vectors are sufficient to dramatically perturb the MV results.

3.4.2. Analysis of the Mismatch

There are several potential causes for the large mismatch observed in the

matched field processing runs on the data. Although sound speed information at the R/P FLIP is very good, one does assume a range independent medium. This may not be accurate for large ranges on the order of 165 km. There is no available range dependent information to improve the processing. Since the experiment was conducted in deep water, the bottom should have only a weak influence in the processing results. Another cause for mismatch is the position errors of the array sensors. The VLA array was deployed in a three transponder network (long baseline) and one channel per array section was navigated during the experiment [Sotirin1989]. Navigation data are available for Tape 915 and 917. They are summarized in Figure 14 for Tape 915 and in Figure 15 for Tape 917. The array shapes are plotted in the North-South and East-West vertical planes. The navigation data indicate that the array behaves, in the first order, like a pendulum and that the largest horizontal displacement across the array aperture is bounded by 15 m. Such displacement corresponds to a 1° tilt. Since 15 m is equal to two wavelength at 200 Hz, array tilt is likely to have a major impact on the matched field processing results. It is investigated in the following.

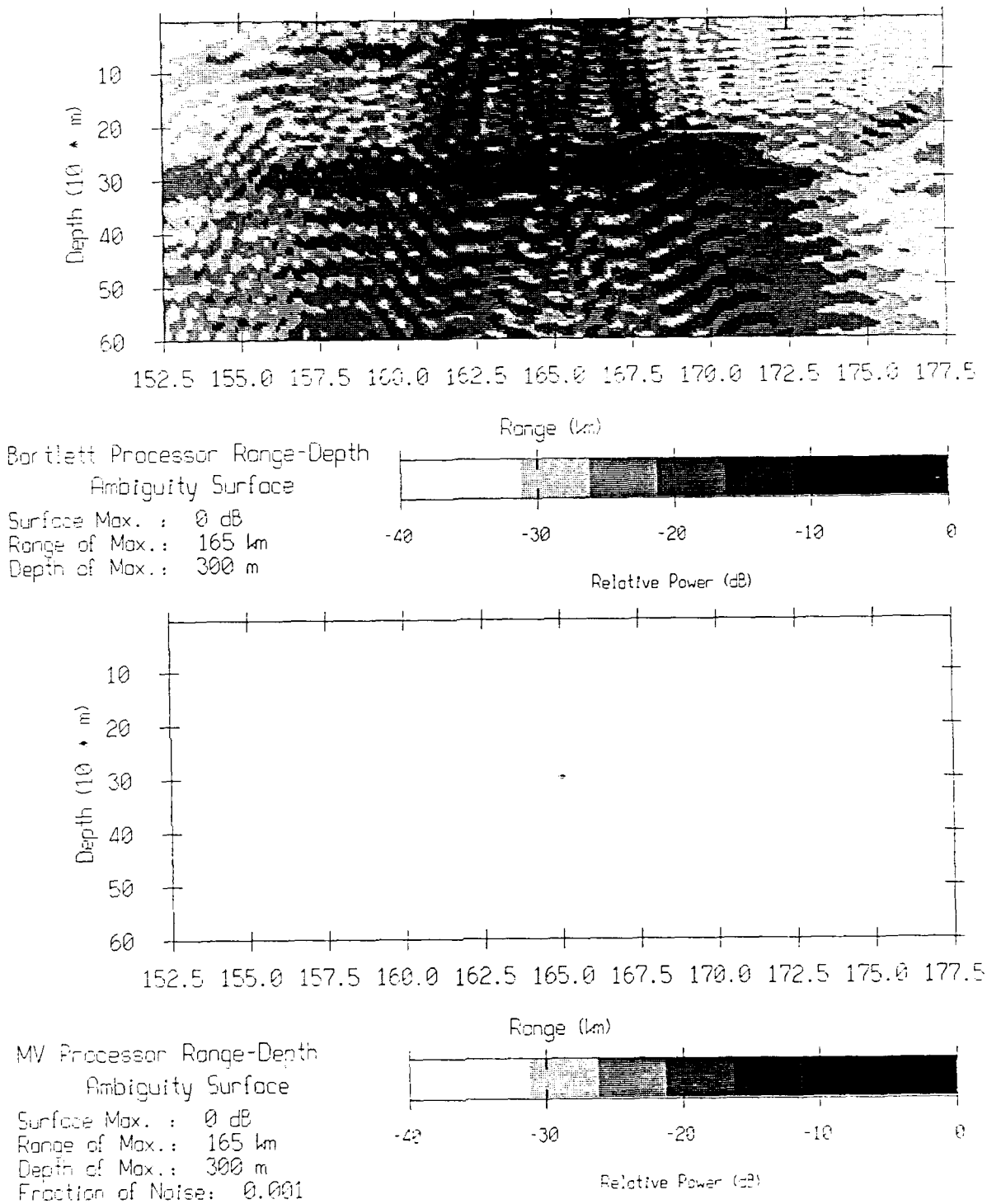

Figure 8: Matched field processing simulation (no noise, no mismatch) for a source depth of 300 m, part 1.

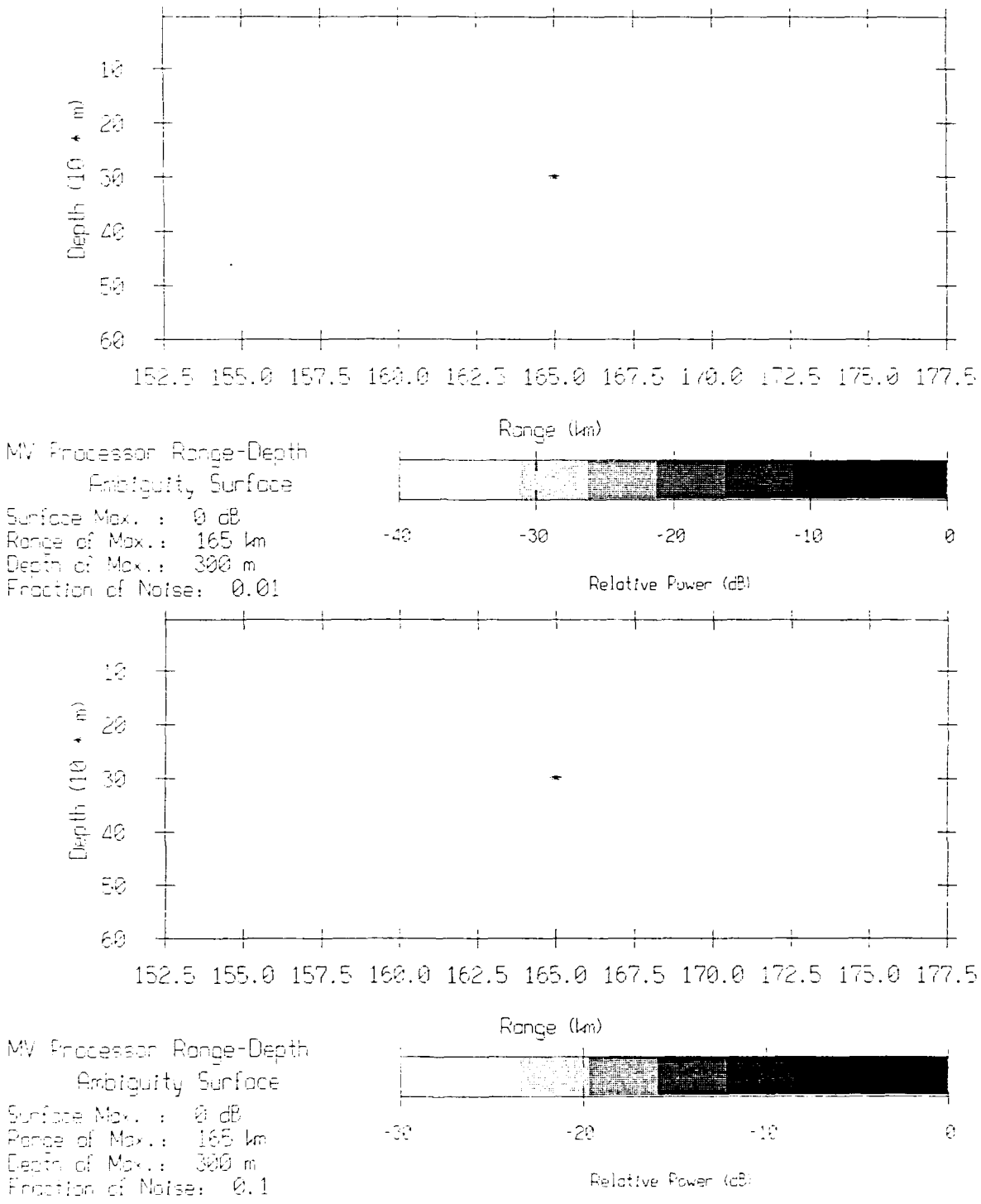

Figure 9: Matched field processing simulation (no noise, no mismatch) for a source depth of 300 m, part 2.

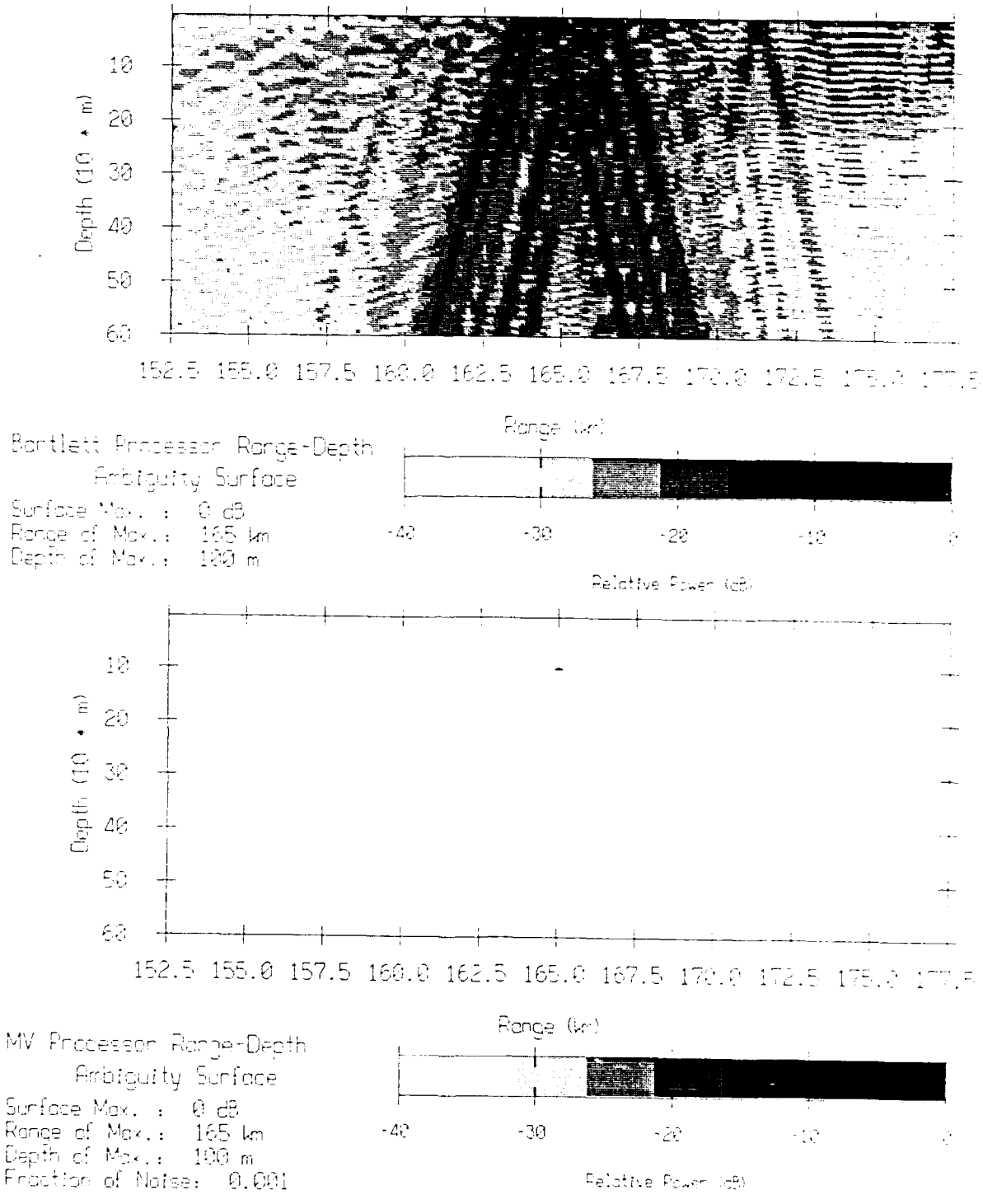

Figure 10: Matched field processing simulation (no noise, no mismatch) for a source depth of 100 m, part 1.

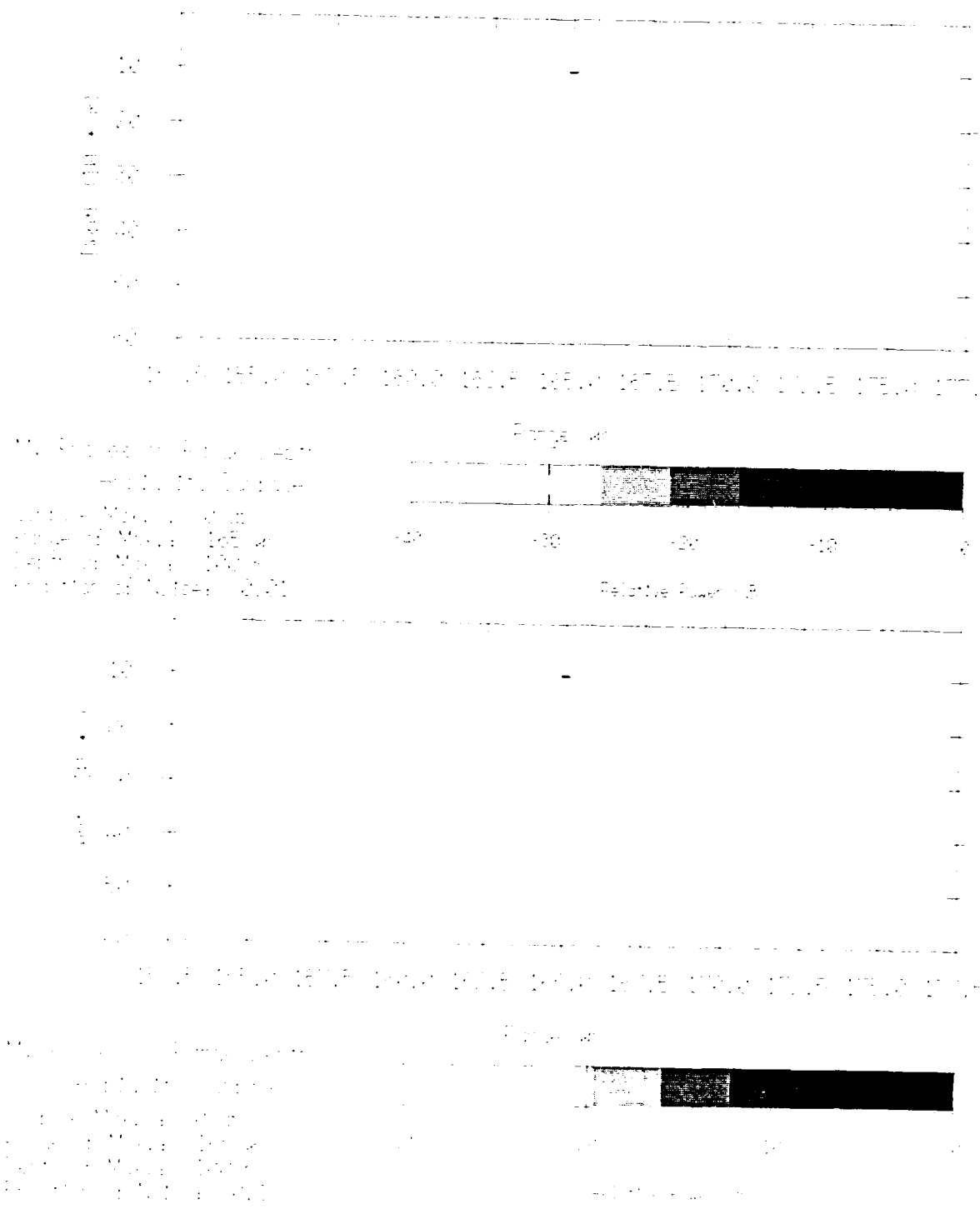

Figure 11: Matched field processing simulation (no noise, no mismatch) for a source depth of 100 m, part 2.

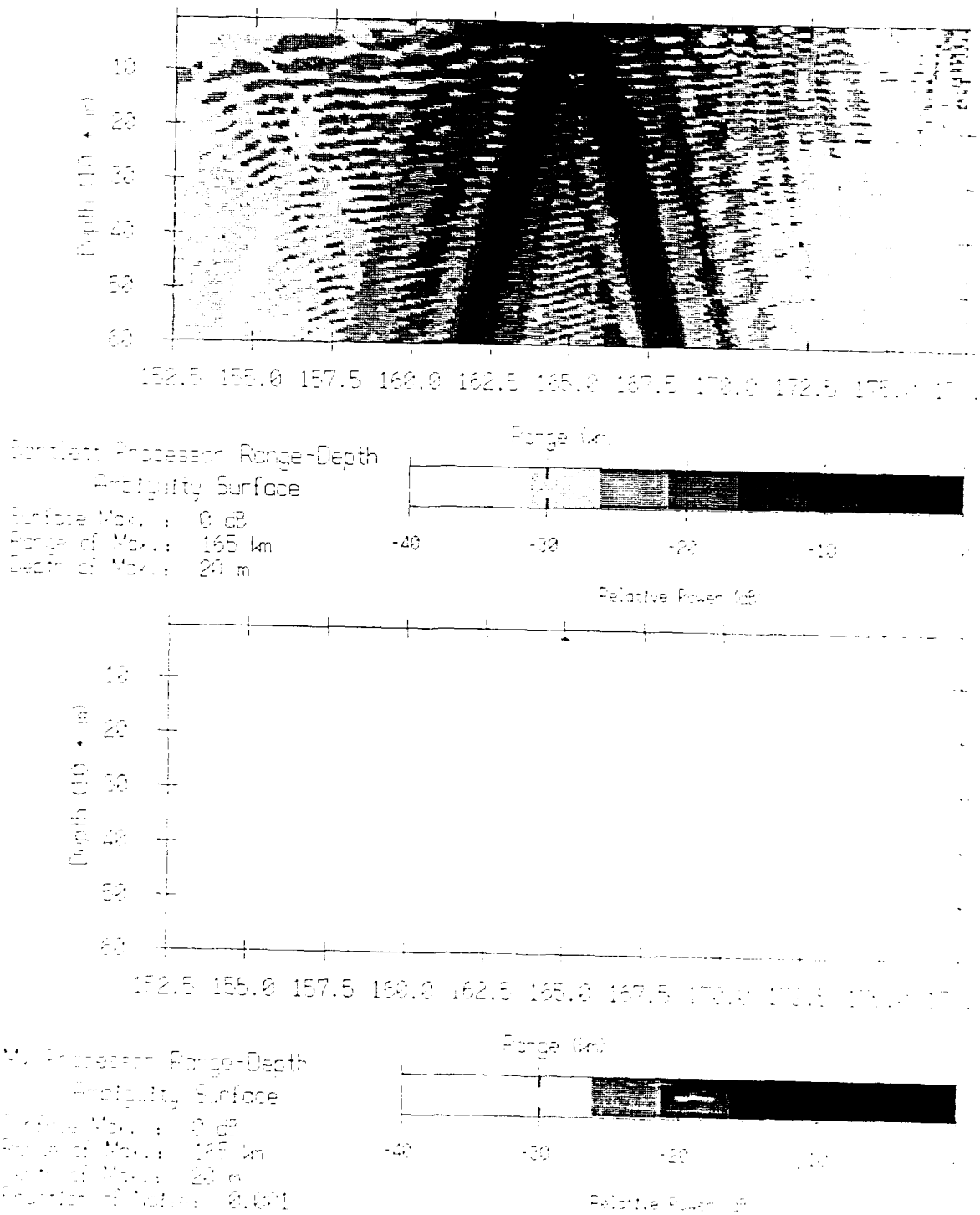

Figure 12: Matched field processing simulation (no noise, no mismatch) for a source depth of 20 m, part 1.

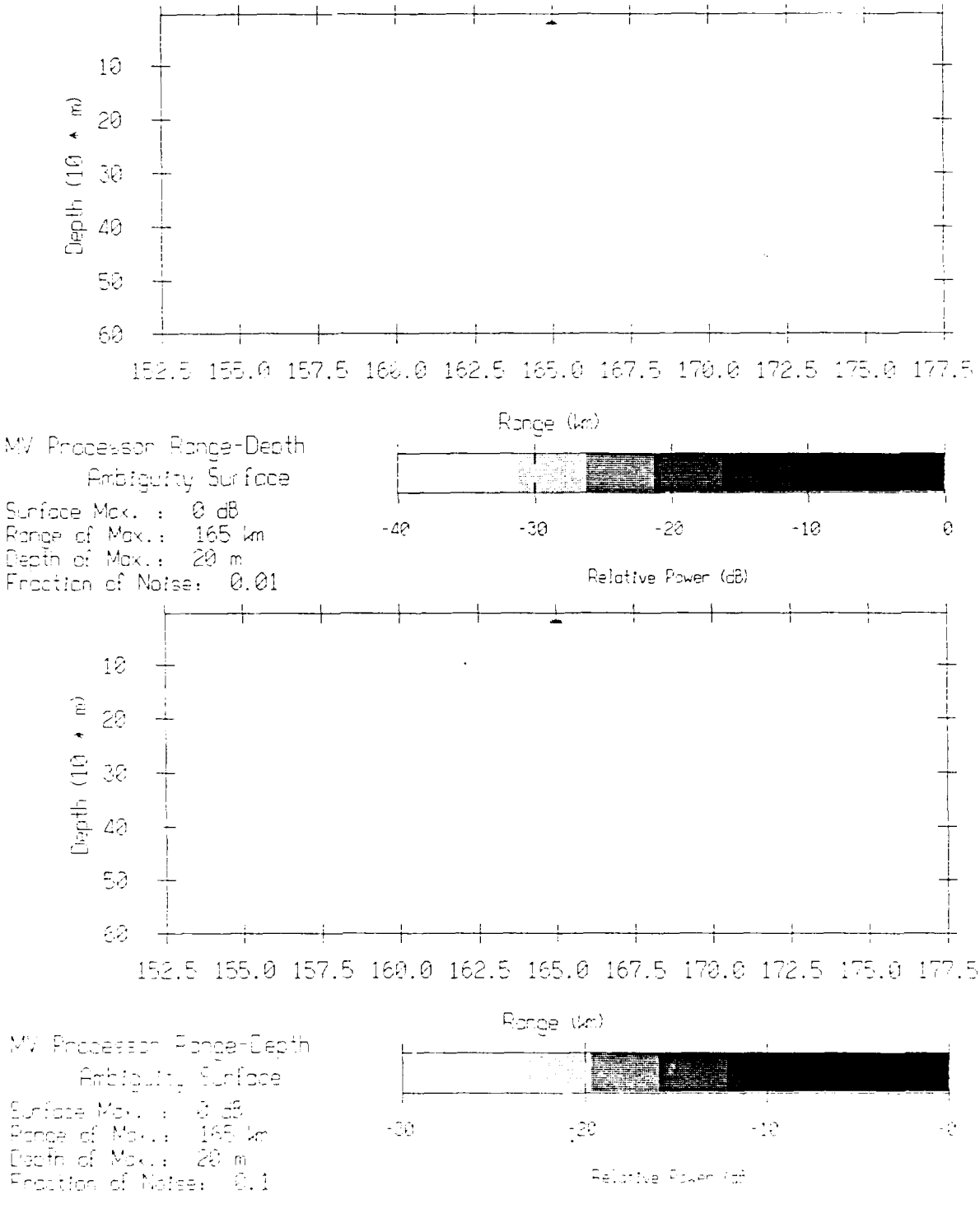

Figure 13: Matched field processing simulation (no noise, no mismatch) for a source depth of 20 m, part 2.

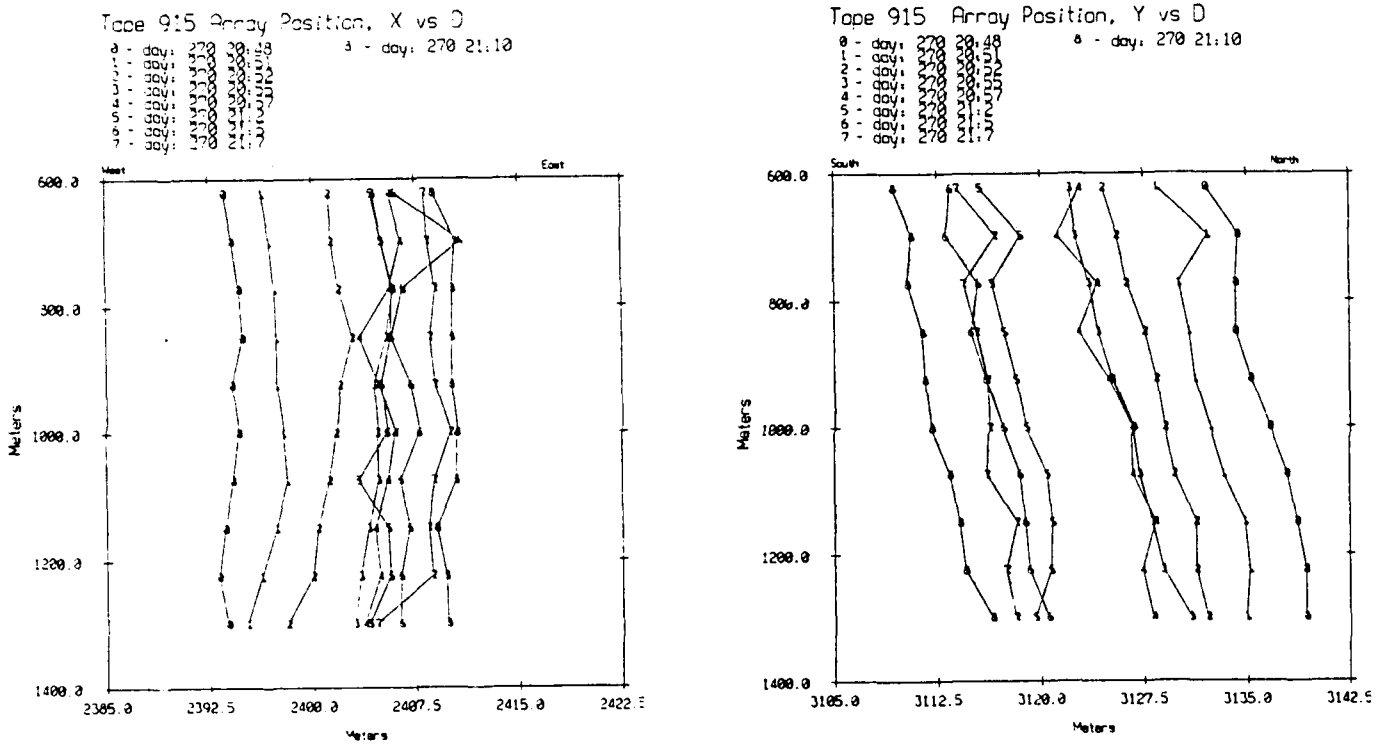

Figure 14: Array navigation for Tape 915.

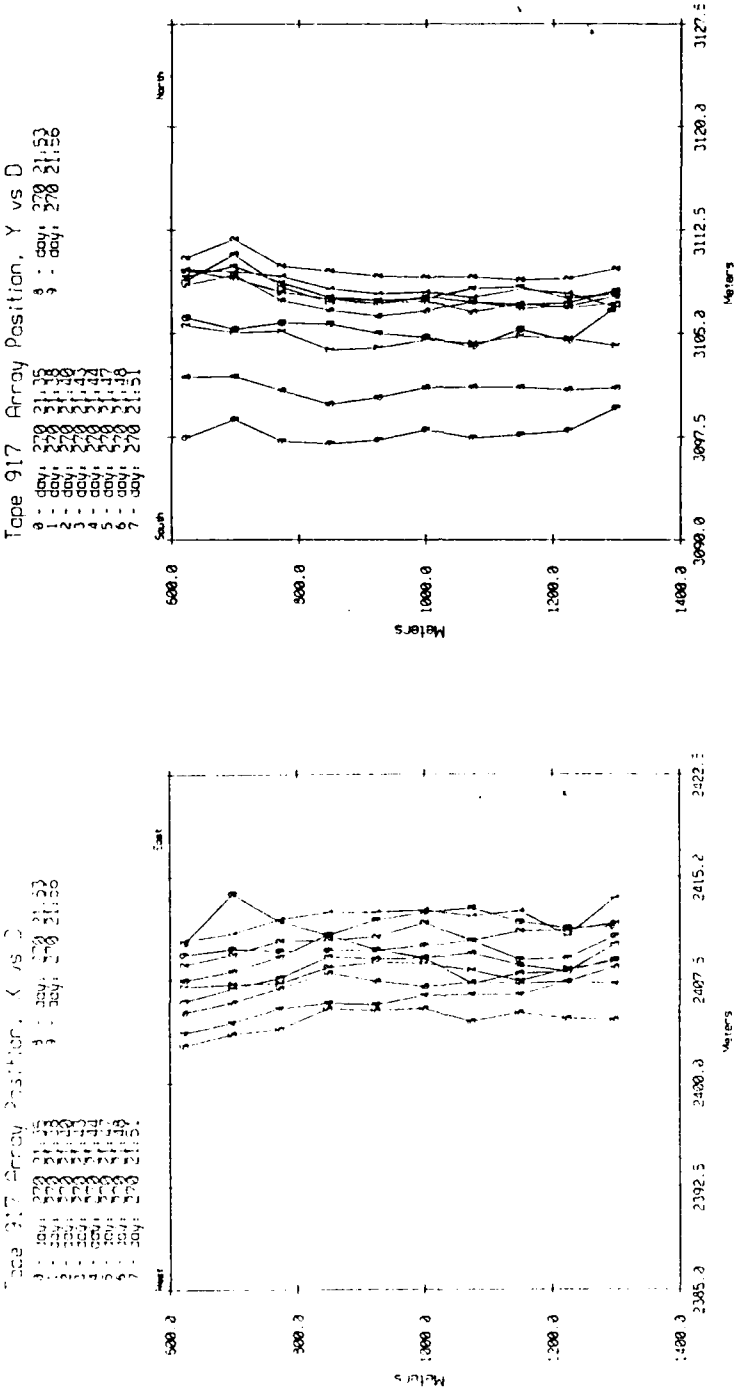

Figure 15: Array navigation for Tape 917.

3.4.3. Tilted Array Simulation

A tilted vertical line array is simulated with a horizontal displacement of 15 m. The source is assumed at 165 km from the array top element and at a depth of 300, 100 and then 20 m. The tilted array simulation geometry is summarized in Figure 16. The replica vectors, which were used earlier, assume a straight line vertical array, thus the impact of mismatch due to array tilt is assessed.

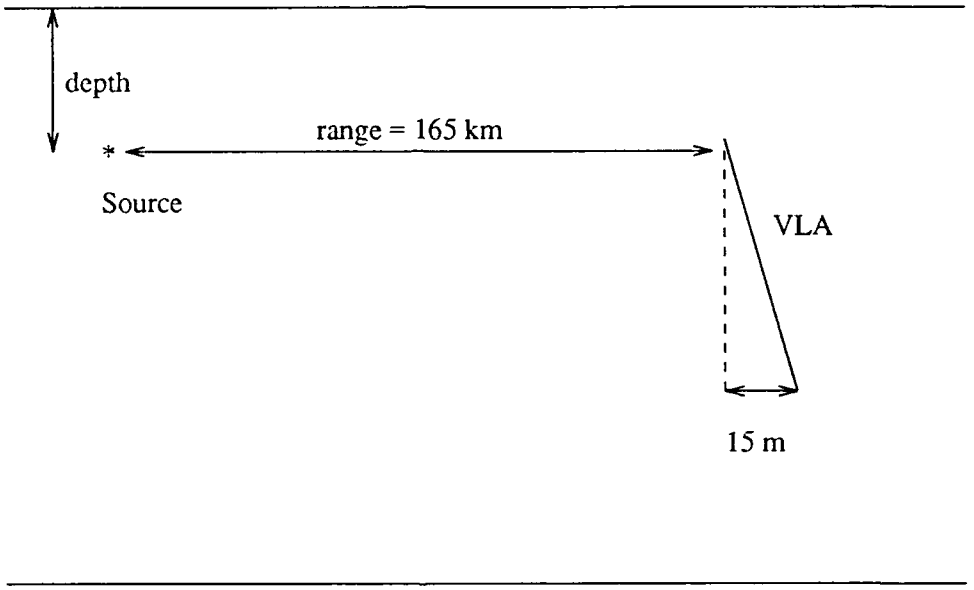

Figure 16: Tilted array simulation

The ambiguity surfaces for a tilted array are plotted in Figure 17 and 18 for a source at 300 m, in Figure 19 and 20 for a source at 100 m, and in Figure 21 and 22 for a source at 20 m. The matched field processing results are summarized in Table 4. Array tilt results in mismatch which significantly reduces the maximum peak power and shifts the position of the peak in range and depth (the probable position of the source). The mismatch also reduces the dynamic range of the ambiguity surfaces to a few dB for the

MV processors. The estimated position of the source is off in range by 4 to 7 km from the true position of the source. The 300 m deep source is localized at a depth of 450 m while the 100 m deep source is localized at a depth of 15 m. These simulated ambiguity surfaces, although they share some similarities with the real data ambiguity surfaces, correspond to a worst case situation where array tilt is maximum. These simulated results indicate that array tilt can be held reponsible for the large mismatch observed in the real data ambiguity surfaces.

Source Depth		Processor			
		Bartlett	MV $\gamma = 10^{-3}$	MV $\gamma = 10^{-2}$	MV $\gamma = 10^{-1}$
Source at 300 m	Depth of Max.	450 m	450 m	450 m	450 m
	Range of Max.	171.75 km	171.75 km	171.75 km	171.75 kmm
	Surface Max.	-8.3 dB	-50 dB	-40 dB	-30 dB
	Dynamic Range	40 dB	0.7 dB	0.7 dB	0.7 dB
	Figure	17	17	18	18
Source at 100 m	Depth of Max.	15 m	15 m	15 m	15 m
	Range of Max.	161 km	161 km	161 km	161 km
	Surface Max.	-4.5 dB	-48.9 dB	-38.9 dB	-28.9 dB
	Dynamic Range	50 dB	1.75 dB	1.75 dB	1.75 dB
	Figure	19	19	20	20
Source at 20 m	Depth of Max.	15 m	15 m	15 m	15 m
	Range of Max.	160.75 km	161 km	161 km	161 km
	Surface Max.	-8.7 dB	-49.8 dB	-39.8 dB	-29.8 dB
	Dynamic Range	50 dB	1 dB	1 dB	1 dB
	Figure	21	21	22	22

Table 4: Tilted array matched field processing simulation

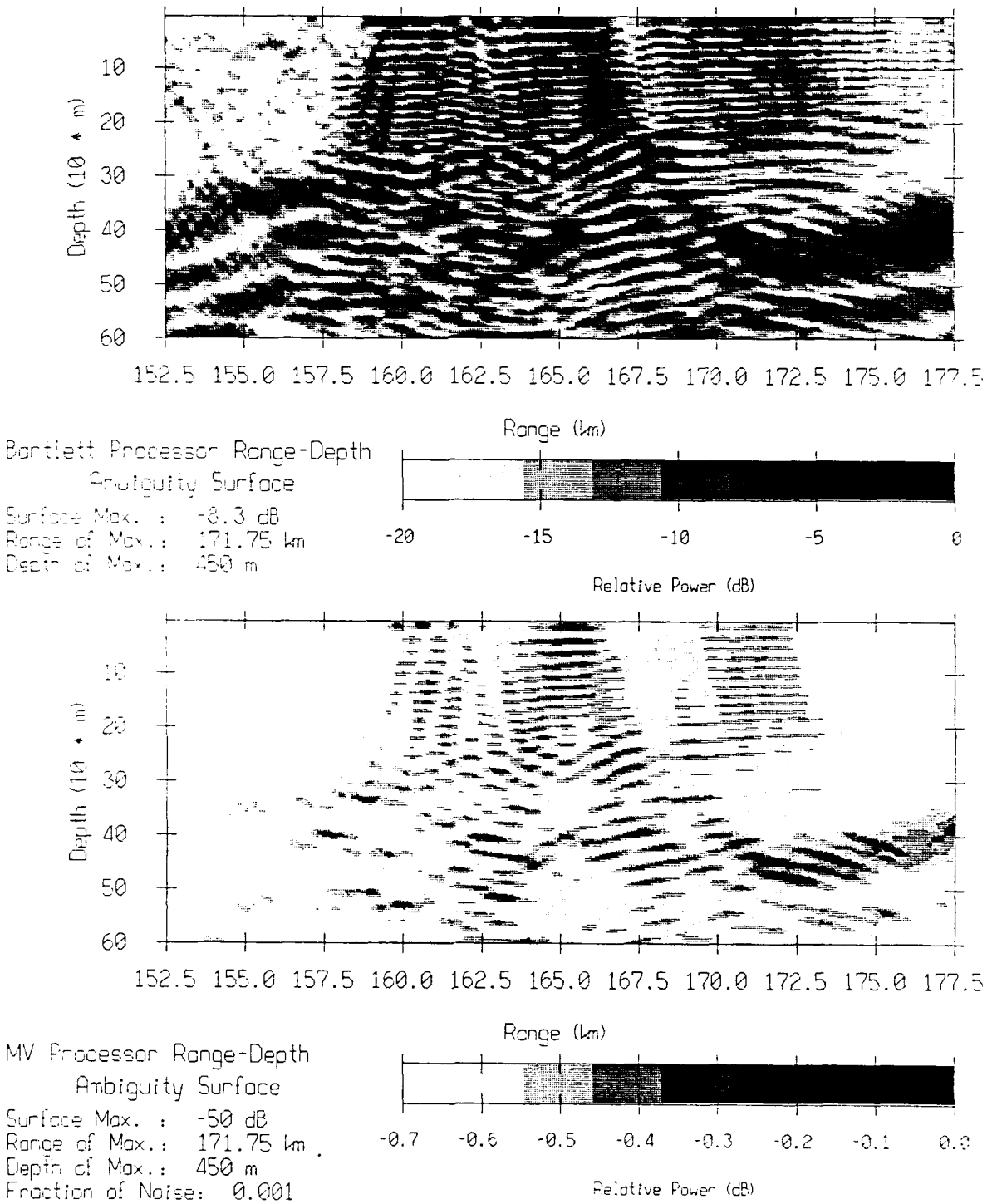

Figure 17: Matched field processing simulation for a tilted array and a source 300 m depth, part 1.

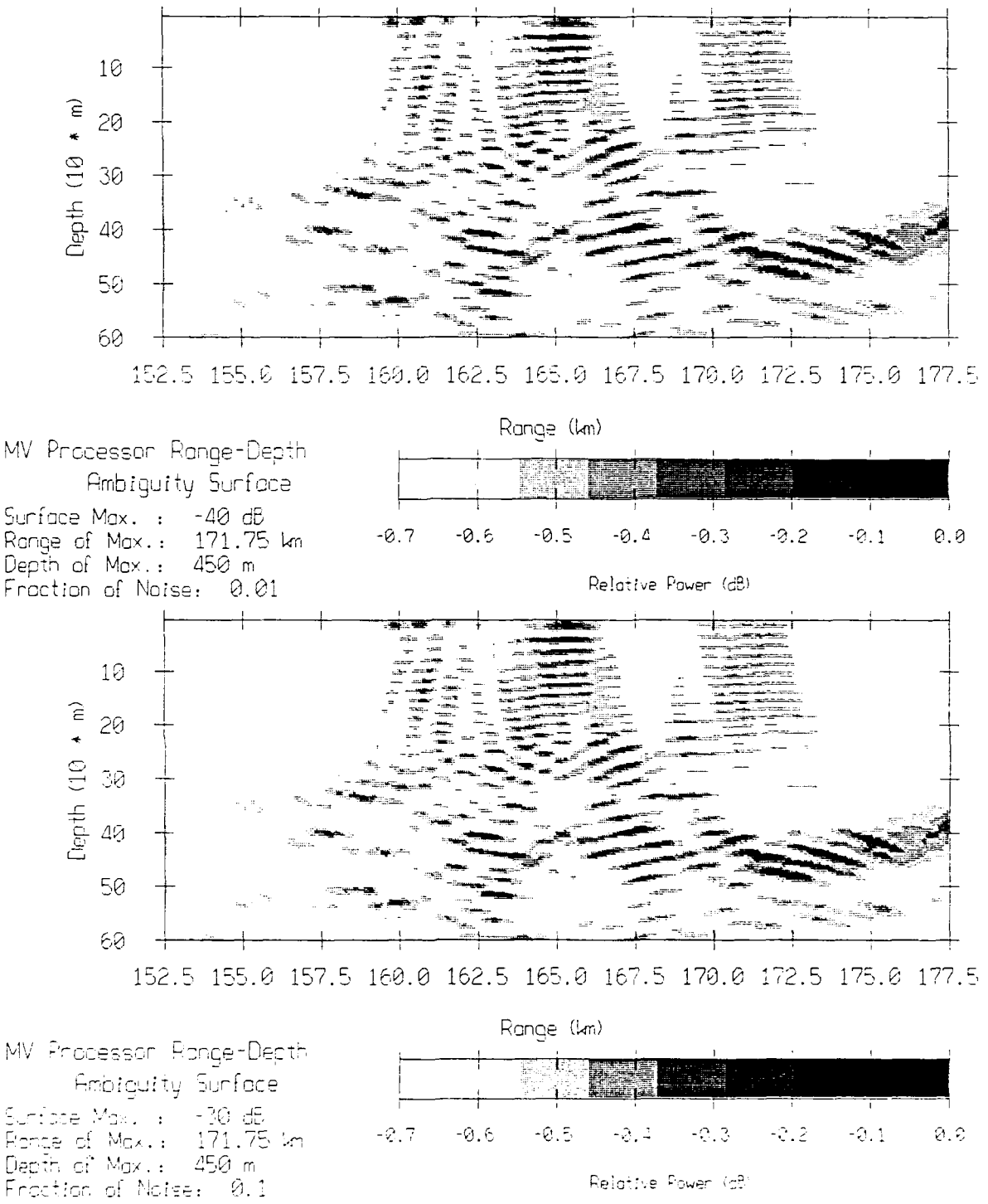

Figure 18: Matched field processing simulation for a tilted array and a source 300 m depth, part 2.

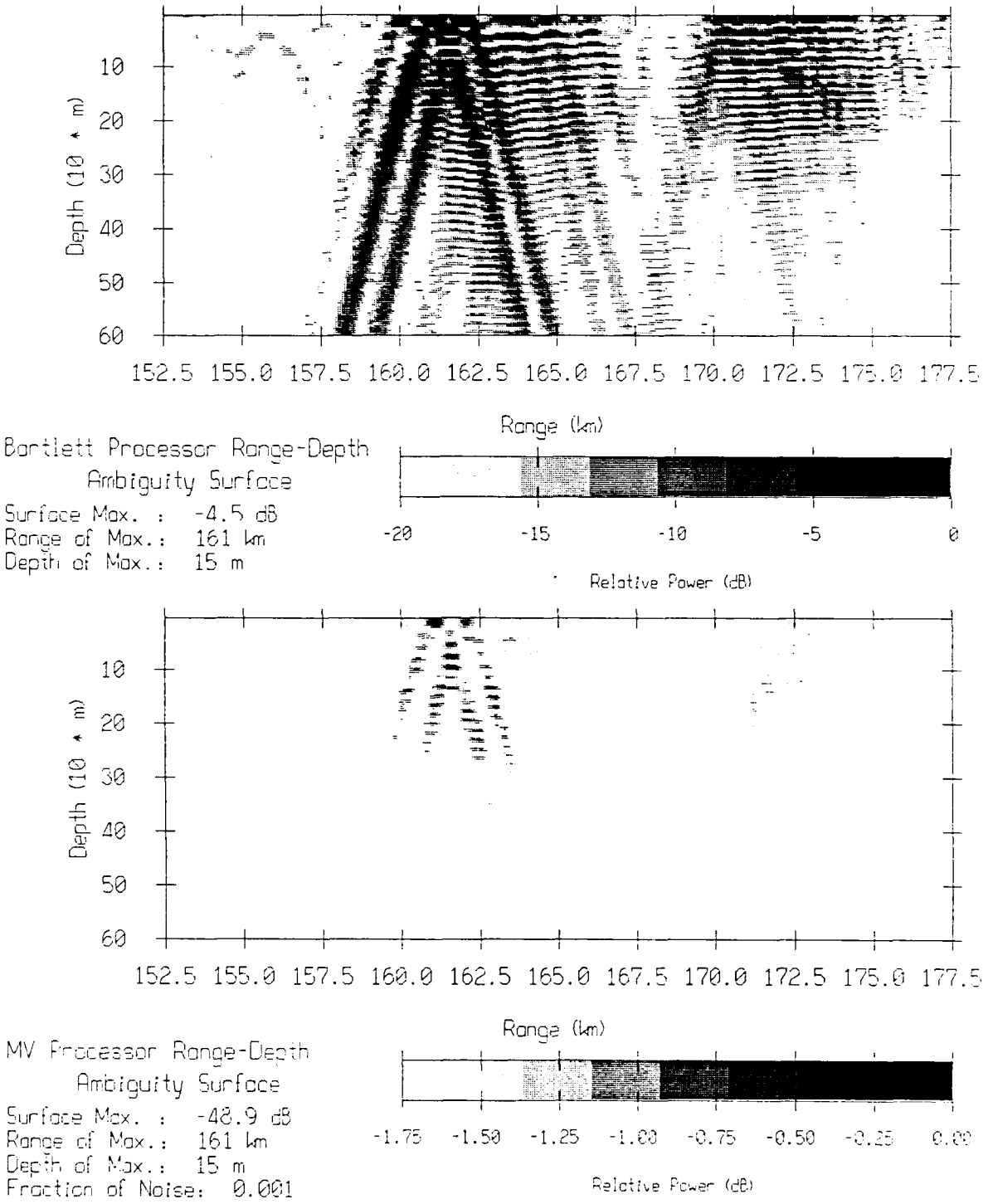

Figure 19: Matched field processing simulation for a tilted array and a source 100 m depth, part 1.

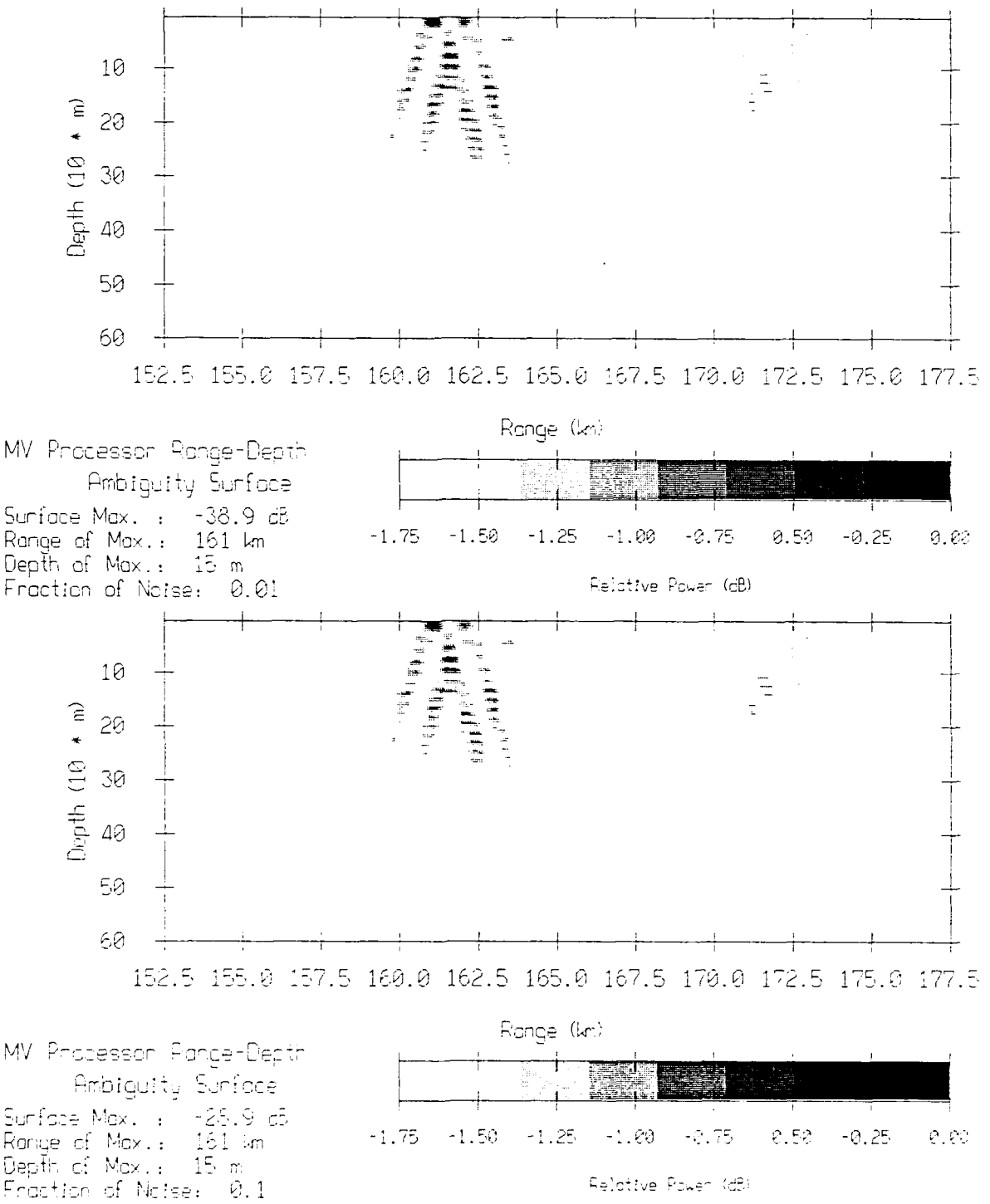

Figure 20: Matched field processing simulation for a tilted array and a source 100 m depth, part 2.

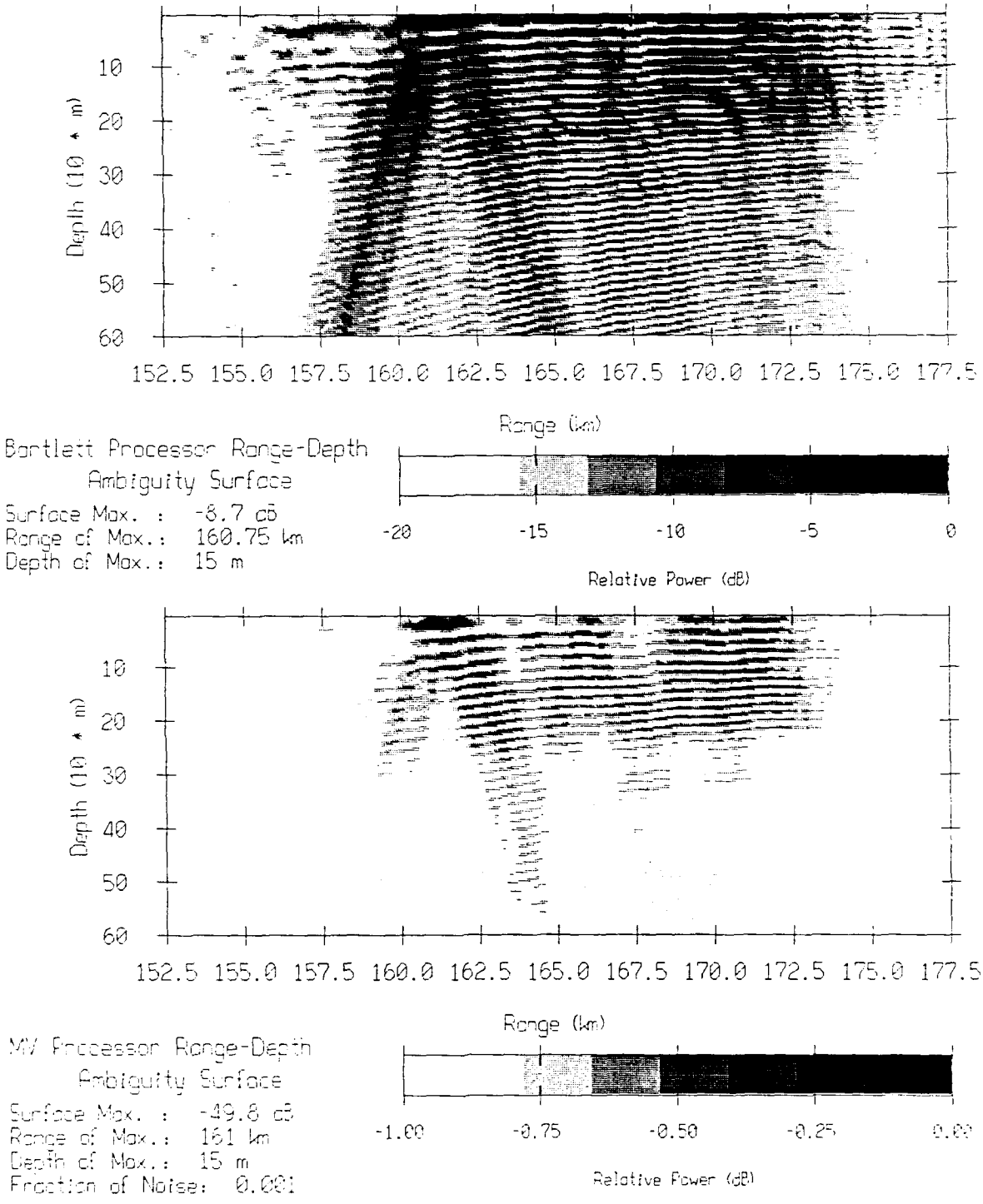

Figure 21: Matched field processing simulation for a tilted array and a source 20 m depth, part 1.

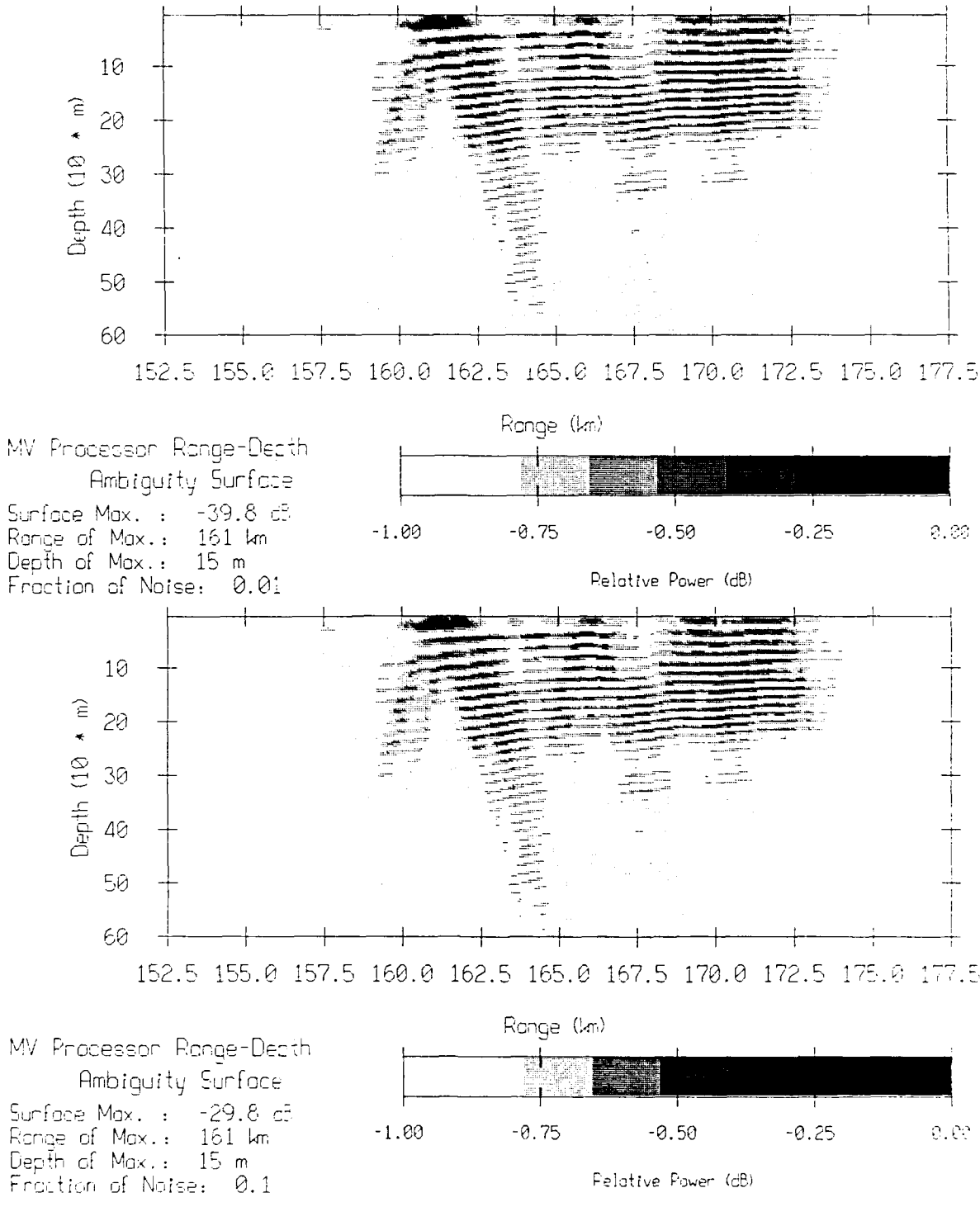

Figure 22: Matched field processing simulation for a tilted array and a source 20 m depth, part 2.

4. Source Tow Matched Field Processing

4.1. Introduction

On Julian Day 272, the USNS NARRAGANSETT began a source tow for 10 hours, starting at 00:00 GMT. The HX90 source was towed at a nominal speed of 5 kts with 300 m of wire out (the probable source depth is 100 m), and was projecting a 200 Hz CW tone. The ship was tracked by radar from the R/P FLIP during the first five hours of the transmission. Data were recorded continuously on 25 tapes from Tape 966 to 990 (each tape corresponds to 23 minutes and 28 seconds). The swell heights recorded at the R/P FLIP were just below 5 feet and wind speeds were between 10 and 15 kts. An XBT cast was taken on the R/P FLIP during the source tow.

4.2. Source Tow Modeling

4.2.1. Sound Speed Profile

The data from the XBT cast collected on the R/P FLIP at 03:00 GMT were utilized with the state equation of [Mackenzie1981] to produce the sound speed profile plotted in Figure 23. The environment at the R/P FLIP is one of a double duct with a large and well defined surface duct in the upper hundred meters. The estimated depth of the towed source is 100 m, right at the boundary of the two waveguides. Therefore, this situation may be difficult to model. The sound speed profile across the water column is synthesized by using a desampled version of the 750 m XBT sound speed profile and by blending it in a desampled version of the deep CTD at the R/P FLIP (the one used in the fixed station modeling). The desampled XBT sound speed profile in the top 750 m and the synthetic sound speed across the whole water column are also plotted in Figure 23.

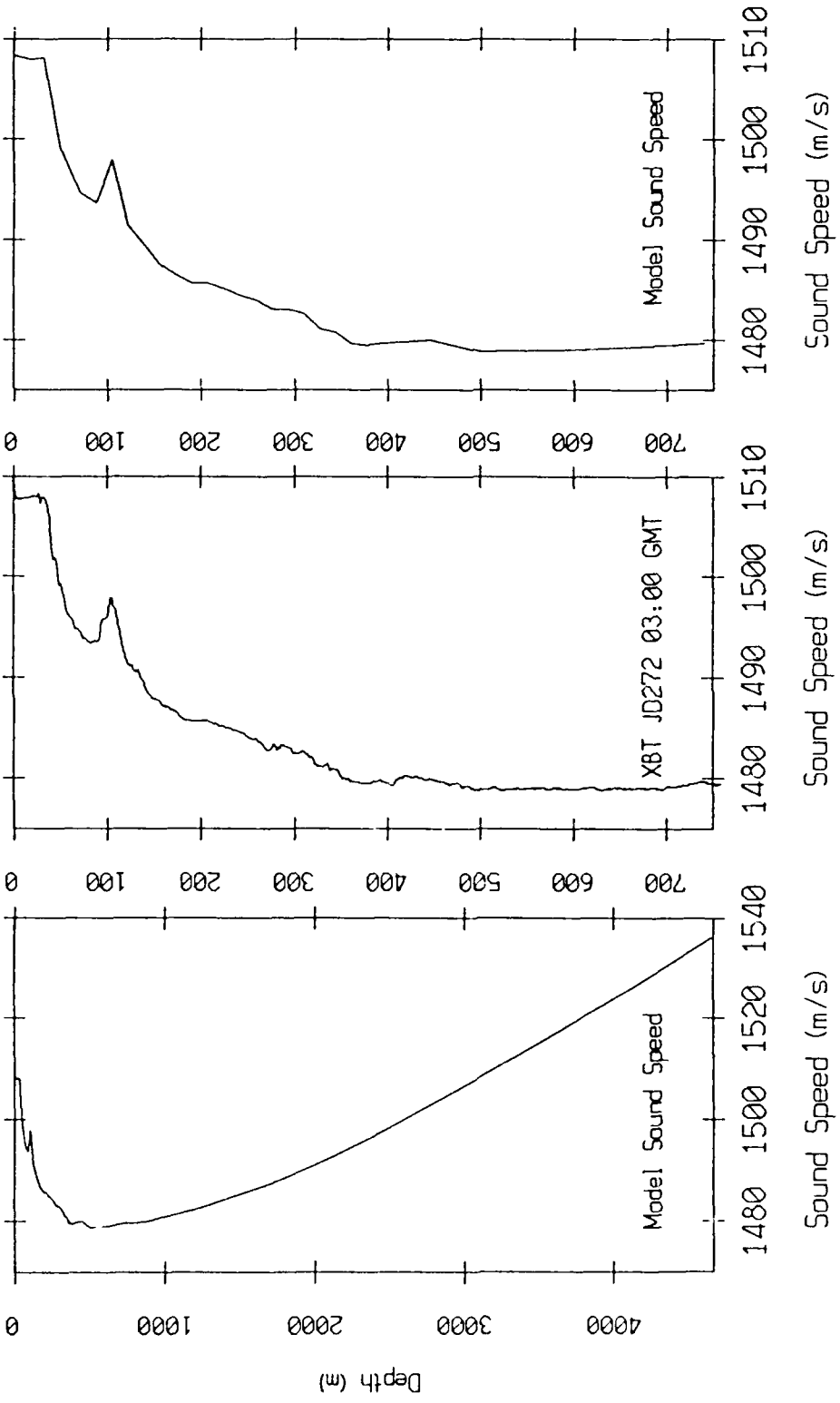

Figure 23: Source tow sound speed profile.

4.2.2. Modeling with ATLAS

As in the case of the fixed station, the ATLAS normal mode model is used to produce the replica vectors for the source tow matched field processing runs. The environmental parameters are similar to the fixed station modeling ones, excepth the sound speed profile. A range independent medium is assumed and a bottom loss table corresponding to a GSM Bottom Province Type 3 is used (Table 1). The ATLAS model predicts the first convergence zone at about 50 km. A fair agreement was found between the arrival structure predicted by the ATLAS model for a source depth of 100 m and the beamformed data [Tran1989].

4.3. Selection of the Matched Field Processing Stations

4.3.1. USNS NARRAGANSETT Tracking

The source tow began at 00:00 GMT on Julian Day 272. During the first four hours and fourty five minutes, the USNS NARRAGANSETT was tracked by the R/P FLIP radar. The tracking information is summarized in Figure 24. The range of the ship as a function of time is derived from the radar tracking information and plotted in Figure 25. The dotted line in Figure 25 allows the interpolation of the ship range after the end of the radar tracking.

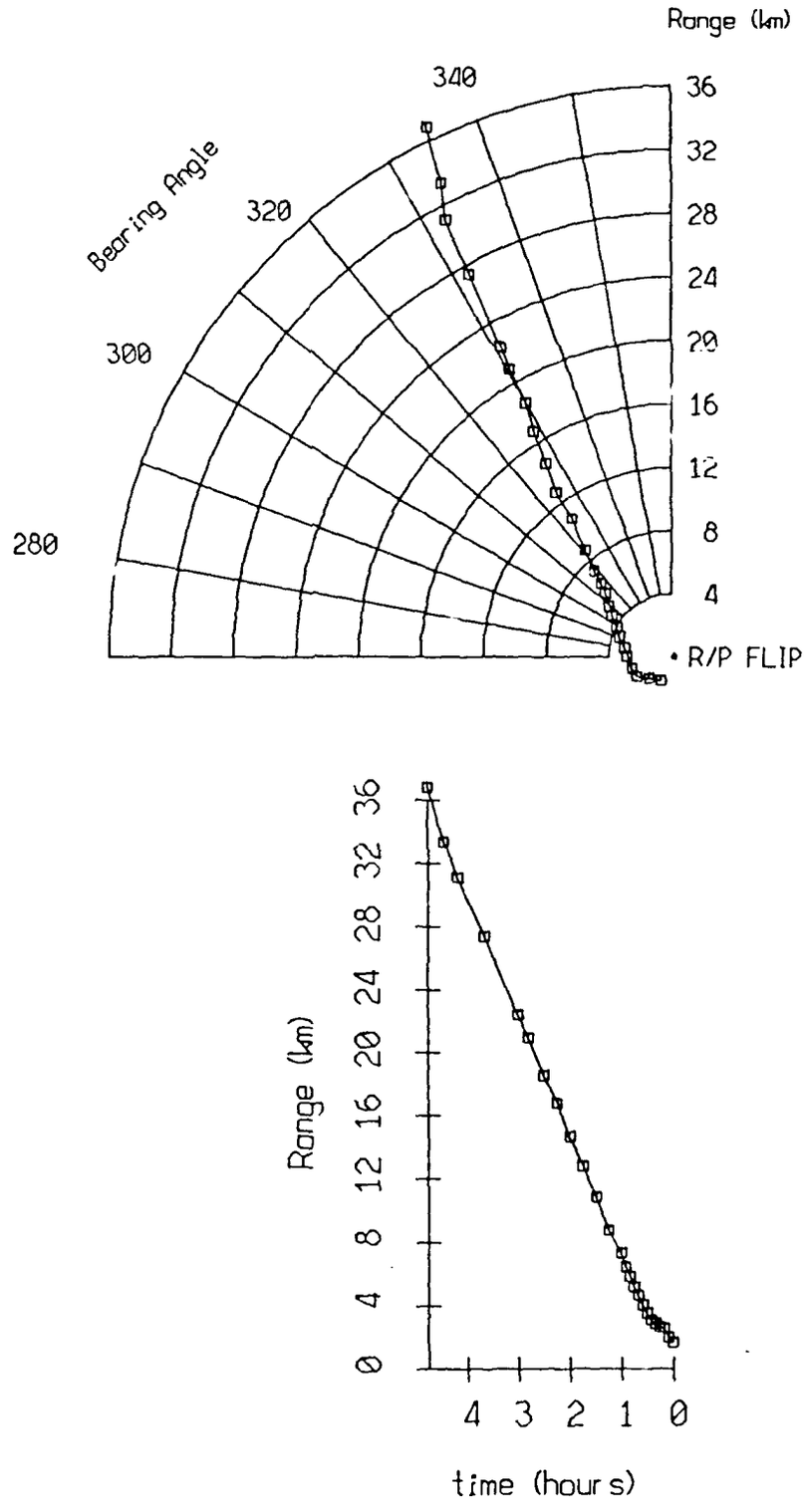

Figure 24: Radar tracking information.

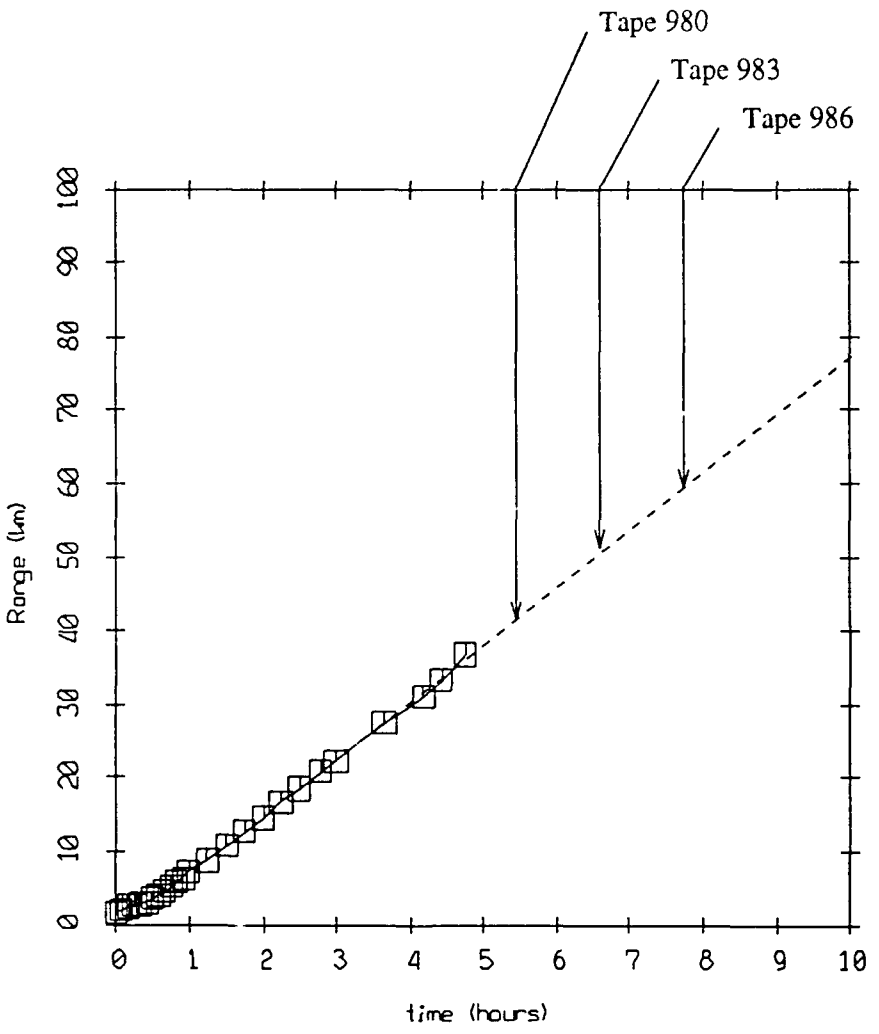

Figure 25: Ship range as a function of time

4.3.2. Selection of the Stations

Four stations are processed using the matched field processing techniques. They are chosen to be the beginning of the first convergence zone, the middle of the first convergence zone, the trailing edge of the first convergence zone, and the beginning of shadow zone following the first convergence zone. The stations are such that there is a 10 km range increment from Station #1 to Station #3, and from Station #3 to Station #4, and

a 5 km increment from Station #1 to Station #2, and from Station #2 to Station #3. Table 5 summarizes the time at which the 4 minutes and 22 seconds long data segment begins for each station. The GMT start time of the data segment allows the estimation of the source range with respect to the VLA.

Station	Tape #	GMT Data Segment Time	Expected Range (km)
1	980	05:33:32	40 to 45
2	981	06:10:06	45 to 50
3	983	06:48:17	50 to 55
4	986	07:51:12	60 to 65

Table 5: Source tow station information

4.4. Doppler Shift

The source is moving away from the VLA receivers at a nominal speed of 5 kts. The VLA array is essentially fixed since deployed from the R/P FLIP in a three point moor. The Doppler shifted received frequency f_r is given by [Camp1970, p 216]

$$f_r = f_t \frac{c}{c+v} \tag{4.1}$$

where f_t the transmitted frequency (i.e. 200 Hz), c the sound speed and v the tow ship speed. Assuming a constant sound speed of 1500 m/s and a tow speed of 5 kts, the received frequency is 199.657 Hz. It is different from 200 Hz by 1.4 times the bin width of the Fourier analysis performed, where the bin width is 0.244 Hz (a 2048-point FFT is used for a -250 Hz to 250 Hz frequency band). The 200 Hz signals from the towed source is strongest in bin 1843.

Another issue is the differential Doppler shift that the different arrivals can experience. If the arrivals have a relative Doppler shift greater than the FFT binwidth, matched field processing will fail to coherently recombine the multipaths. The differential Doppler shift is easily obtained from Equation 4.1 by assuming that the source project sound with a given take-off angle θ with respect to the horizontal, while the source

has only a horizontal displacement. While there is no Doppler shift for sound propagating vertically ($\theta = 90^o$), the Doppler shift is maximal for horizontally propagating sound ($\theta = 0^o$). If v denotes the ship horizontal speed, θ the take-off angle of the sound at the source, the Doppler shift is given by

$$\Delta f = \frac{\cos\theta}{\cos\theta + \frac{v}{c}} \tag{4.2}$$

v is replaced in Equation 4.1 by its projection on the direction θ (that is by $v\cos\theta$) to produce Equation 4.2. The Doppler shift as a function of take-off angle is plotted in Figure 26. The Differential shift is within half the 0.244 Hz binwidth for all practical take-off angles θ (i.e. such that $\theta \leq 70^o$).

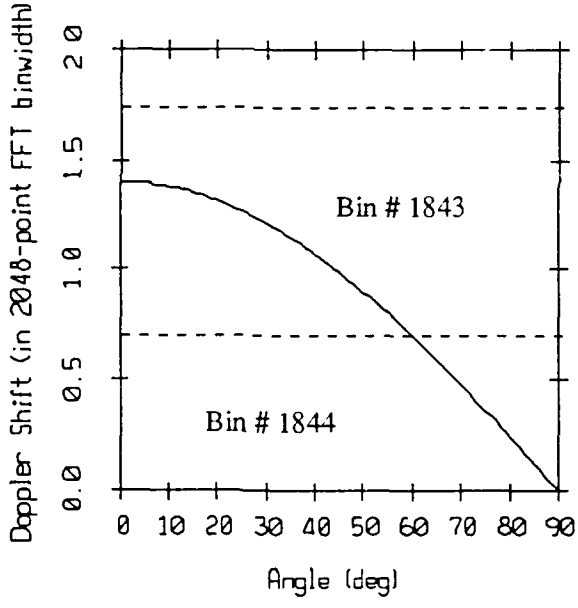

Figure 26: Doppler shift as a function of take-off angle

The Doppler shift is neglected in this study and the effects due to frequency variations are not considered in the calculation of the replica vectors. The range variations of the source are not considered either. This simple approach is justified in the following.

The pressure field computed by the ATLAS normal mode model can be written as [Gordon1984, p 4]

$$p = \sum_{m=1}^{m} \frac{1}{N_m} \left[\frac{2\pi}{k_m r} \right]^{1/2} U_m(z_s)\, U_m(z)\, e^{i \kappa_m r} \tag{4.3}$$

where N_m is a generalized normalization factor, U_m the m^{th} mode eigenfunction, z the depth of the receiver, z_s the depth of the source, κ_m the horizontal wavenumber of the m^{th} mode and r the horizontal range from the source to the receiver. The contribution of the m^{th} mode has a phase given by $\kappa_m r$ The normalized modal eigenfunctions are gray-level displayed in Figure 27 for the whole water column and in Figure 28 for the top 500 m. A 100 m deep source excite a group of modes around mode number 71 and the m^{th} mode discussed in the following can be assumed to belong to this group of excited modes. For a moving source, the phase of the m^{th} mode can be expressed as

$$\Phi = (\kappa_m + d\kappa_m)\,(r + dr) \tag{4.4}$$

where dr is the distance over which the source moves and $d\kappa_m$ the error in wavenumber due to a slight Doppler frequency shift. The phase errors when using $k_m r$ can be evaluated by keeping only the first order terms

$$\Phi - \kappa_m r \approx \kappa_m\, dr + d\kappa_m\, r \tag{4.5a}$$

$$\Delta\Phi = \kappa_m\, r \left(\frac{dr}{r} + \frac{d\kappa_m}{\kappa_m} \right) \tag{4.5b}$$

$$\frac{\Delta\Phi}{\Phi} \approx \frac{dr}{r} + \frac{d\kappa_m}{\kappa_m} \tag{4.5c}$$

Since the source moves over 750 m over the time necessary to estimate the array covariance matrix between 40 and 60 km, the relative error due to source motion in range is at most on the order of 1.9 %.

The relative phase error due to wavenumber variations is shown negligible in the following. The error in wavenumber is

$$d\kappa_m = \kappa_m(\omega + d\omega) - \kappa_m(\omega) \tag{4.6a}$$

$$d\kappa_m = \frac{d\kappa_m}{d\omega}\, d\omega \tag{4.6b}$$

where ω is the circular frequency. Since $\frac{d\kappa_m}{d\omega}$ is the inverse of the group velocity v_g, Equation 4.6b can be expressed as

$$d\kappa_m = \frac{d\omega}{v_g} \tag{4.7}$$

The Doppler shift $d\omega$ is given by

$$d\omega = -\frac{\omega V}{c_p + V} \tag{4.8}$$

where V is the speed of the source, c_p the phase velocity of the m^{th} mode. Since c_p is much larger than V, Equation 4.8 can be expressed as [Ozard1989]

$$d\kappa_m = -\frac{\omega V}{c_p\, v_g} \tag{4.9a}$$

$$d\kappa_m = -\kappa_m \frac{V}{v_g} \tag{4.9b}$$

so that

$$\frac{d\kappa_m}{\kappa_m} = -\frac{V}{v_g} \tag{4.10}$$

Here, $V \# 3$ m/s and v_g is approximately constant. The relative error in horizontal wavenumber computed using the ATLAS model group velocities is plotted in Figure 29 against mode number. It is bounded by 0.18 % and an order of magnitude lower than the phase errors due to range effects.

This preliminary remarks indicates that Doppler shift results in negligible phase errors compared to source range variations. Neglecting Doppler effects in the replica vectors calculations appear justified.

4.5. Source Tow Matched Field Processing Result

Matched field processing is performed using the Bartlett processor and the MV processor with stabilization factors equal to 10^{-3}, 10^{-2} and 10^{-1}. The sequence of the four selected stations provides an opportunity to test on real data the capabilities of matched field processing to localize a moving source. The ambiguity surface are computed

between 35 and 60 km for the first three stations and between 47.5 and 72.5 km for the last station. As before, a 250 m range and 5 m depth cell is used. The maximum depth of the ambiguity surface is 600 m. The results are gray-level displayed in Figure 30 to 37. The gray levels span the full dynamic range of each ambiguity surface and correspond to a scale in dB re μPa. The surfaces are normalized by their highest peak power which can be used for localization. Table 6 summarizes the results of the matched field processing on the source tow data.

The localization in range is excelient since the ranges of the highest peak in the ambiguity surfaces correspond to the predicted ranges for each station given in Table 5. The localization in depth gives, as in the case of the fixed stations, mixed results. The depth of the highest peak is either shallower or deeper than the expected source depth around 100 m. Because of the multiplicity of the sidelobes, it is difficult to estimate precisely where the source is. The dynamic range in the ambiguity surfaces indicates a large loss due to mismatch for the MV processor.

Tape		Processor			
		Bartlett	MV $\gamma = 10^{-3}$	MV $\gamma = 10^{-2}$	MV $\gamma = 10^{-1}$
980	Depth of Max.	200 m	50 m	50 m	50 m
	Range of Max.	41.5 km	42.75 km	42.75 km	42.75 km
	Surface Max.	88.2 dB	54.9 dB	61.2 dB	69.1 dB
	Dynamic Range	35 dB	8.5 dB	6.5 dB	5 dB
	Figure	30	30	31	31
981	Depth of Max.	50 m	40 m	40 m	40 m
	Range of Max.	44.25 km	46.25 km	46 km	46 km
	Surface Max.	80.4 dB	49.5 dB	54.9 dB	61.5 dB
	Dynamic Range	30 dB	9 dB	7 dB	5 dB
	Figure	32	32	33	33
983	Depth of Max.	135 m	135 m	20 m	135 m
	Range of Max.	51.75 km	51.75 km	50.75 km	50.75 km
	Surface Max.	82.2 dB	49.2 dB	56.7 dB	63.2 dB
	Dynamic Range	30 dB	9 dB	7 dB	6 dB
	Figure	34	34	35	35
986	Depth of Max.	15 m	10 m	10 m	10 m
	Range of Max.	60.25 km	60 km	60.25 km	60.25 km
	Surface Max.	78.2 dB	49.2 dB	54.8 dB	62.0 dB
	Dynamic Rang	25 dB	9.5 dB	8 dB	7 dB
	Figure	36	36	37	37

Table 6: Summary of the matched field processing (source tow data)

4.6. Matched Field Processing Simulation

As in the case of the fixed station processing, simulation results are now presented to help the interpretation of the results of the matched field processing on the real data.

4.6.1. Analysis of Mismatch

As pointed out in the previous section, the results show a somewhat large mismatch. The source tow matched field processing runs are performed on a much shorter range than the fixed stations, therefore the assumption of a range independent medium appears justified. The sound speed profile is derived from an XBT cast taken during the source tow and sound speed mismatch is unlikely. The impact of the source motion on the ambiguity surfaces is investigated. Like in the case of the fixed stations, array tilt is expected to have a major impact on the performance of the matched field

processing techniques and will also be discussed.

4.6.2. Simulation of the Tow

A source tow simulation for Station #2 is performed, where the source is assumed at a depth of 100 m in a noise-free environment and moves away from the VLA array. 4 minutes and 22 seconds worth of data are used to estimate the real data covariance matrix thus for a ship speed of 5 kts or 2.75 m/s, the source displacement is 721 m or 3 range cells (each cell is 250 m wide). The 100 m deep moving source is simulated by extracting the unnormalized complex ATLAS pressure fields that correspond to ranges equal to 47.5 km, 47.75 km and 48 km. Denoting those complex vectors by $\mathbf{X}_0$, $\mathbf{X}_1$, $\mathbf{X}_2$, the covariance matrix is computed by using

$$\mathbf{R} = \frac{1}{3\,\mathbf{X}_0^H \mathbf{X}_0} \left[\mathbf{X}_0 \mathbf{X}_0^H + \mathbf{X}_1 \mathbf{X}_1^H + \mathbf{X}_2 \mathbf{X}_2^H \right] \tag{4.11}$$

The replica vector that corresponds to $\mathbf{X}_i$ is given by $\frac{\mathbf{X}_i}{(\mathbf{X}_i^H \mathbf{X}_i)^{1/2}}$ In this simulation, the "true" source position is considered at 47.5 km from the VLA. Matched field processing is performed on this covariance matrix and the ambiguity surfaces are plotted in Figure 38 and 39. The only mismatch is due to the averaged covariance matrix. The ambiguity surfaces are similar to the ones of Figure 40, which correspond to the perfect case where there is no mismatch (a non moving source is assumed at 47.5 km and 100 m depth). The highest peaks in Figure 38 and 39 are at the right range-depth cell but their power is reduced by almost 3 dB for the Bartlett processor and almost 5 dB for the MV processor. The pressure field sampled by the VLA is not stationary since the source moves away in range. This simulation shows that averaging over time snapshots to estimate the covariance matrix results in a reduction of the maximum peak power and a slight broadening of the main peaks. But it also shows that averaging does not create enough mismatch to destroy the ambiguity surfaces and to reduce, in a dramatic way, their dynamic range. Thus, the amount of averaging proposed in Section 2 and used to estimate the covariance

matrix appears acceptable.

To illustrate the undesirable effects of using a larger number of averages (i.e. using a longer data segment) to estimate the array covariance matrix, the ambiguity surfaces for a source moving over 1500 m or 6 range cells are calculated and plotted in Figure 41 and 42 This simulates the case where 252 dyadic vector outer-products are used to compute the covariance matrix with a 2048-point FFT operating on the data. These ambiguity surfaces show a large peak power reduction due to mismatch, almost 5 dB for the Bartlett processor and almost 8 dB for the MV processors. Furthermore the ambiguity surface for the Bartlett processor appears qualitatively quite different from the one with no mismatch.

4.6.3. Simulation of Tilt

As in the case of the fixed stations, the array was navigated in the three transponder net. The shapes of the array in the North-East and East-West vertical planes as well as from above in a horizontal plane are plotted in Figure 43, 44 and 45 for Tapes 980, 983 and 986. The navigation shows that the array is tilted with maximum horizontal displacement from top to bottom on the order of 15 m. The array was fairly straight when Tape 986 was recorded and mismatch due to tilt should minimal in this case.

A tilted array is simulated at a range of 47.5 km from the VLA in Figure 46 and 47. The source is assumed at a depth of 100 m. There is no noise and no other mismatch than array tilt. As expected, there is a large loss due to mismatch for the MV processors. The power of main peak is significantly reduced as well as the dynamic range in the ambiguity surface. The localization in range is underestimated by 1.75 km and the source depth is estimated at 95 m instead of 100 m.

4.6.4. Tow and Tilt Simulation

Since averaging over space and array tilting occur simultaneously in the case of

the real data, a simulation involving both phenomenon is presented for all four stations. A tilted array is simulated with a 15 m horizontal displacement from top to bottom, with the source at 100 m depth and moving over 3 range cells starting at 42 km for Station #1, at 47.5 km for Station #2, at 52 km for Station #3 and at 62 km for Station #4. The covariance matrix is computed by

$$\mathbf{R} = \frac{\sum_{i=1}^{3} \mathbf{X}_{r_i} \mathbf{X}_{r_i}^H}{\mathbf{X}_{r_1}^H \mathbf{X}_{r_1}} \tag{4.12}$$

where r_1 belongs to the set of ranges {42, 47.5, 52, 62} and $r_i = r_1 + 0.25\,(i-1)$, $i \neq 1$. The ambiguity surfaces are computed in each case for the Bartlett processor, and the three implementations of the MV processor. Good similarity is observed with the experimental runs for the first three stations. For Tape 986 or Station #4, the simulation results are different from the experimental run. This is not surprising since the array tilt, in this case, is minimal. The simulation results are summarized in Table 8. The simulation shows that array tilt coupled with averaging over range results in poor estimate of the source depth for the three first stations. The range estimate is generally close to the true range. It is generally off by 1.75 km except for Station #4. The matched field processing performed on Station #4 produces a good estimate of the source depth but a poor estimate of the source range (the error is either 4.75 km or 5 km). Also, the MV processors suffer the most loss due to mismatch and the most reduction of dynamic range in the ambiguity surfaces.

Station		Processor			
		Bartlett	MV $\gamma = 10^{-3}$	MV $\gamma = 10^{-2}$	MV $\gamma = 10^{-1}$
1	Depth of Max.	70 m	60 m	60 m	60 m
	Range of Max.	41.25 km	41.5 km	41.5 km	41.5 km
	Surface Max.	-5 dB	-47.8 dB	-37.8 dB	-27.8 dB
	Dynamic Range	40 dB	3 dB	3 dB	3 dB
	Figure	48	48	49	49
2	Depth of Max.	95 m	35 m	35 m	35 m
	Range of Max.	46 km	46.75 km	46.75 km	46.75 km
	Surface Max.	-4.95 dB	-47 dB	-37 dB	-27 dB
	Dynamic Range	50 dB	4 dB	4 dB	4 dB
	Figure	50	50	51	51
3	Depth of Max.	55 m	20 m	20 m	20 m
	Range of Max.	50.75 km	50.25 km	50.25 km	50.25 km
	Surface Max.	-6 dB	-46.2 dB	-36.2 dB	-26.2 dB
	Dynamic Range	45 dB	4.7 dB	4.7 dB	4.7 dB
	Figure	52	52	53	53
4	Depth of Max.	110 m	110 m	110 m	110 m
	Range of Max.	66.25 km	67 km	67 km	67 km
	Surface Max.	-9 dB	-50 dB	-40 dB	-30 dB
	Dynamic Range	38 dB	1.1 dB	1.1 dB	1.1 dB
	Figure	54	54	55	55

Table 8: Summary of the coupled tilt and tow simulation

5. Conclusions

This study demonstrates, using real data, that matched field processing is a viable processing technique at 200 Hz with a 900 m long vertical line array. Because of the high source level used in this transmission experiment, the source is easily detected and detection issues are not discussed. This report demonstrate the good capabilities of range localization of a source in deep water and for the 200 Hz mid-frequency. The environmental information collected at the time of the experiment allows an appropriate modeling of the acoustic transmissions using the ATLAS normal mode model. While the acoustic modeling, still, is imperfect, the source can be localized with good accuracy in range. Mismatch exists mainly because of a 1° tilt. This tilt is severe at the operating frequency since it corresponds to twice the wavelength at 200 Hz. Simulations show that array tilt causes slight range localization errors but potentially large errors for depth localization. Source depth estimation appears more sensitive to mismatch.

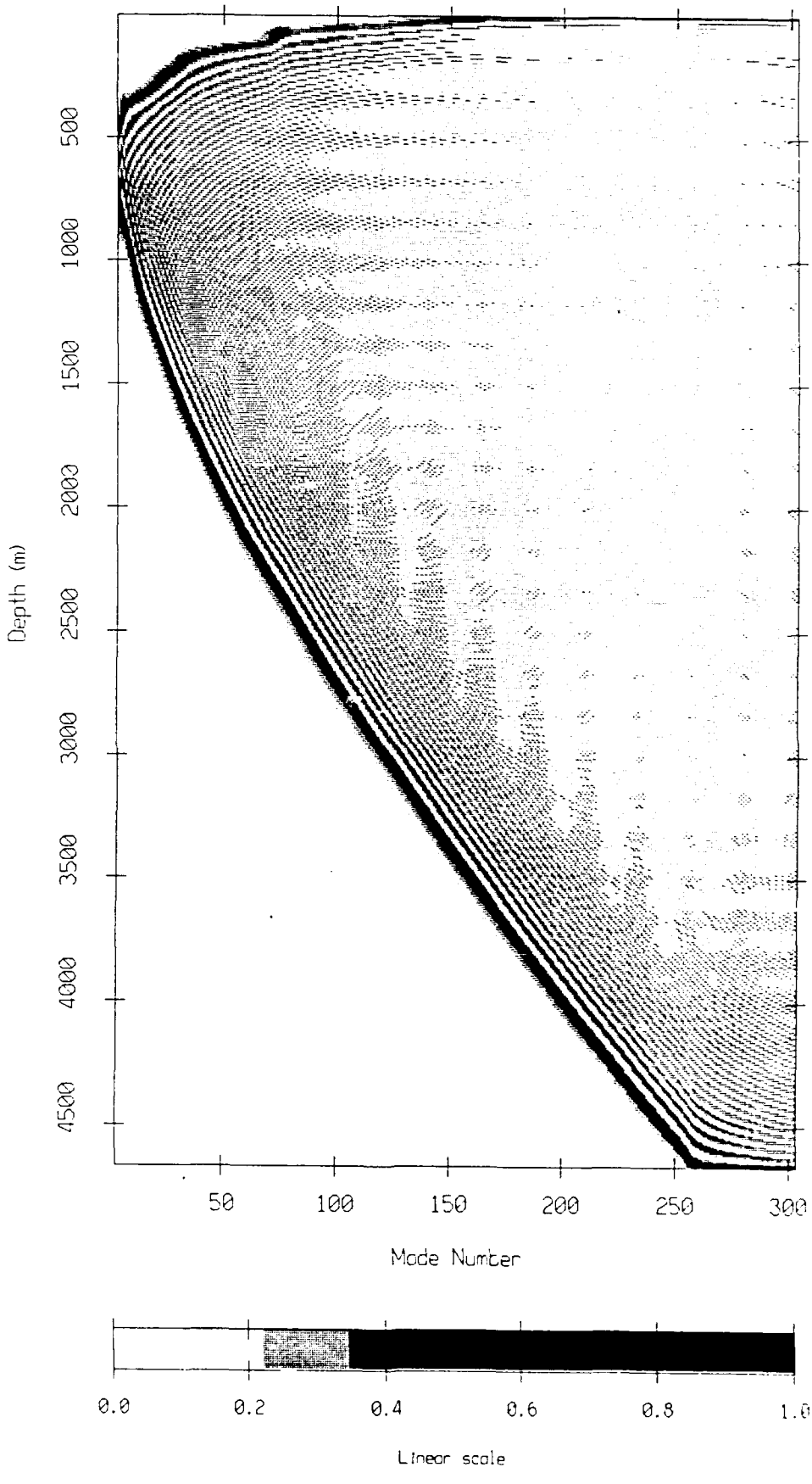

Figure 27: Modal Eigenfunction absolute value versus depth.

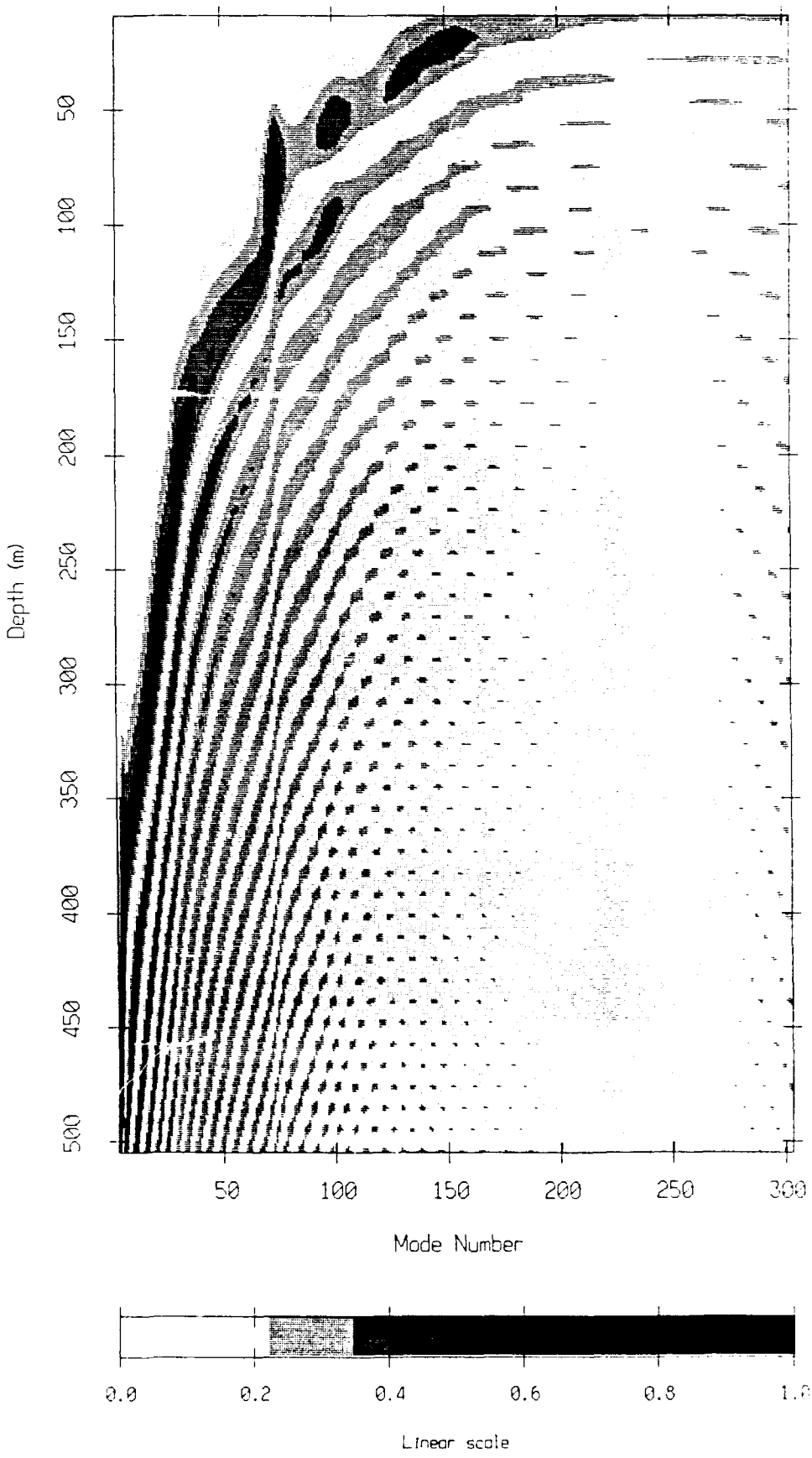

Figure 28: Modal Eigenfunction absolute value versus depth up to 500 m .

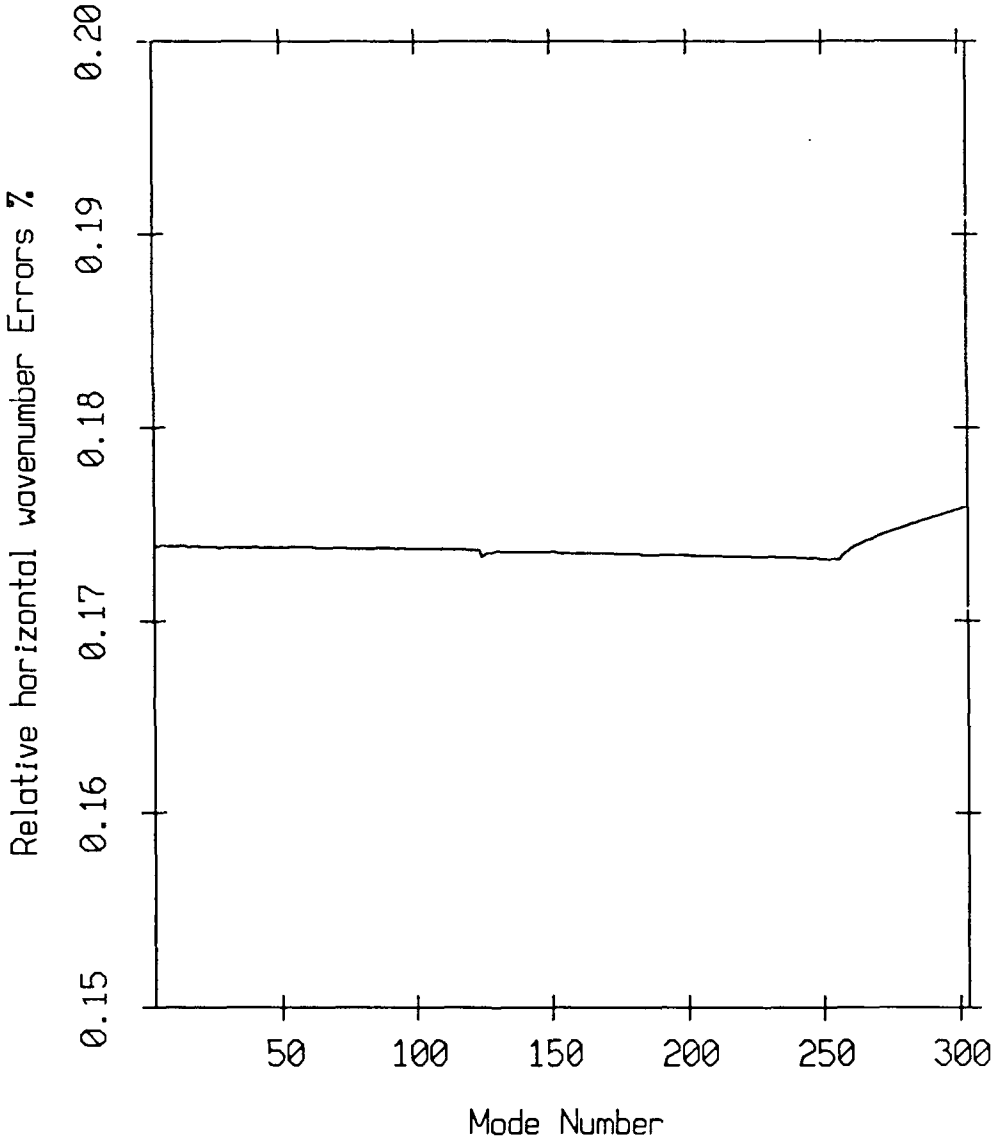

Figure 29: Relative error in horizontal wavenumber.

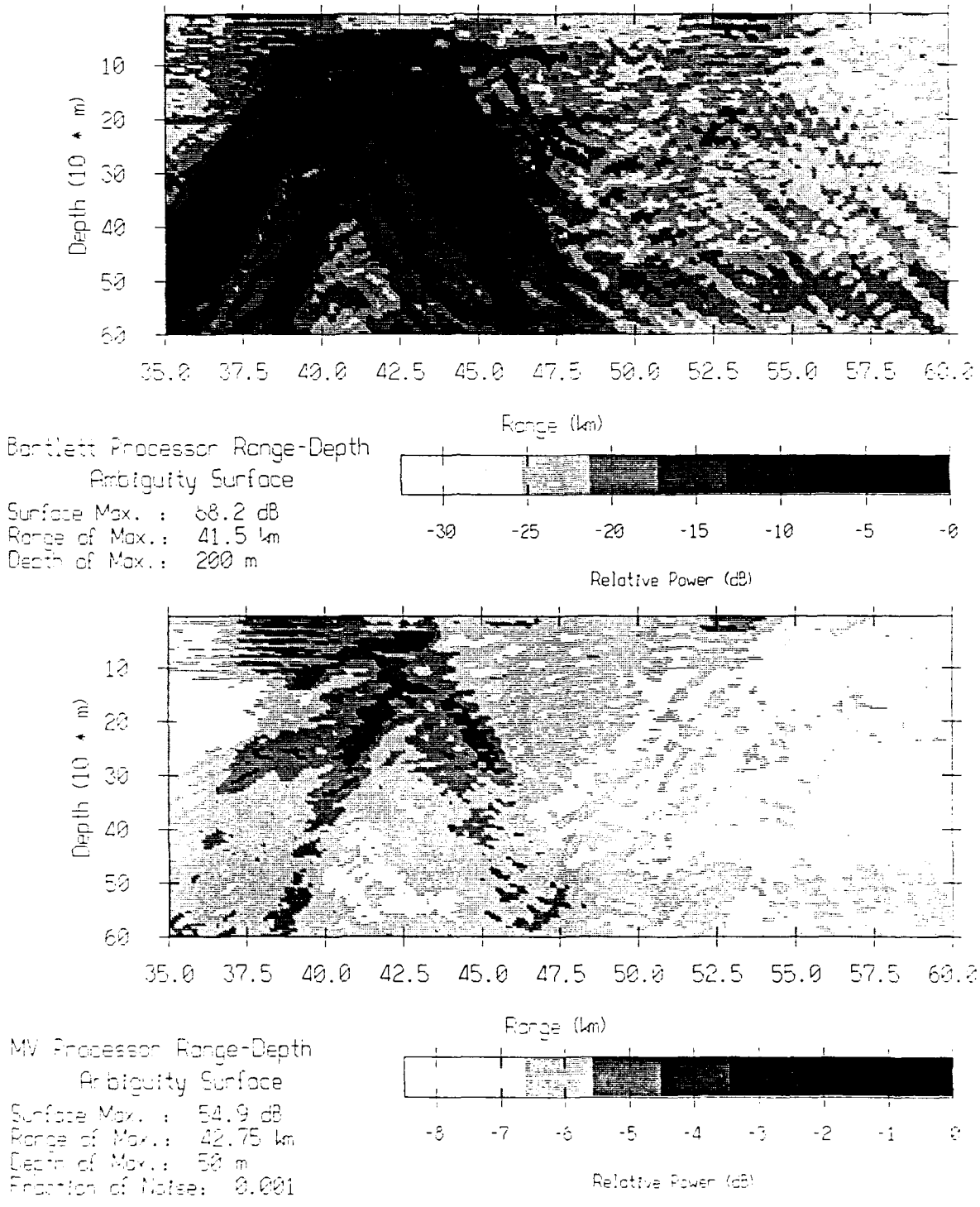

Figure 30: Matched field processing on the data of Tape 980, part 1.

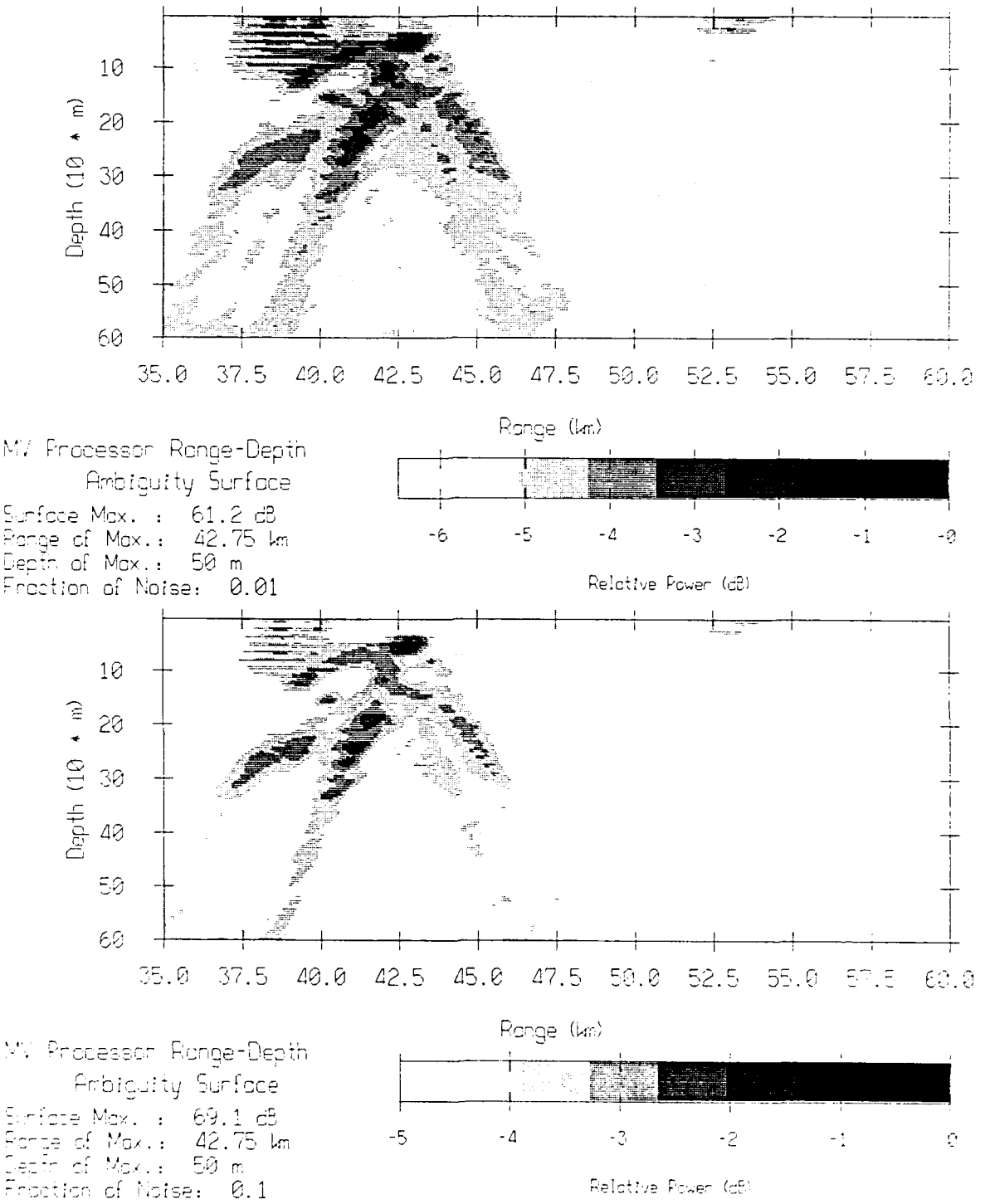

Figure 31: Matched field processing on the data of Tape 980, part 2.

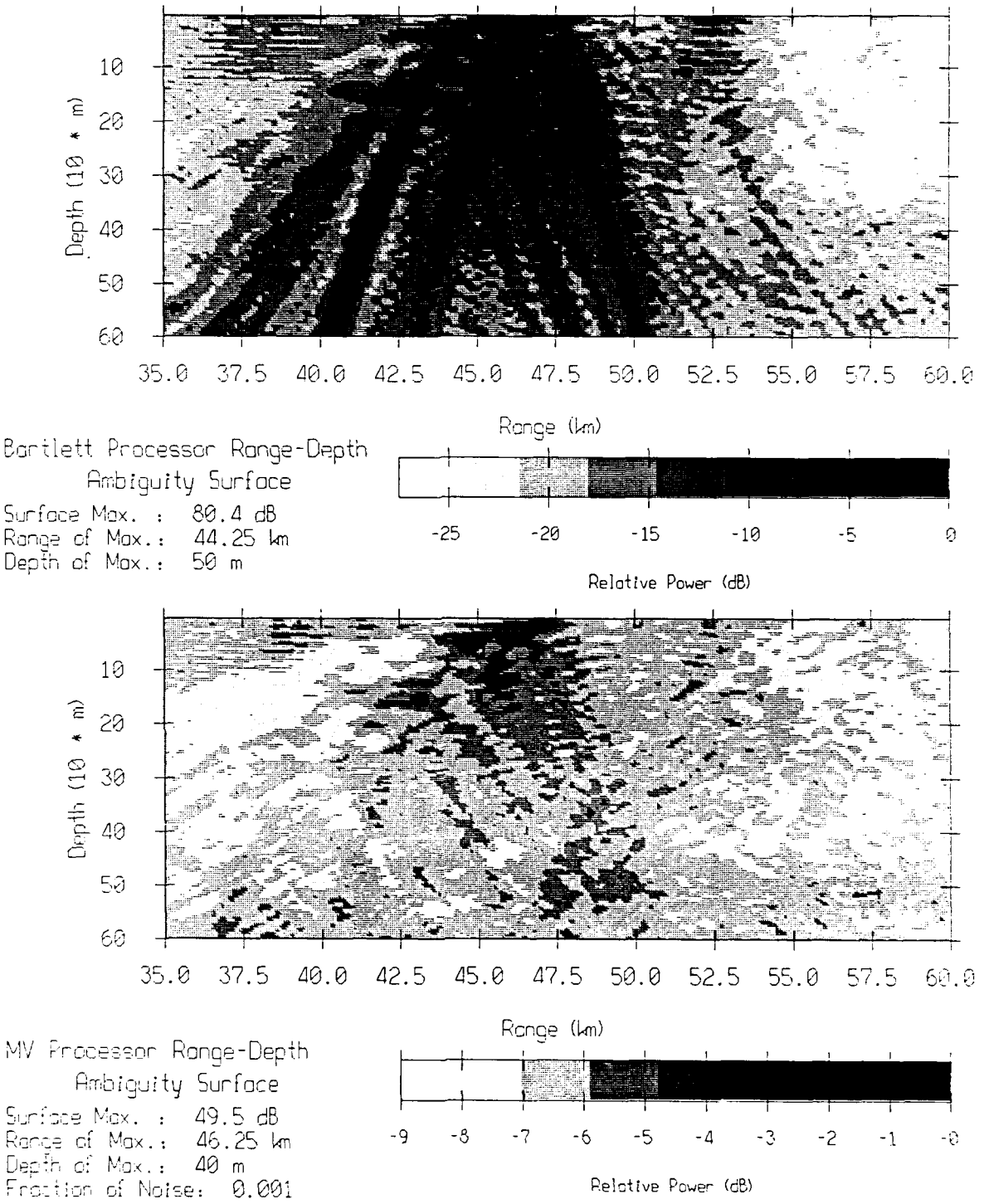

Figure 32: Matched field processing on the data of Tape 981, part 1.

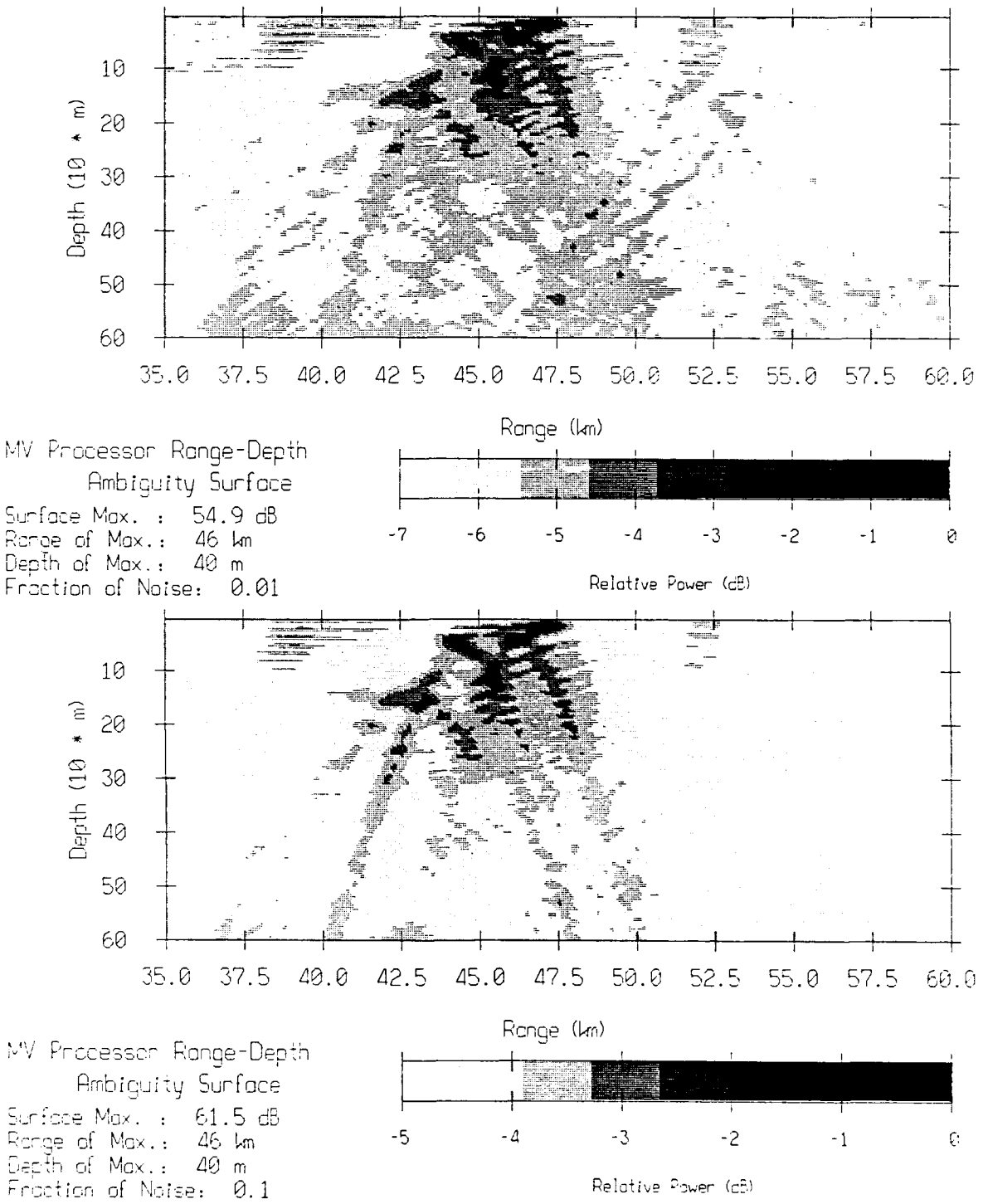

Figure 33: Matched field processing on the data of Tape 981, part 2.

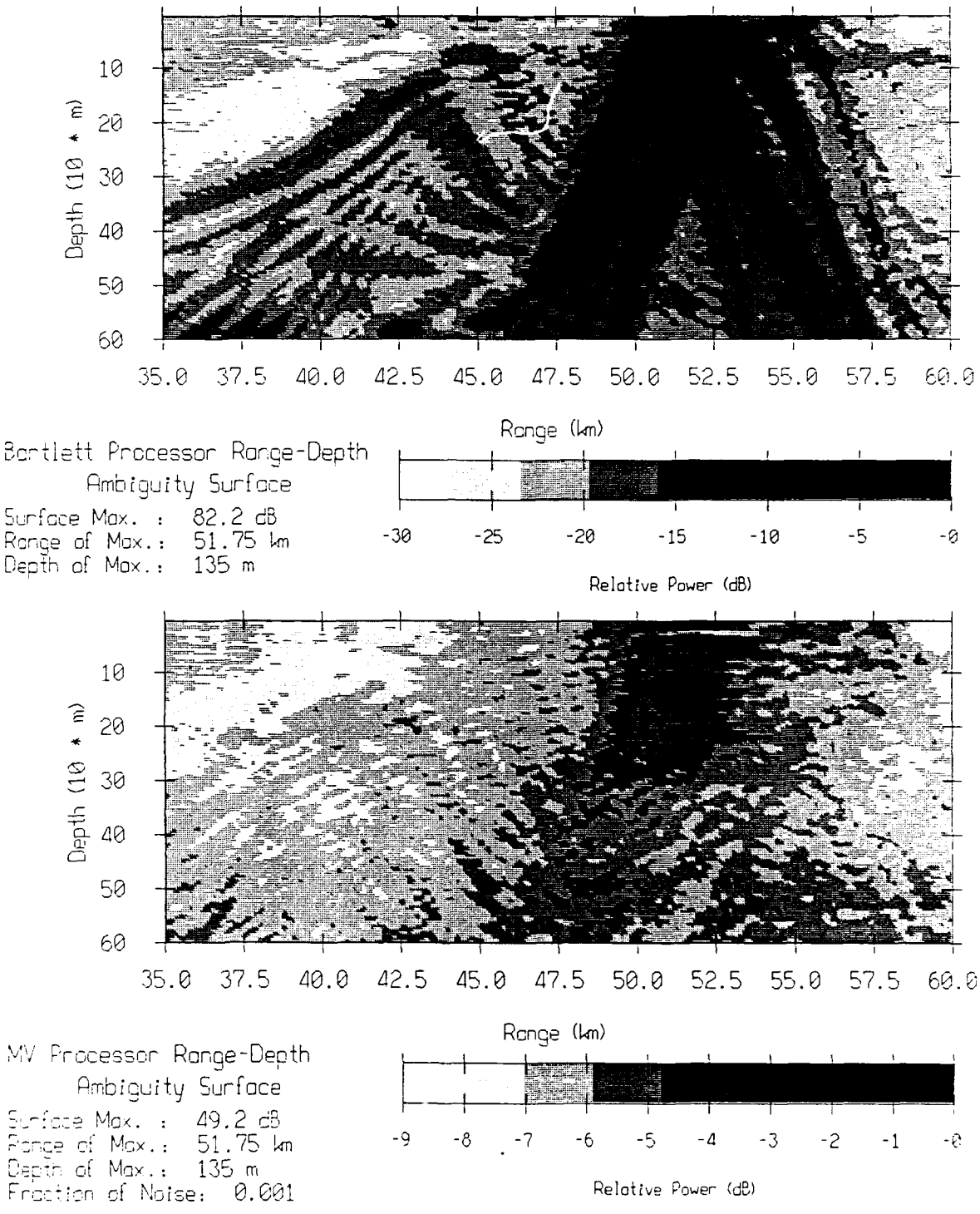

Figure 34: Matched field processing on the data of Tape 983, part 1.

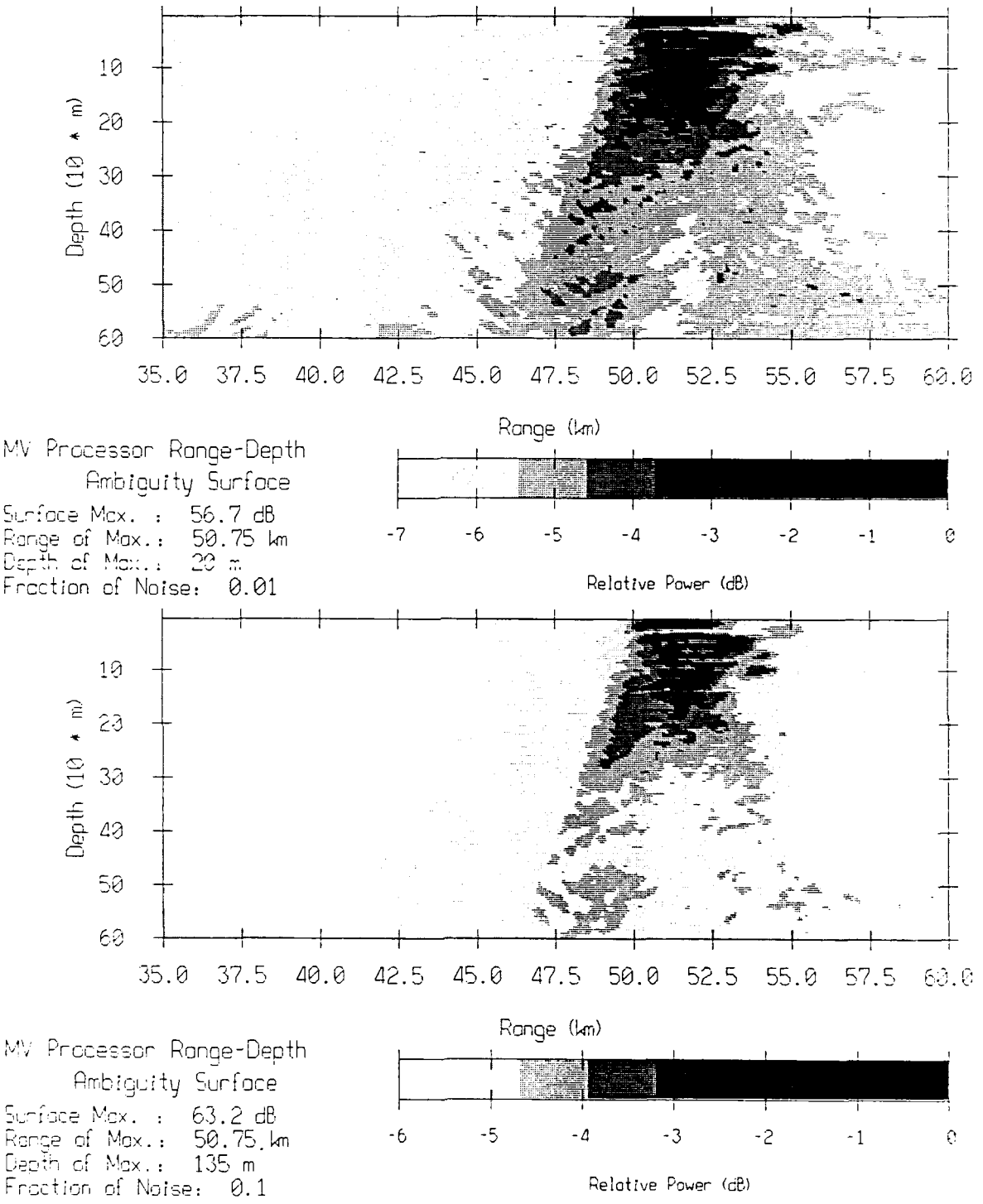

Figure 35: Matched field processing on the data of Tape 983, part 2.

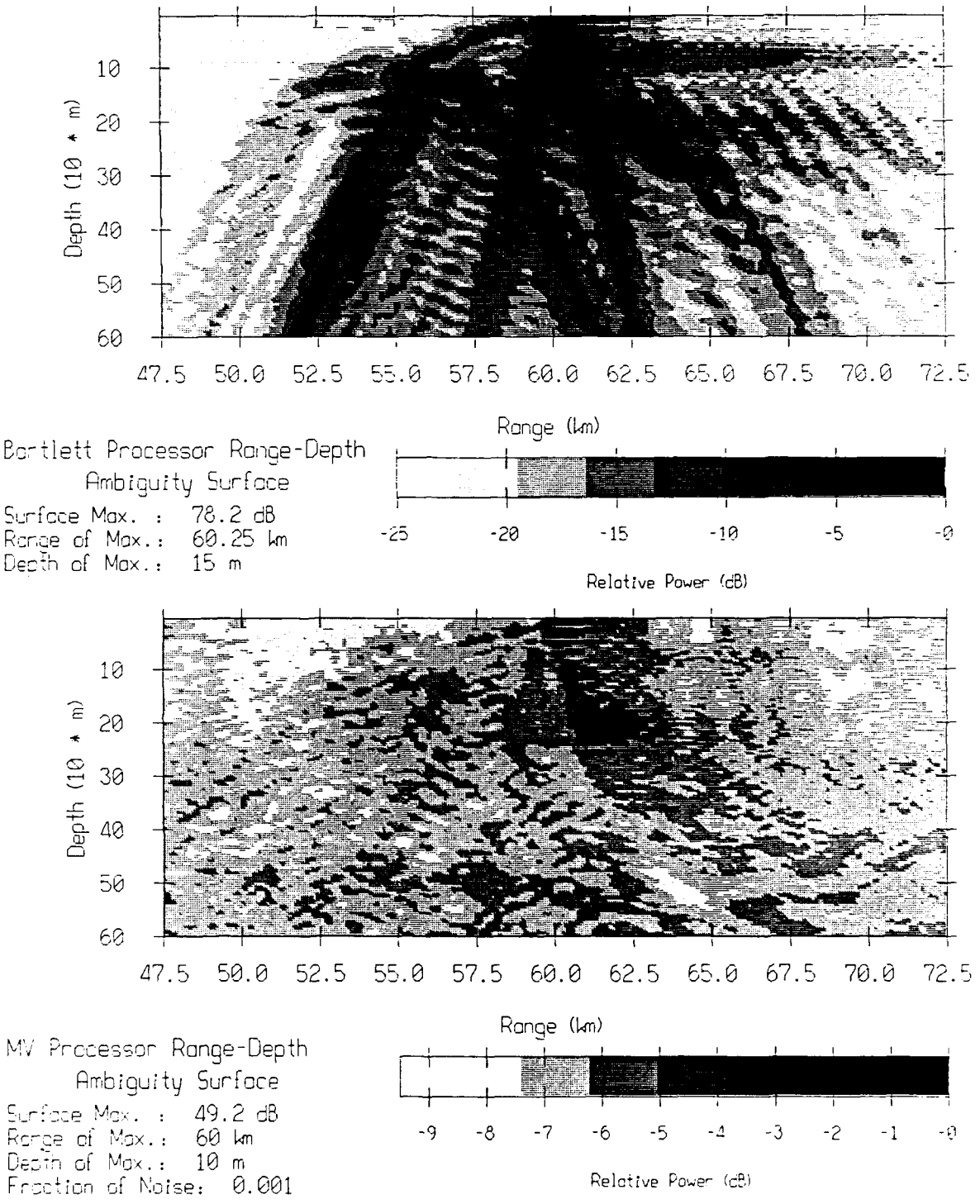

Figure 36: Matched field processing on the data of Tape 986, part 1.

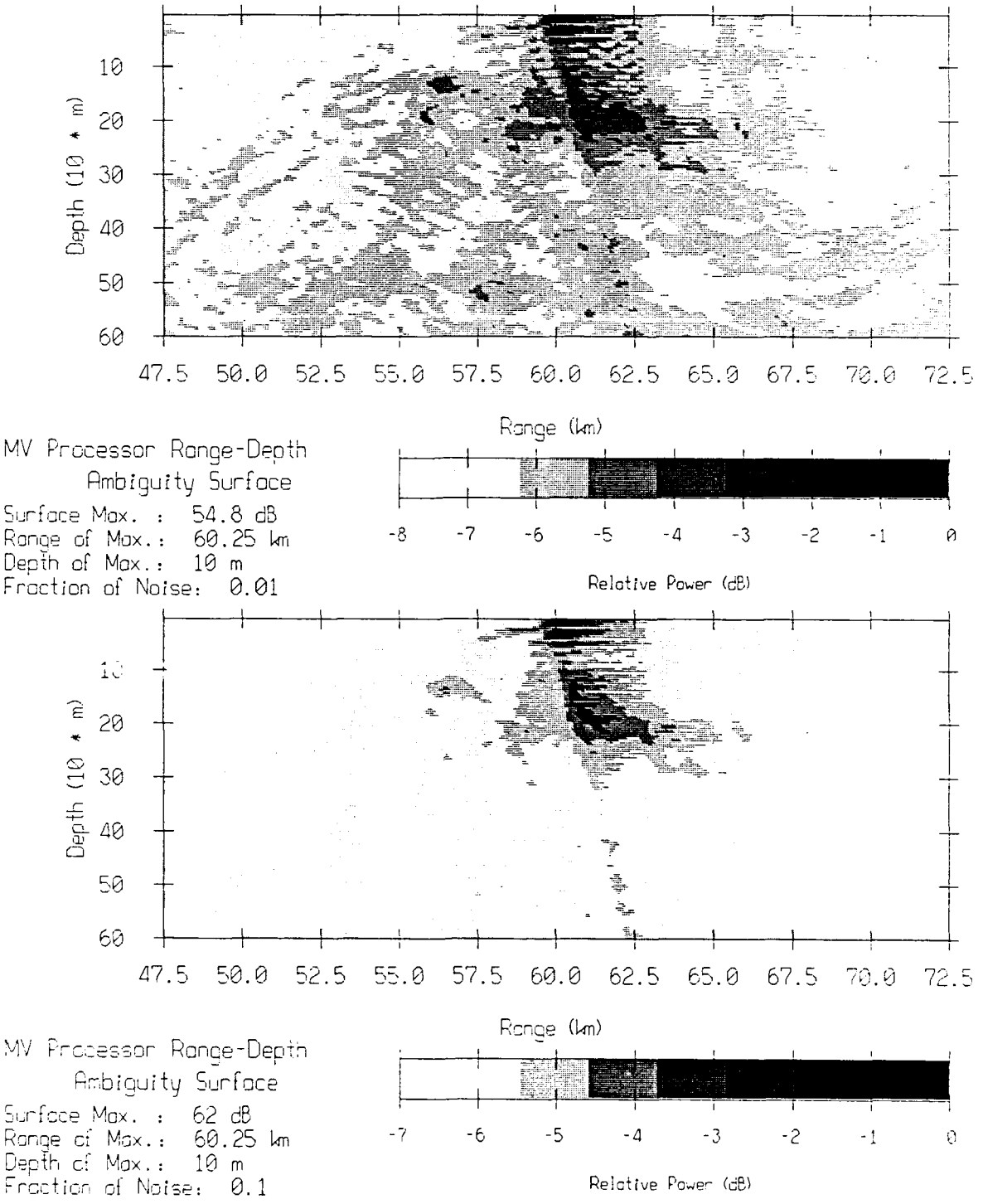

Figure 37: Matched field processing on the data of Tape 986, part 2.

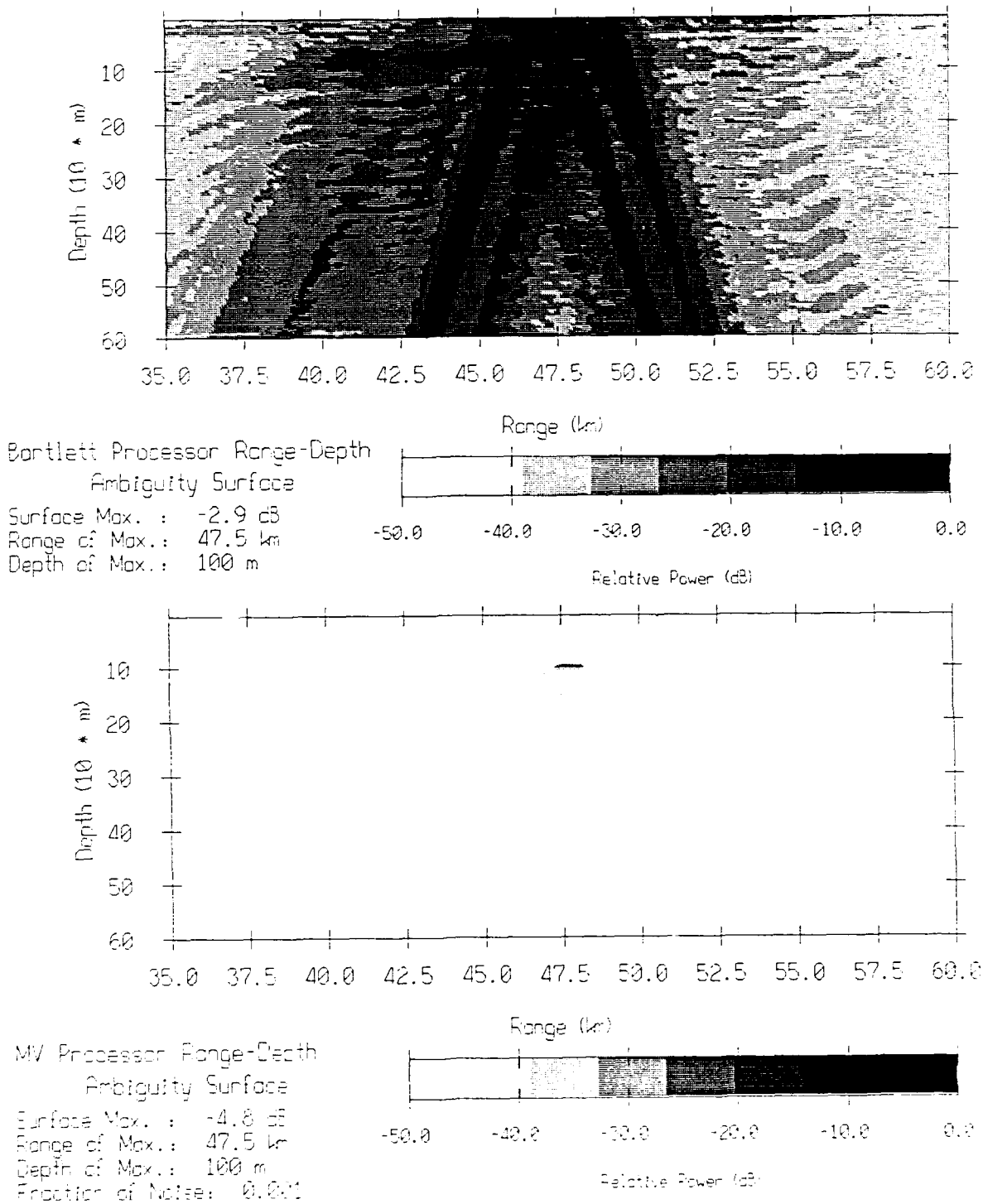

Figure 38: Source tow matched field processing simulation, part 1.

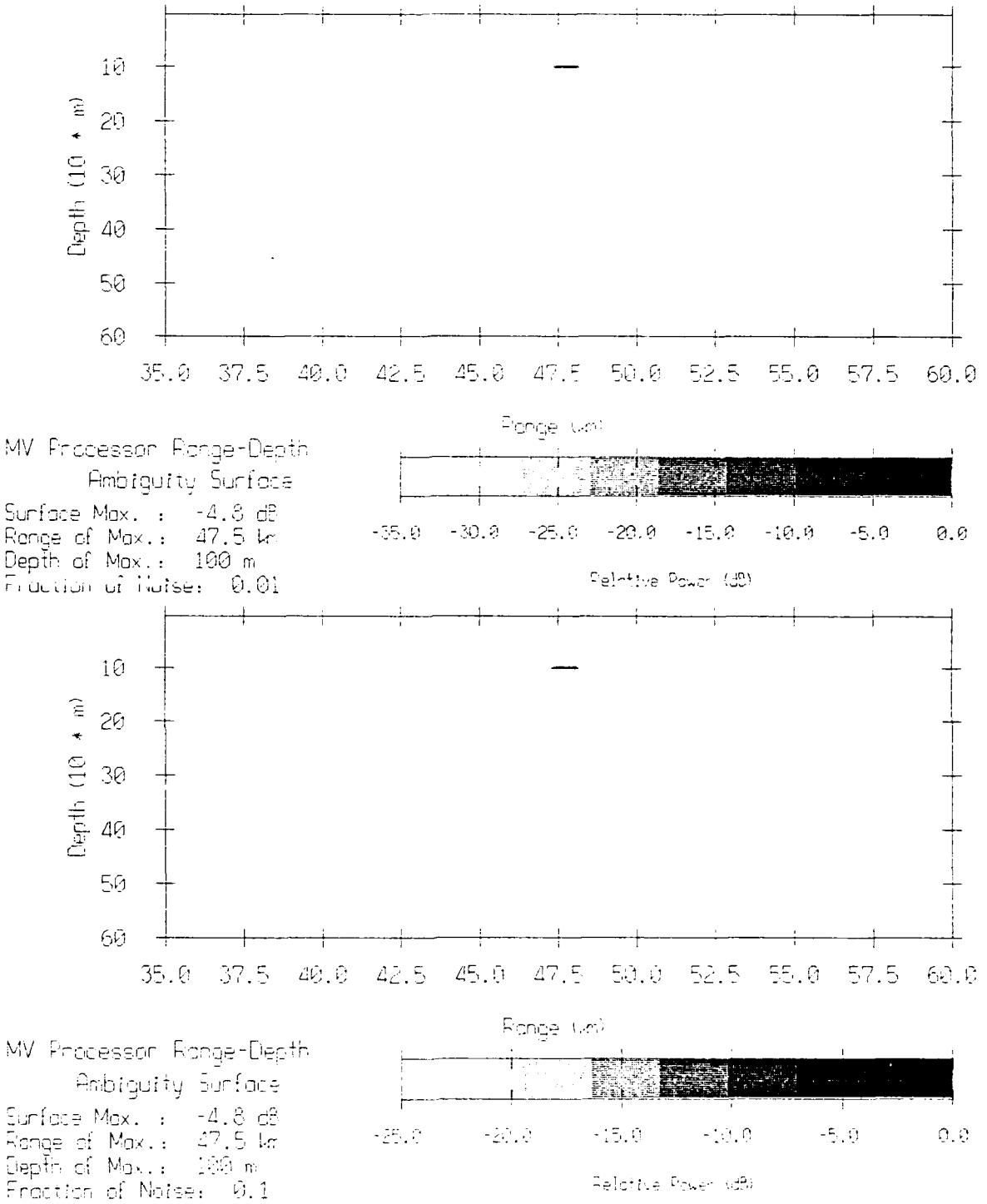

Figure 39: Source tow matched field processing simulation, part 2.

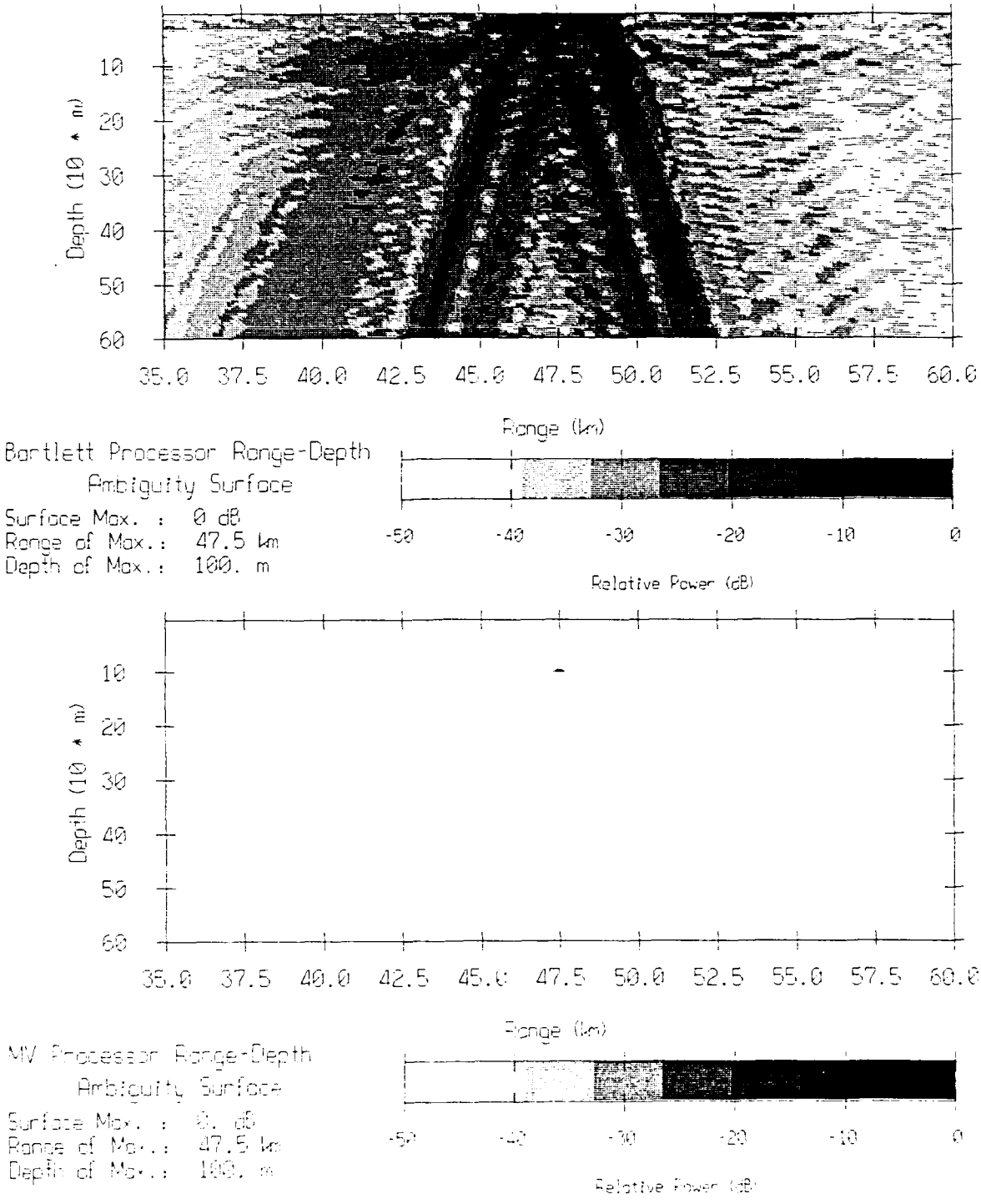

Figure 40: No mismatch and no noise matched field processing simulation.

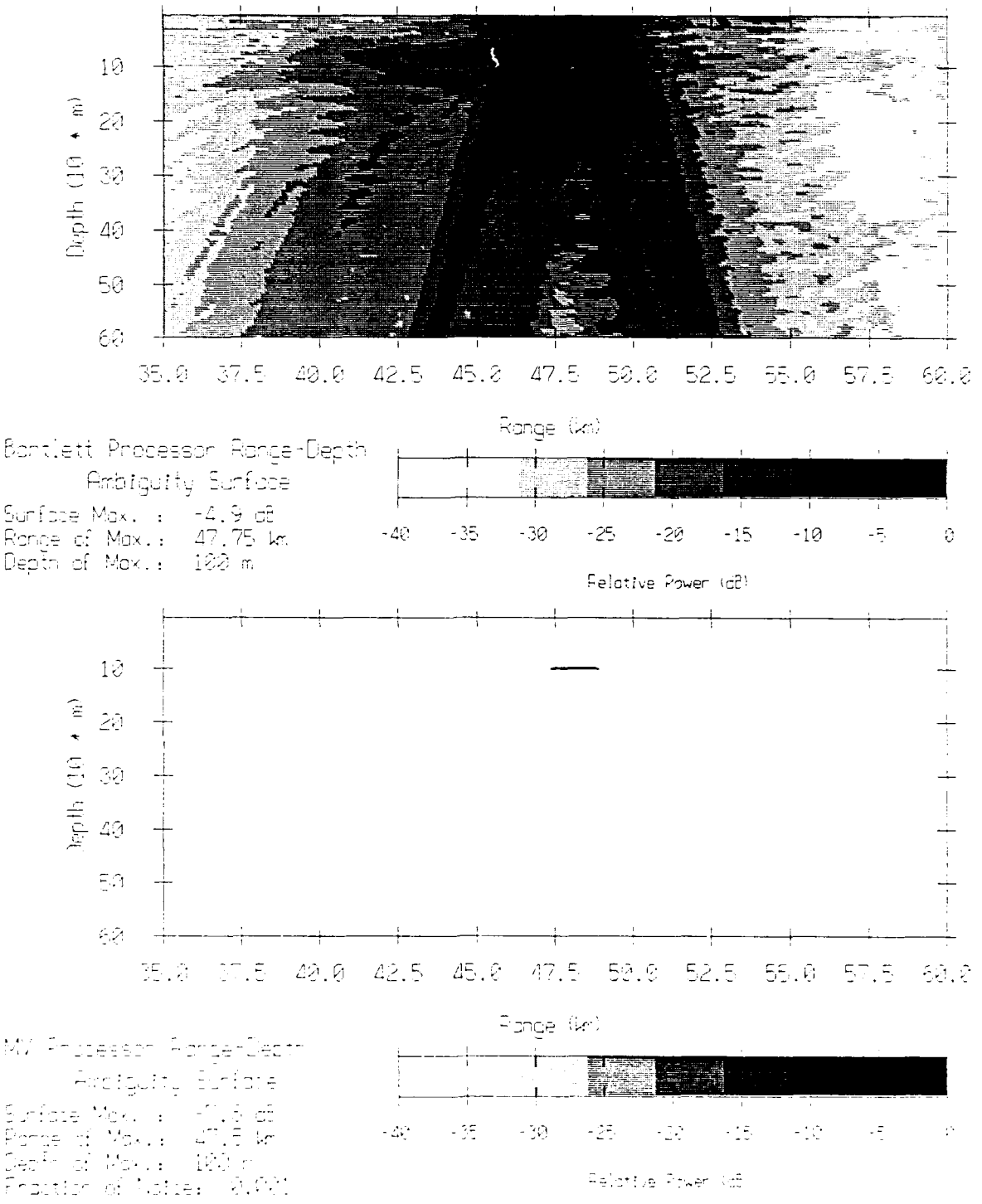

Figure 41: Source tow matched field processing simulation (long averaging time), part 1.

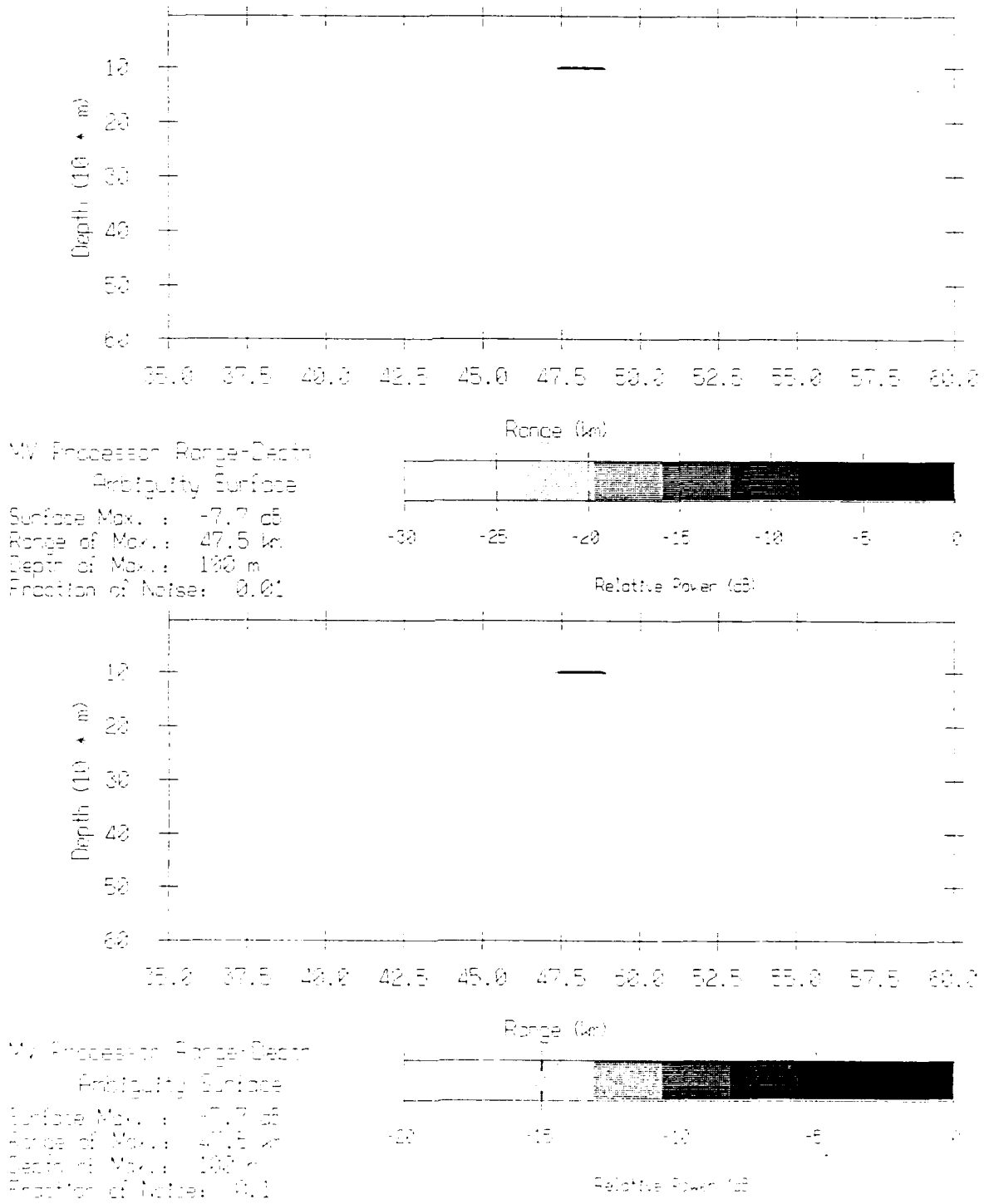

Figure 42: Source tow matched field processing simulation (long averaging time), part 2.

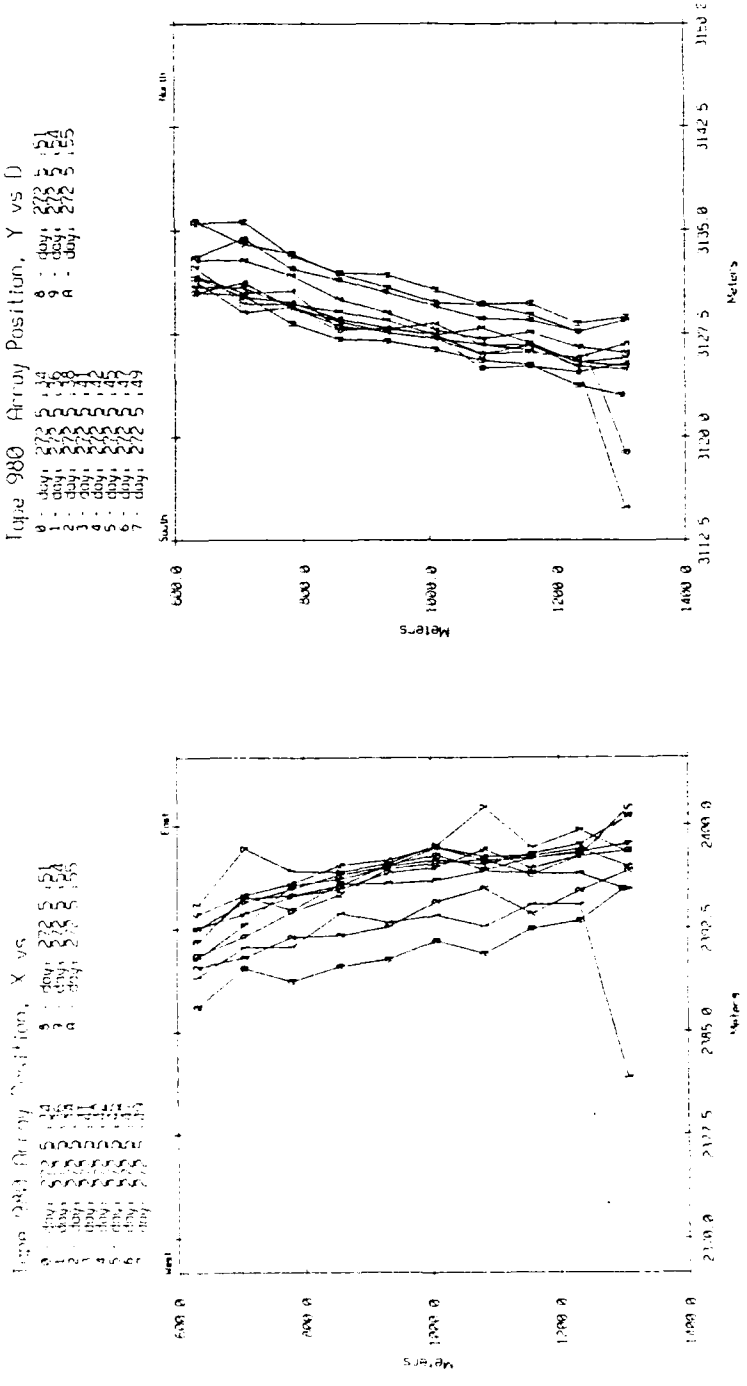

Figure 43: Array navigation for Tape 980.

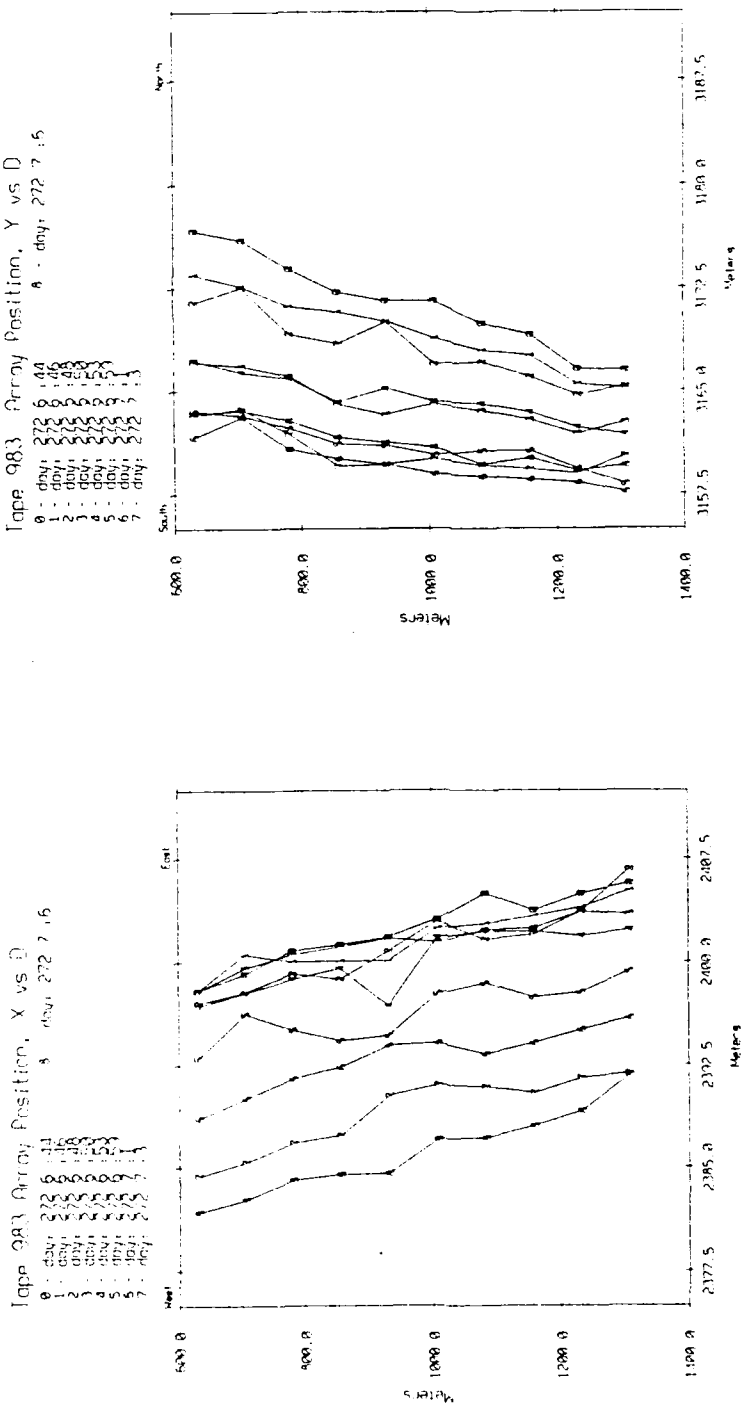

Figure 44: Array navigation for Tape 983.

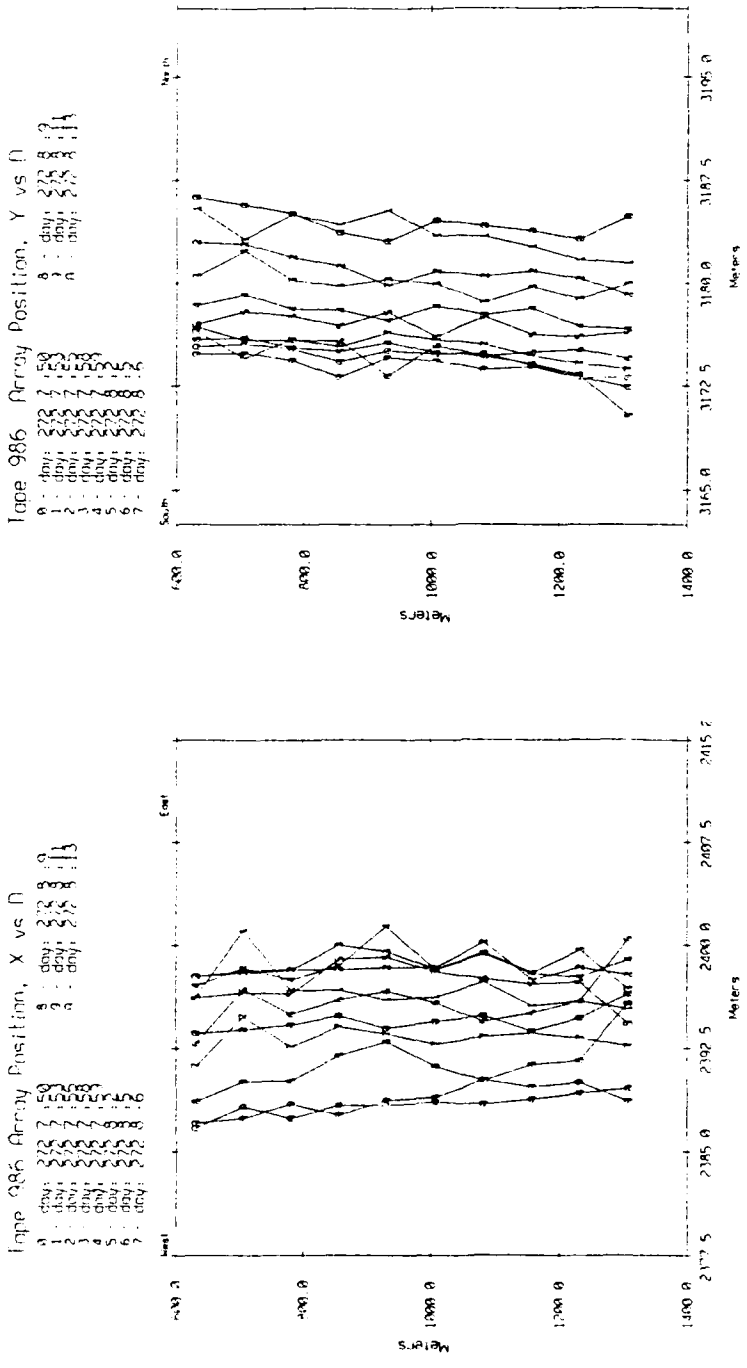

Figure 45: Array navigation for Tape 986.

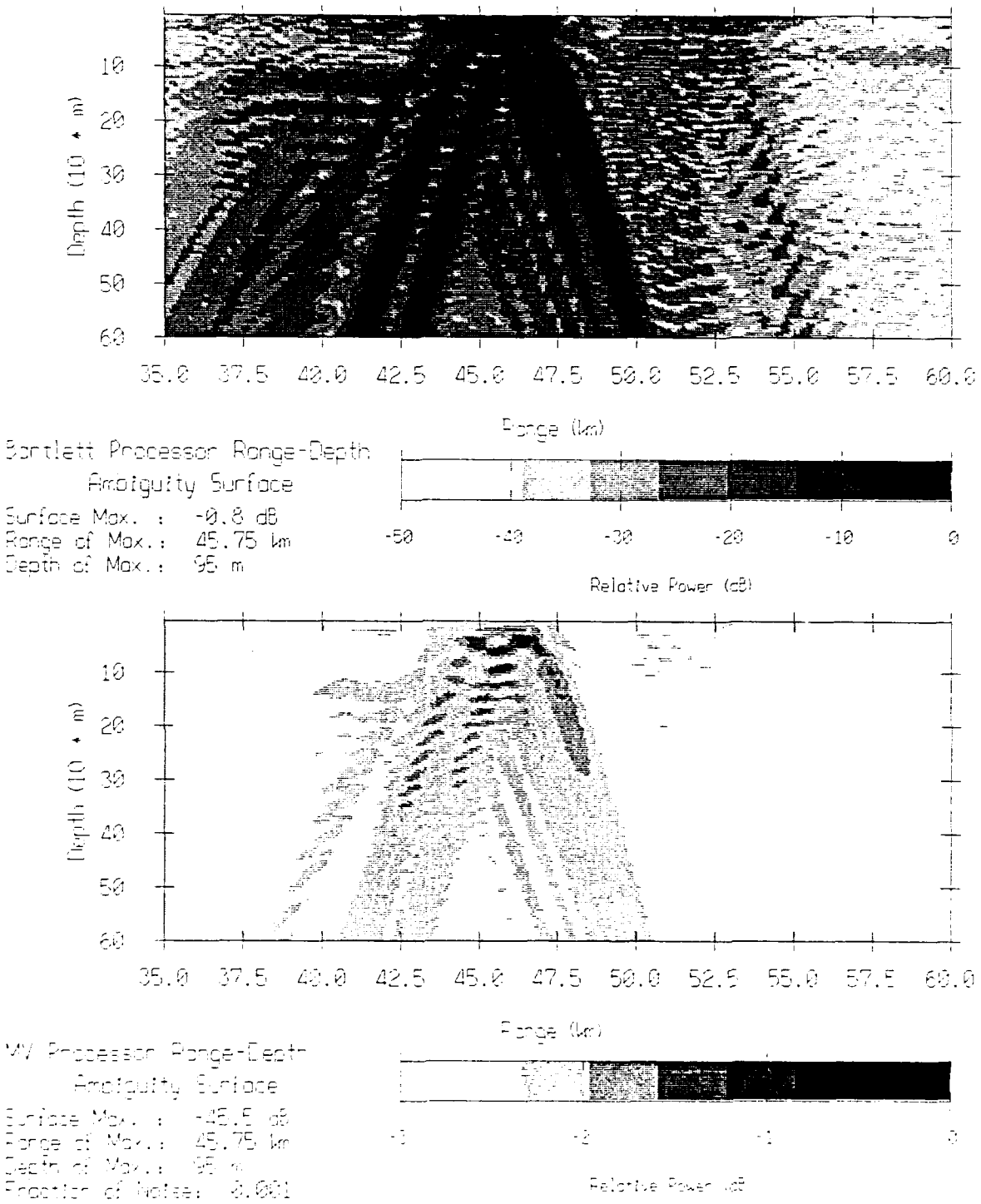

Figure 46: Tilted array matched field processing simulation, part 1.

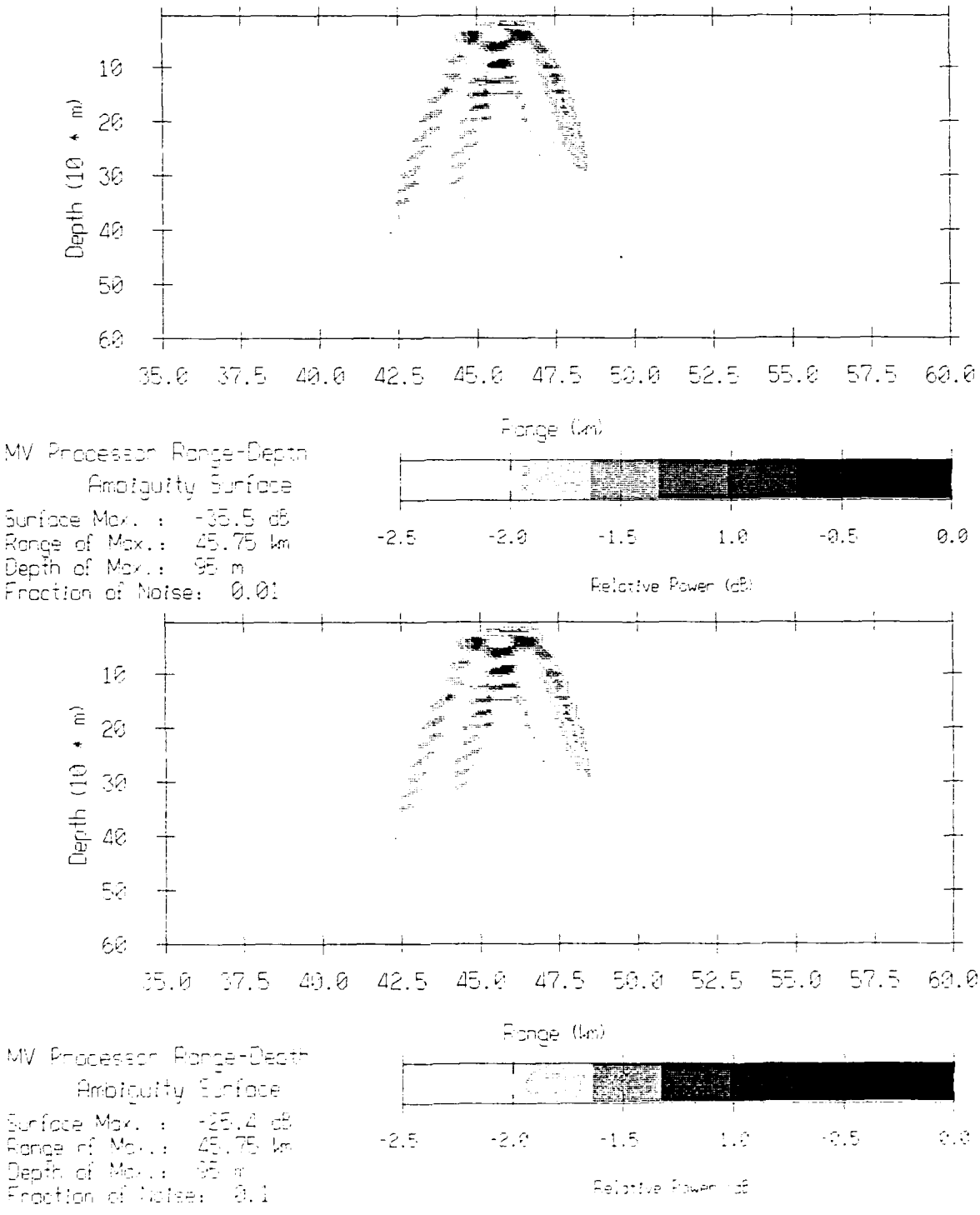

Figure 47: Tilted array matched field processing simulation, part 2.

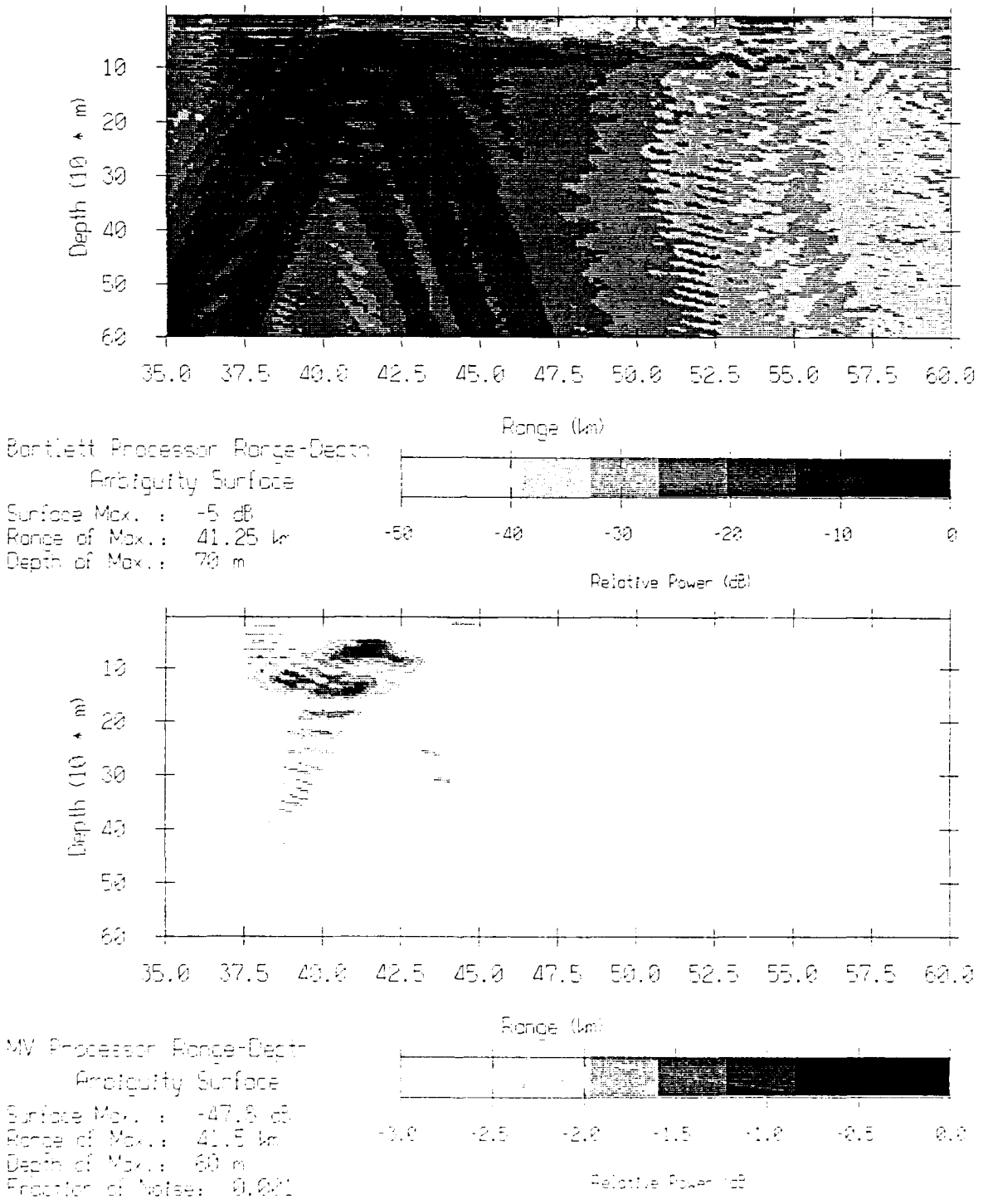

Figure 48: Matched field processing simulation (tilted array and towed source at 42 km), part 1.

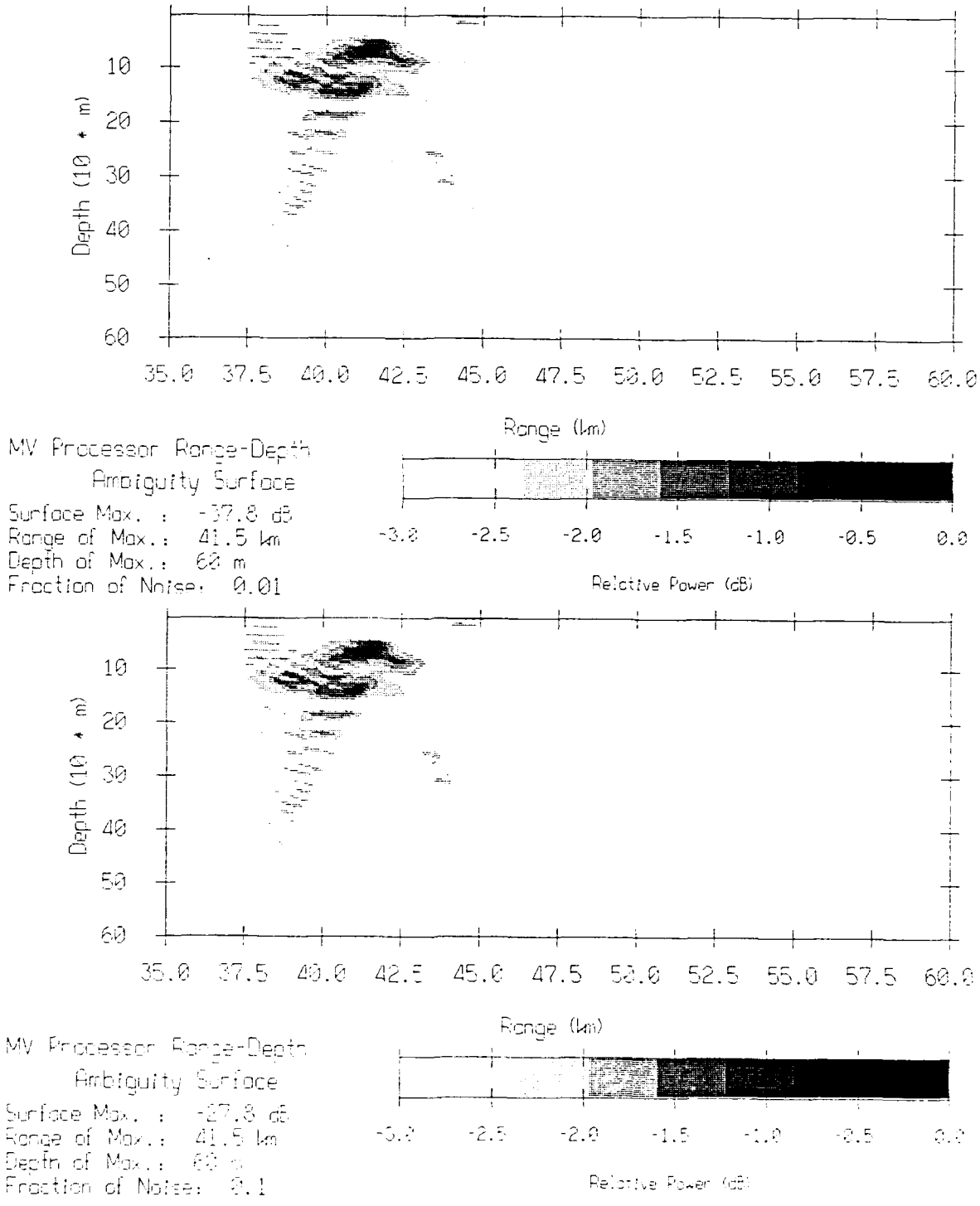

Figure 49: Matched field processing simulation (tilted array and towed source at 42 km), part 2.

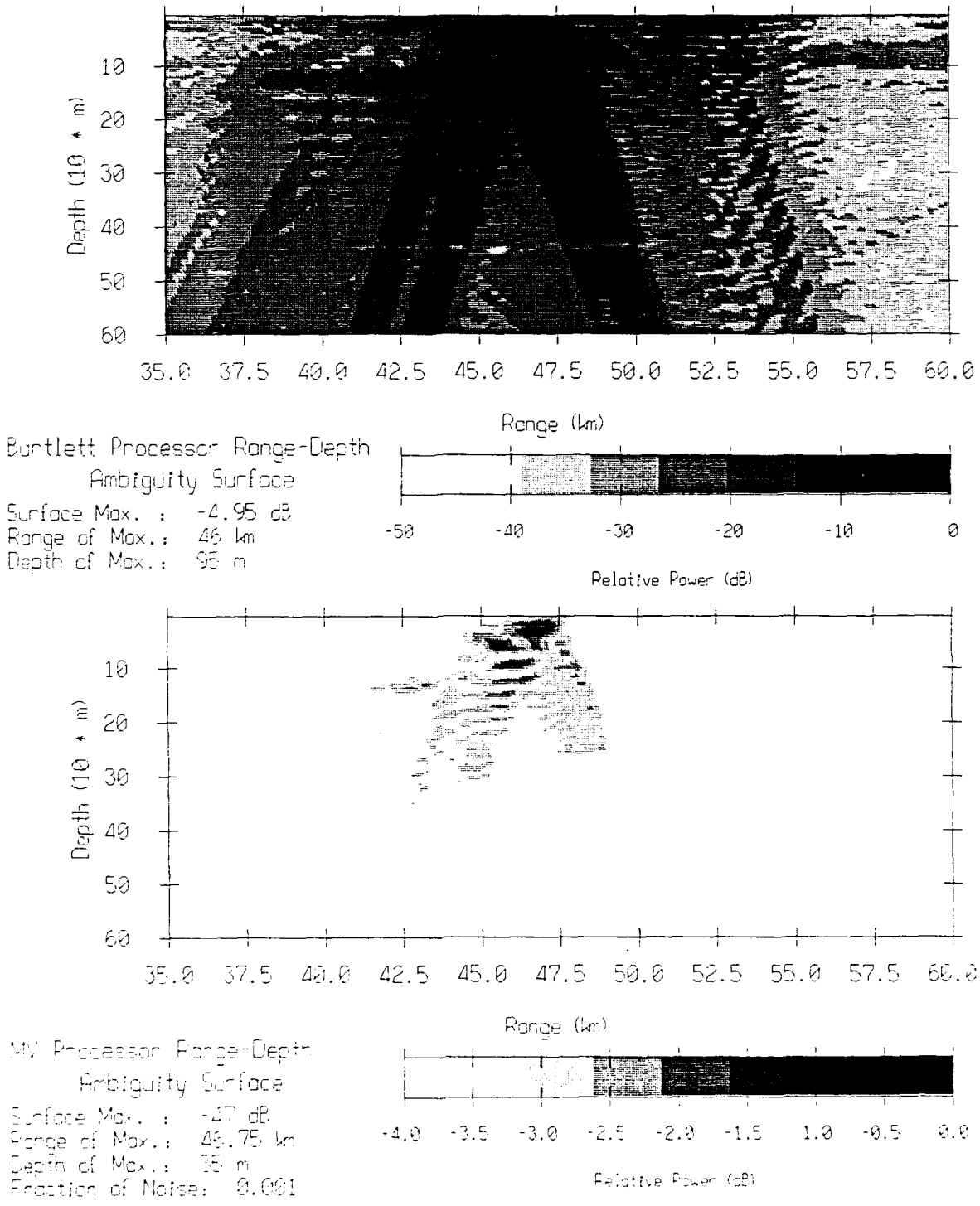

Figure 50: Matched field processing simulation (tilted array and towed source at 47.5 km), part 1.

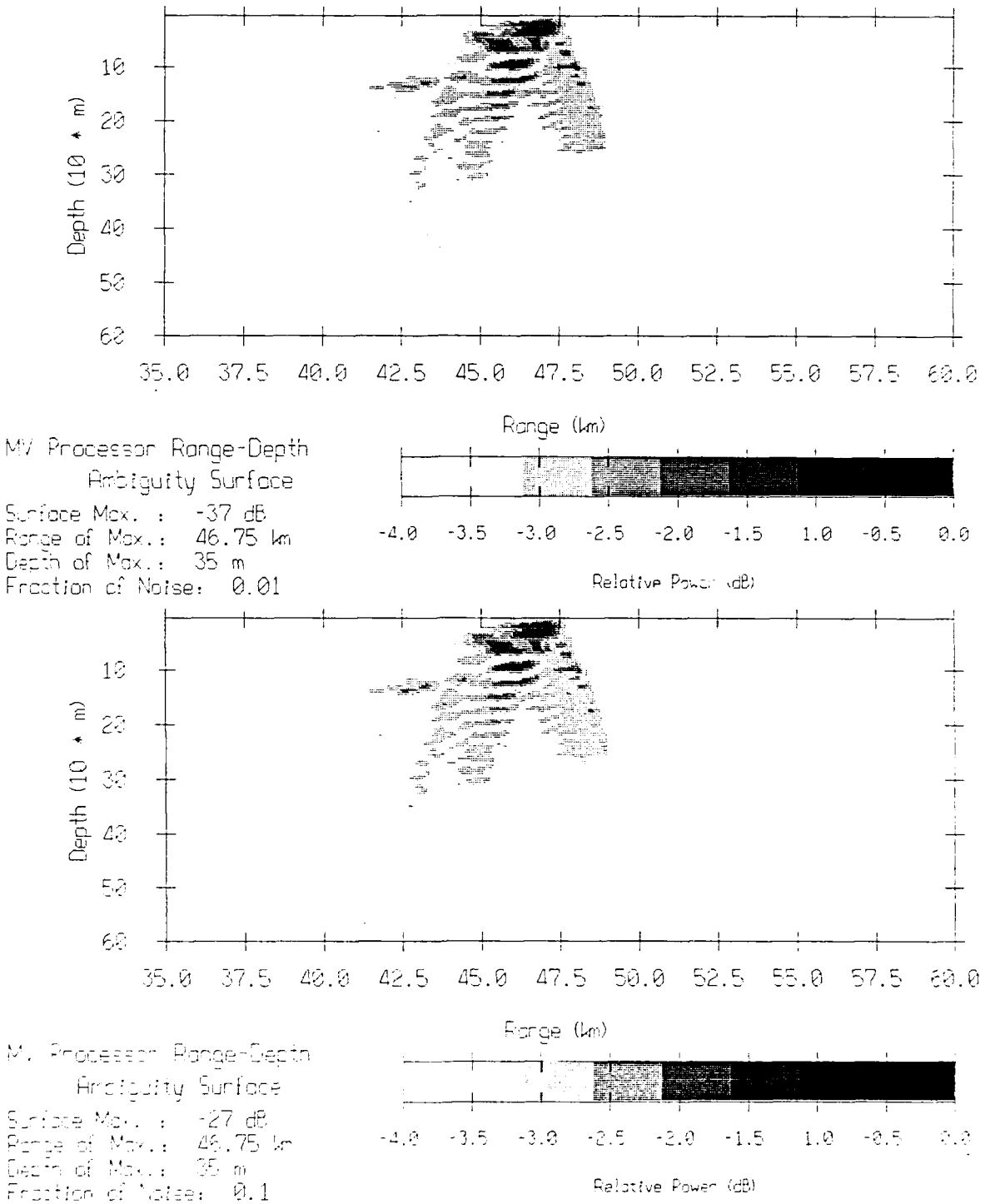

Figure 51: Matched field processing simulation (tilted array and towed source at 47.5 km), part 2.

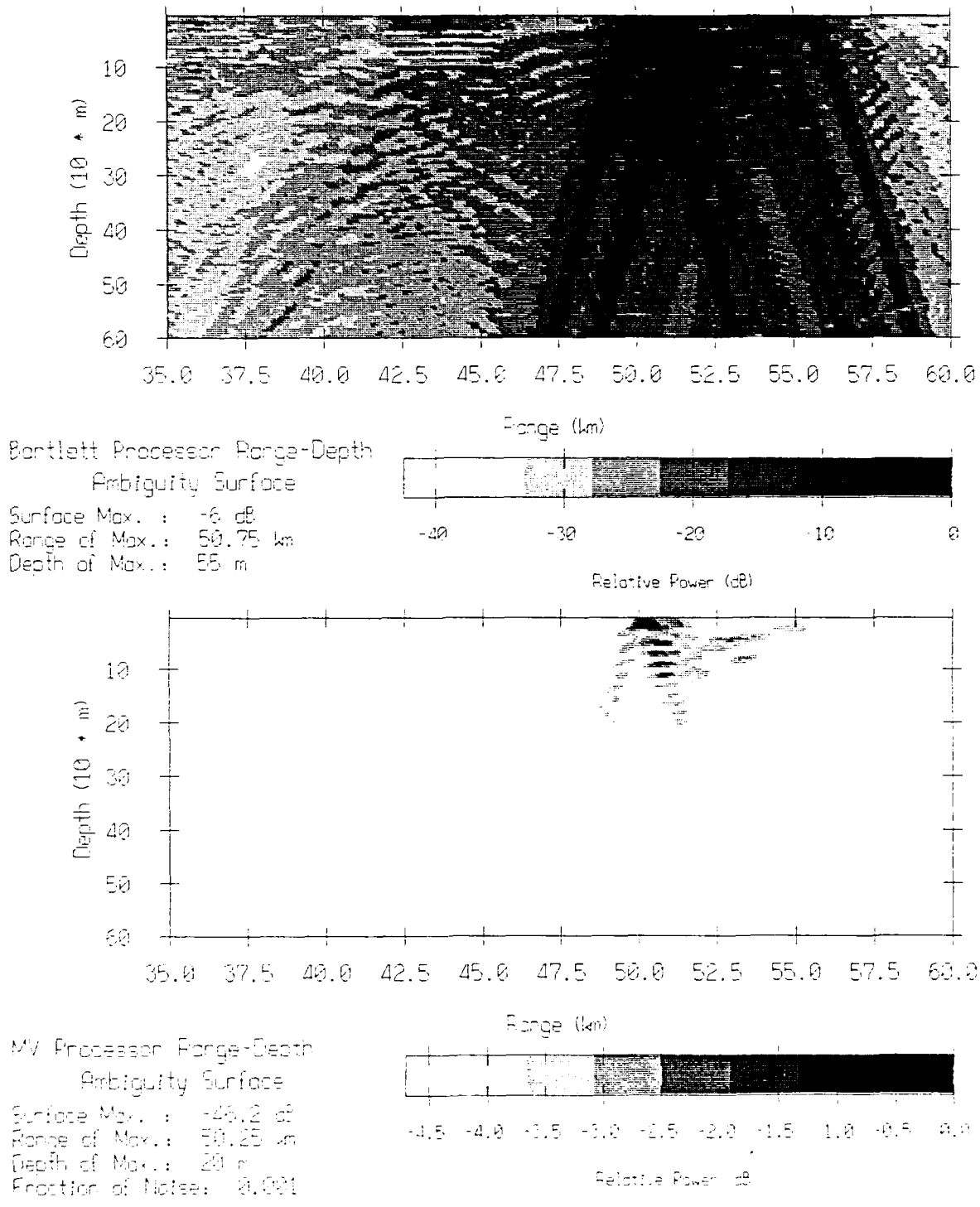

Figure 52: Matched field processing simulation (tilted array and towed source at 52 km), part 1.

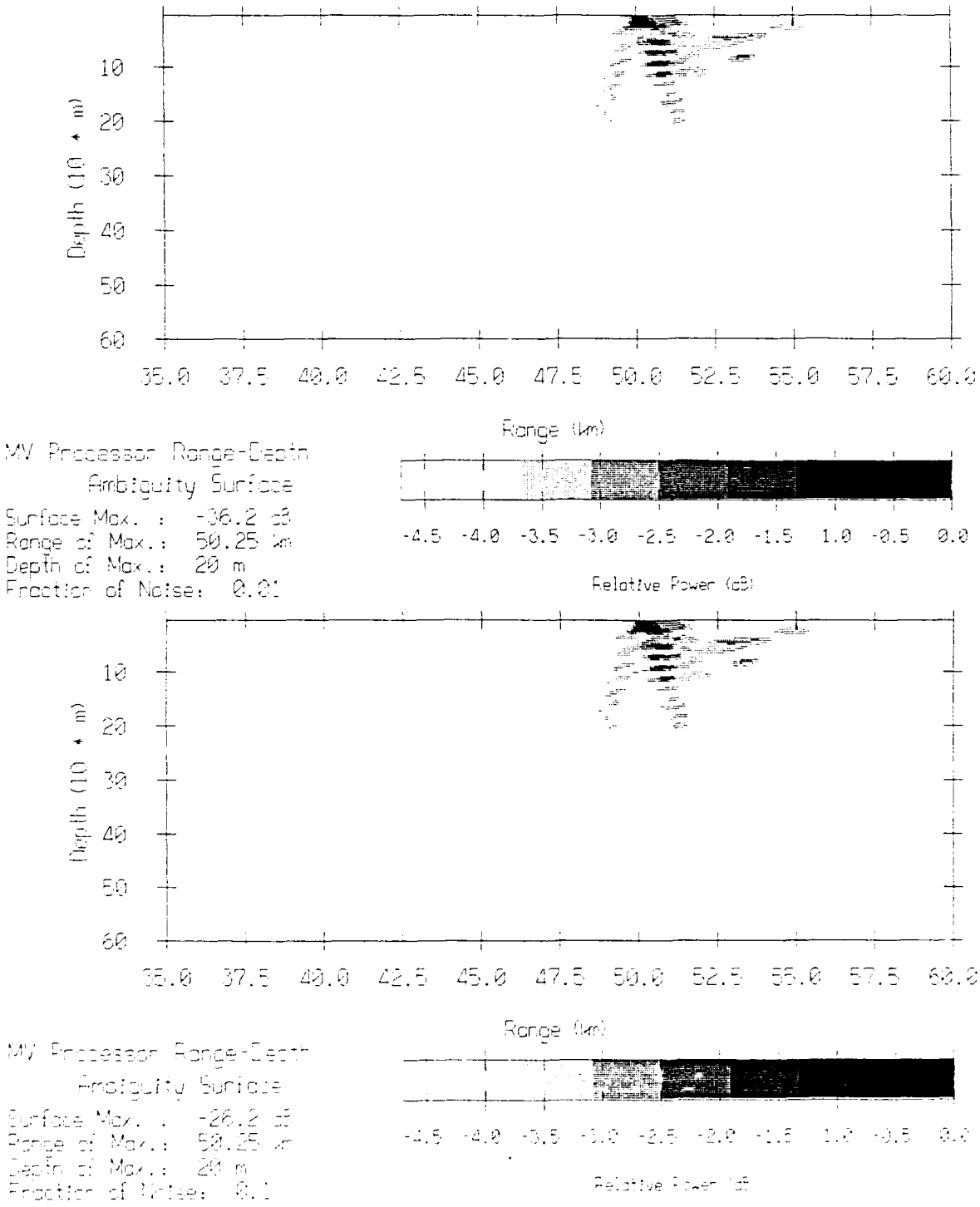

Figure 53: Matched field processing simulation (tilted array and towed source at 52 km), part 2.

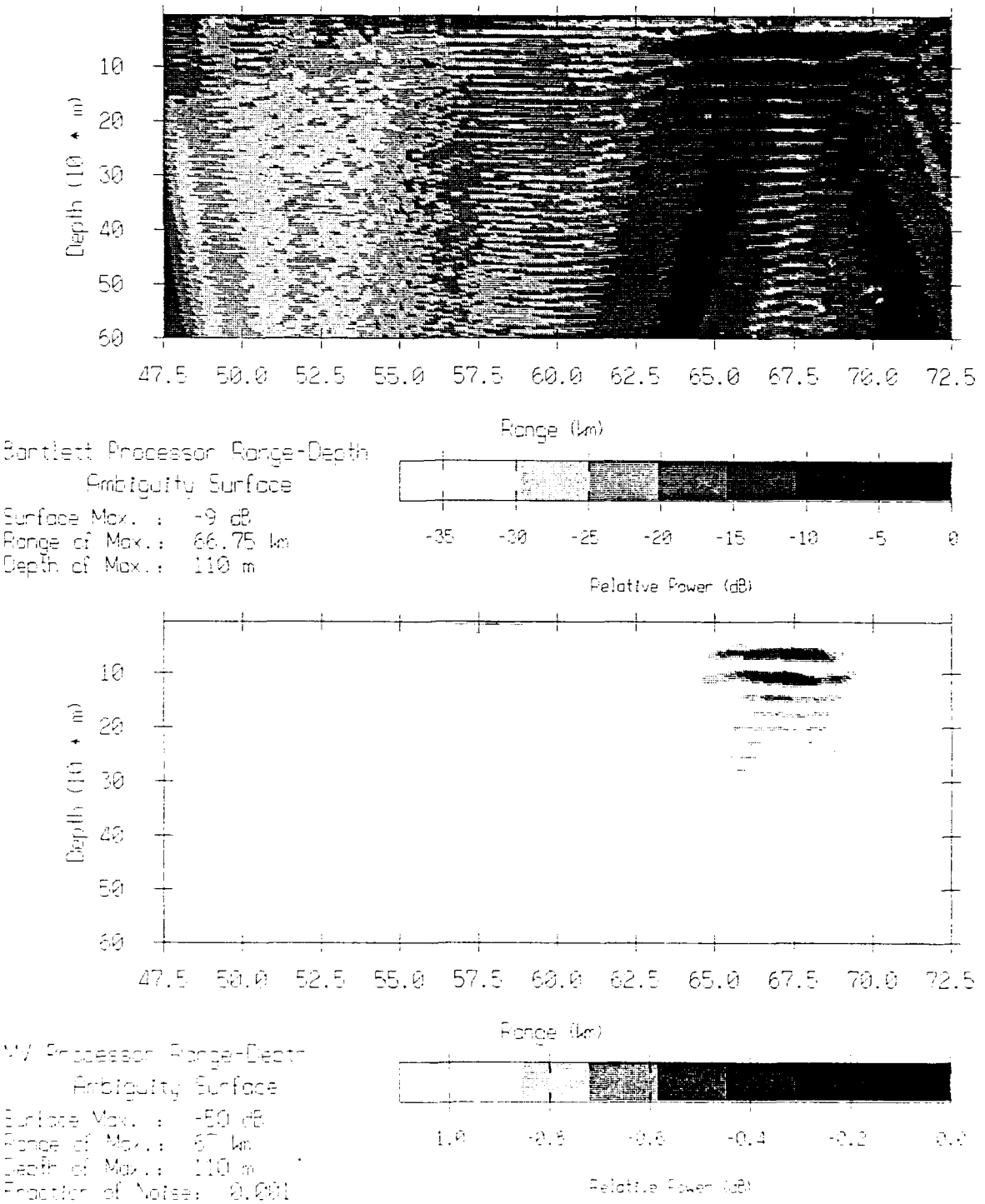

Figure 54: Matched field processing simulation (tilted array and towed source at 62 km), part 1.

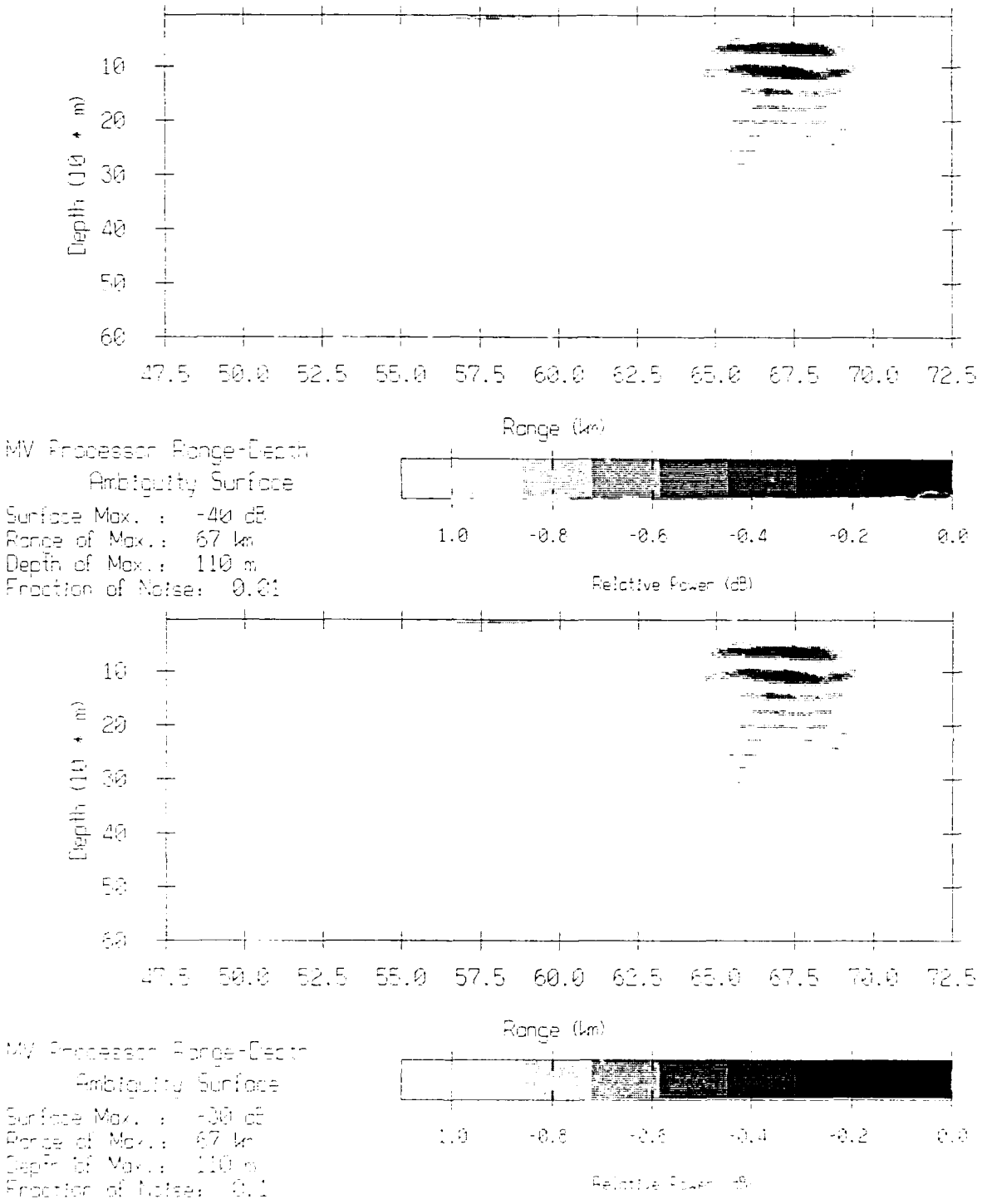

Figure 55: Matched field processing simulation (tilted array and towed source at 62 km), part 2.

References

Baggeroer, A. B. and W. A. Kuperman, "Matched Field Processing Source Localization in Correlated Noise as an Optimum Parameter Estimation Problem," *J. Acoust. Soc Am.*, vol. 83, no. 2, pp. 571-587, 1988.

Baxley, P. A. and J-M. Tran, "The Adverse Effects of a Mismatched Surface Layer in Matched Field Depth Discrimination," *Fourth Matched Field Processing Workshop*, Defence Research Establishement Pacific, Victoria, B.C. Canada, September 6-8 1989.

Camp, L., in *Underwater Acoustics*, Wiley, N.Y. , 1970.

Capon, J., "High Resolution Frequency-Wavenumber Spectrum Analysis," *Proc. IEEE*, vol. 57, pp. 1408-1418, 1969.

DelBazo, D. R., C. Feuillade, and Mary M. Rowe , "Effects of water-depth mismatch on matched field localization in shallow water," *J. Acoust. Soc. Am.*, vol. 83, no. 6, June 1988.

Feuillade, C., D. R. DelBazo, and Mary M. Rowe, "Environmental mismatch in shallow-water matched field processing: Geoacoustic parameter variability," *J. Acoust. Soc. Am.*, vol. 85, no. 6, June 1989.

Fizell, R. G., "Application of high-resolution processing to range-depth estimation using ambiguity function methods," *J. Acoust. Soc. Am.*, vol. 82, no. 2, pp. 606-613, August 1987.

Fofonoff, N. P., *Algoritms for the Computation of Fundamental Properties of Seawater*, Technical Paper 44, Unesco Division of Marine Sciences, Paris, France , 1983.

Gordon, D. F. and H. P. Bucker, *Arctic Acoustic Propagation Model with Ice Scattering*, NOSC Technical Report 985, 30 September 1984.

Mackenzie, K. V., "Nine-term Equation for Sound Speed in the Oceans," *J. Acoust. Soc. Am.*, vol. 70, no. 3, p. 808, September 1981.

Ozard, J. M. and P. Brouwer, "Doppler Effects and Matched Field Processing," *Fourth Matched Field Processing Workshop* , Defence Research Establishement Pacific, Victoria, B.C. Canada , September 6-8 1989.

Porter, M. B., R. L. Dicus, and R. G. Fizell, "Simulations of Matched Field Processing in a Deep-Water Pacific Environment," *IEEE J. Oceanic Engineering*, vol. OE-12, no. 1, pp. 173-181, January 1987.

Tolstoy, A., "Sensitivity of matched field processing to sound speed profile mismatch for vertical arrays in a deep water Pacific environment," *J. Acoust. Soc. Am.*, vol. 85, no. 6, June 1989.

Tran, J-M. and W. S. Hodgkiss, "Analysis of 200 Hz CW Tome Propagation Signals Recorded During the September 1987 SVLA Experiment," *MPL Technical Memorandum in process*, Marine Physical Laboratory, Scripps Institution of Oceanography, San Diego, CA.

Weinberg, H., *Generic Sonar Model,* NUSC Technical Document 5971-D, 6 June 1985.